



# **UNIVERSIDAD DE INVESTIGACIÓN DE TECNOLOGÍA EXPERIMENTAL YACHAY**

**Escuela de Ciencias Biológicas e Ingeniería**

## **DEVELOPMENT OF A NEURAL NETWORK FOR ANALYSIS OF EXTERNAL RADIOTHERAPY TREATMENT FOR BREAST CANCER**

Trabajo de integración curricular presentado como requisito para la obtención  
del título de Ingeniera Biomédica

**Autor:**

Deynna Lizbeth Sevilla Flores

**Tutor:**

PhD. Diego Almeida Galarraga

**Co-Tutor:**

M.Sc. Paula Rodríguez Ormaza

Urcuquí, mayo 2024

## Anexo 2 – Autoría

### AUTORÍA

Yo, **SEVILLA FLORES DEYNNA LIZBETH**, con cédula de identidad 1004754774, declaro que las ideas, juicios, valoraciones, interpretaciones, consultas bibliográficas, definiciones y conceptualizaciones expuestas en el presente trabajo; así como, los procedimientos y herramientas utilizadas en la investigación, son de absoluta responsabilidad de el/la autora (a) del trabajo de integración curricular. Así mismo, me acojo a los reglamentos internos de la Universidad de Investigación de Tecnología Experimental Yachay.

Urcuquí, Febrero, 2024.

  
Deynna Lizbeth Sevilla Flores  
CI:1004754774

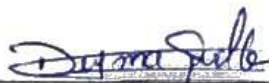
### **Anexo 3 – Autorización de Publicación**

#### **AUTORIZACIÓN DE PUBLICACIÓN**

Yo, **SEVILLA FLORES DEYNNA LIZBETH**, con cédula de identidad 1004754774, cedo a la Universidad de Investigación de Tecnología Experimental Yachay, los derechos de publicación de la presente obra, sin que deba haber un reconocimiento económico por este concepto. Declaro además que el texto del presente trabajo de titulación no podrá ser cedido a ninguna empresa editorial para su publicación u otros fines, sin contar previamente con la autorización escrita de la Universidad.

Asimismo, autorizo a la Universidad que realice la digitalización y publicación de este trabajo de integración curricular en el repositorio virtual, de conformidad a lo dispuesto en el Art. 144 de la Ley Orgánica de Educación Superior

Urcuquí, Febrero, 2024.



**Deynna Lizbeth Sevilla Flores**  
CI:1004754774

## **Dedication**

*This Work is dedicated to my dear angels: Mauro, Domi, and Pauli. To my lovely parents: Win and Nelvi for their great effort, and dedication and for never leaving me alone. My sisters who make my life colorful each day: Eimi, Adita, and Madi*

*For my dear friend Oscarl, who was my support of my university life and whom gave me a lot of moments of happiness.*

*For two great dear teachers for believing in my potential and always helping me, Diego and Paula.*

*With love  
Dey*

## Acknowledgments

I want to thank God for my life and each of the experiences I have had, like this one, Yachay Tech will always be my second home. I feel very blessed to have two great parents who have taught me and guided me to be who I am. I am happy to have three wonderful sisters, who in the moments I have cried have dried my tears and will always be my best friends.

Thanks to my favorite people that I love a lot, who rescued me and were my stick when I had a bad time and I shared a lot moments of happiness: Ali, Emi and Diego. Besides in this beautiful stage, I have had the pleasure of meeting great people who have been supportive and whom I can now call friends Antonio, Brenda and Pame for being my friends from day one and accompanying me throughout this stage, in the laughter and the tears.

To another great people who were an important support to me: Sebas, Majo and Rony. To my other friends who are not at the university but always gave me words of encouragement, being my second family: Geovany, Jorgito, Andy, Aby, and Jeny. I thank each of those I have mentioned for offering me their friendship, and more people that are not here but that I also love them.

To each of my dear professors in the Biomedical Engineering program, for being a voice of encouragement, and teaching us to love science. Thank you, Professor Diego. A, Paula. R Fernando. V, Nelson. V, Fernando. A. Also to Karlita Alarcon for always being so sweet and pretty when I went to the offices.

This thesis was written thanks to all of you.

*With love  
Dey*

## Resumen

Este estudio se centra en mejorar la precisión de la planificación y predicción de dosis de radiación en el tratamiento del cáncer de mama. Se utiliza una base de datos compuesta por 740 imágenes de resonancia magnética (RM) para el entrenamiento y 140 imágenes de tomografía computarizada (TC) para la validación. Se realiza una comparación entre dos enfoques: las Redes Neuronales (RN) y el Modelo Monte Carlo (MMC).

Para abordar esta tarea, se desarrolla un modelo híbrido que combina las RN, utilizando las arquitecturas ResNet50 y U-Net, y el MMC. Los resultados obtenidos se presentan tanto cualitativa como cuantitativamente. La precisión de las RN, evaluada mediante métricas específicas, alcanza un 97.1% de precisión. Por otro lado, el MMC se evalúa utilizando desviación estándar y dosis máxima y mínima, evidenciando resultados similares en la dosis máxima absorbida.

Es importante destacar que la diferencia media de dosis entre las RN y el MMC es mínima, con valores de 2.15 Gy y 2.19 Gy, respectivamente. Este estudio representa un avance significativo en la mejora de la precisión en la planificación de dosis de radiación para el tratamiento del cáncer de mama. Se aprovechan las capacidades de la inteligencia artificial y la simulación Monte Carlo en este contexto, ofreciendo resultados prometedores que contribuyen al campo de la radioterapia.

**Palabras Clave:** Redes Neuronales Convolucionales, Modelo Monte Carlo, Cáncer de mama, Radioterapia, Terapia Intensiva Modulada, Predicción de dosis, Haces.

## **Abstract**

This study focuses on improving the accuracy of radiation dose planning and prediction in breast cancer treatment. A database consisting of 740 magnetic resonance imaging (MRI) images for training and 140 computed tomography (CT) images for validation is used. A comparison is made between two approaches: Neural Networks (NN) and Monte Carlo Modeling (MCM).

To address this task, a hybrid model is developed combining the NN, using the ResNet50 and U-Net architectures, and the MCM. The results obtained are presented both qualitatively and quantitatively. The accuracy of the NNs, evaluated by specific metrics, reaches 97.1% accuracy. On the other hand, the MCM is evaluated using standard deviation and maximum and minimum dose, showing similar results in the maximum absorbed dose.

It is important to note that the mean dose difference between NN and MCM is minimal, with values of 2.15 Gy and 2.19 Gy, respectively. This study represents a significant advance in improving the accuracy of radiation dose planning for breast cancer treatment. It harnesses the capabilities of artificial intelligence and Monte Carlo simulation in this context, offering promising results that contribute to the field of radiotherapy.

**Key Words:** Convolutional Neural Network, Monte Carlo Model, Breast Cancer, Radiotherapy, Intensity Modulated Therapy, Dose Prediction, Beam

# Contents

<b>Chapter 1: Introduction</b> .....	<b>1</b>
1.1 Background .....	1
1.2 Problem Statement .....	2
1.3 General Objectives .....	3
1.4 Specific Objectives .....	3
1.5 Hypothesis .....	3
<b>Chapter 2: Literature Review</b> .....	<b>5</b>
2.1 Basics of Breast Cancer .....	5
2.1.1 Types of Cancer .....	6
2.1.2 Stages of Cancer .....	7
2.1.3 Types of Treatment .....	8
2.2 Techniques to Obtain Medical Images .....	10
2.2.1 Magnetic Resonance Imaging (MRI) .....	11
2.2.2 Computer Tomography (CT) .....	14
2.2.3 Contrast between MRI and CT .....	15
2.3 Radiotherapy .....	16
2.3.1 Types of Radiotherapy .....	17
2.3.2 Equipment of Radiotherapy .....	18
2.4 Artificial Intelligence .....	20
2.4.1 Types of learnings .....	20
2.4.2 Neural Networks .....	22
2.4.3 ResNet50 .....	23
2.4.4 U-Net .....	24
2.5 Monte Carlo Method (MCM) .....	25
2.5.1 Boltzmann Transport Equation .....	25
2.5.2 MC in Radiotherapy Treatment .....	26
2.6. Computational Sources .....	27
2.7 Related Works .....	28
<b>Chapter 3: Methodology</b> .....	<b>30</b>
3.1 Data Set .....	31
3.2 Preprocessing .....	32

3.2.1 Thresholding .....	32
3.2.2 Segmentation .....	34
3.3 Neural Network .....	35
3.3.1 Computational analysis: ResNet50 .....	36
3.3.2 Computational analysis: U-Net .....	37
3.3.3 Strategies of Training and Validation .....	39
3.4 Monte Carlo Simulation .....	40
3.4.1 MatRad .....	40
3.4.1 Development of MCM.....	40
<b>Chapter 4: Results .....</b>	<b>43</b>
4.1 Results of CNN .....	43
4.1.1 Hyperparameters .....	43
4.1.2 Plots of Learning .....	44
4.2 Volume Analysis .....	48
4.2.1 Differences between Radiotherapy and Chemotherapy .....	49
4.3 Radiation Dose .....	51
4.3.1 Results of CNN on dosage prediction .....	51
4.3.2 Results of MC on dosage prediction .....	53
4.4 T-test .....	53
<b>Chapter 5: Discussion .....</b>	<b>64</b>
5.1 Analysis between MCM and CNN .....	64
5.2 Comparison with other studies .....	66
<b>Chapter 6: Conclusions and Future Works .....</b>	<b>67</b>
6.1 Conclusions .....	67
6.2 Future Works .....	68

# List of Figures

<b>Figure 1.1</b> H1 and H2 representation .....	4
<b>Figure 2.1</b> Types of Breast Cancer .....	6
<b>Figure 2.2</b> Stages of Breast Cancer .....	7
<b>Figure 2.3</b> MRI Components .....	12
<b>Figure 2.4</b> Process of obtaining an image from a MRI.....	13
<b>Figure 2.5</b> CT Components .....	15
<b>Figure 2.6</b> Process of obtaining an image from CT .....	15
<b>Figure 2.7</b> Components of LINAC for IMRT .....	19
<b>Figure 2.8</b> Learning hierarchies in artificial intelligence.....	20
<b>Figure 2.9</b> Deep learning Neural Network .....	22
<b>Figure 2.10</b> Convolutional Neural Network .....	23
<b>Figure 2.11</b> Residual Learning: Building blocks ResNet50 .....	24
<b>Figure 3.1</b> Block diagram of the research methodology .....	30
<b>Figure 3.2</b> Preprocessing of Data.....	32
<b>Figure 3.3</b> Original and Threshold images .....	33
<b>Figure 3.4</b> Block diagram of the thresholding process .....	33
<b>Figure 3.5</b> Threshold and Segmented images .....	34
<b>Figure 3.6</b> Segmentation process .....	35
<b>Figure 3.7</b> Network architecture and parameters at each layer based on ResNet50.....	35
<b>Figure 3.8</b> Network architecture and parameters at each layer based on U-Net.....	37
<b>Figure 3.9</b> CNN Final Model .....	38
<b>Figure 3.10</b> Distribution of Data Set.....	39
<b>Figure 3.11</b> GUI of Workflow .....	40
<b>Figure 3.12</b> GUI of Plan Parameters.....	41
<b>Figure 3.13</b> GUI of Optimization Parameters .....	41
<b>Figure 3.14</b> GUI of Visualization.....	41
<b>Figure 3.15</b> Tumor Segmentation .....	42
<b>Figure 3.16</b> Schematic visualization of the concept of rays and bixel .....	44
<b>Figure 4.1</b> Plots of training and validation accuracy and loss of ResNet50 .....	48
<b>Figure 4.2.</b> Plots of training and validation accuracy and loss of U-Net.....	48

<b>Figure 4.3</b>	Plots of training and validation accuracy and loss of the General CNN Model ..	49
<b>Figure 4.4</b>	Confusion Matrix .....	50
<b>Figure 4.5</b>	Accuracy, Precision, Recall, and F1 score of different models .....	50
<b>Figure 4.6</b>	Segmentation of Volumes .....	51
<b>Figure 4.7</b>	Difference in tumor size before and after Chemotherapy state 1 .....	52
<b>Figure 4.8</b>	Difference in tumor size before and after Radiotherapy State 1 .....	52
<b>Figure 4.9</b>	Difference in tumor size before and after Chemotherapy state 2 .....	53
<b>Figure 4.10</b>	Difference in tumor size before and after Radiotherapy state 2 .....	53
<b>Figure 4.11</b>	Patient ACRIN-FLT-005 CNN-Dose distribution .....	54
<b>Figure 4.12</b>	Patient ACRIN-FLT-005 MCM-Dose distribution .....	56
<b>Figure 4.13</b>	Tumor dose distribution .....	57
<b>Figure 4.14</b>	Progress of Fluence Optimization (ACRIN-FLT-005) .....	58
<b>Figure 4.15</b>	DVH of ACRIN-FLT-005 patient .....	58
<b>Figure 4.16</b>	3D representation of dose and beam distribution .....	60
<b>Figure 4.17</b>	Angles of Beams .....	61
<b>Figure 4.18</b>	Longitudinal profile beam 1 .....	62
<b>Figure 4.19</b>	Lateral profile beam 5 .....	62
<b>Figure 4.20</b>	Longitudinal profile beam 1 .....	63
<b>Figure 4.21</b>	Lateral profile beam 5 .....	63
<b>Figure 4.22</b>	Shapes of beam 1 .....	65
<b>Figure 4.22</b>	Shapes of beam 5 .....	65
<b>Figure 5.1</b>	Distribution of dose data of CNN and MCM .....	69
<b>Figure 6.1</b>	Breast Anatomical Structure including intramammary nodes .....	71

# List of Tables

<b>Table 2.1.</b> Comparison between Chemotherapy and Radiotherapy .....	10
<b>Table 2.2</b> Comparison between MRI and CT .....	16
<b>Table 2.3</b> Summary of the literature referring to CCN on breast cancer .....	28
<b>Table 2.4</b> Summary of the literature referring to MCMC on radiotherapy treatment.....	29
<b>Table 3.1</b> Descriptions for classes and subclasses of Data Distribution .....	31
<b>Table 4.1</b> Hyperparameters used in the training of neural networks.....	47
<b>Table 4.2</b> Dose Prediction Results of CNN.....	55
<b>Table 4.3</b> Results of metrics of MCM simulation for dose Calculation .....	59
<b>Table 5.1</b> Advantages and Disadvantages of Models.....	68
<b>Table 5.2</b> Comparison of different methods.....	69

# List of Equations

<b>Equation 2.1</b> Activation function equation .....	23
<b>Equation 2.2</b> Boltzman Transpot equation .....	25
<b>Equation 2.3</b> Derived Equation of BTE .....	26
<b>Equation 4.1</b> Equation to Calculate Accuracy .....	50
<b>Equation 4.2</b> Equation to Calculate Precision .....	50
<b>Equation 4.3</b> Equation to Calculate Recall or Sensibility .....	50
<b>Equation 4.4</b> Equation to Calculate F1 score .....	50

# List of Abbreviations

**MCM** : Monte Carlo Model

**CNN**: Convolutional Neural Network

**CT**: Computerized Tomography

**MRI**: Magnetic Resonance Image

**PET**: Positron Emission Tomography

**CAT**: Computer Axial Tomography

**LINAC**: Linear Accelerator

**IMT**: Intensity Modulated Therapy

**IMRT**: Intensity Modulated Radiation Therapy

**AI**: Artificial Intelligence

**DNN**: Deep Neural Network

**ANN**: Artificial Neural Network

**RNN**: Recurrent Neural Network

**BTE**: Boltzman Transport Equation

**IDE**: Integrated Development Environment

**GUIs**: Graphical User Interfaces

**VMAT**: Volumetric Modulated Arc Therapy

**PNN**: Probabilistic Neural Network

**SRS**: Stereotactic Radiosurgery

**DICOM**: Digital Imaging and Communications in Medicine

**GPU**: Digital Imaging and Communications in Medicine

**RAM**: Random Access Memory

**ACC**: Accuracy

**NN**: Neural Network

**TN**: True Negative

**TP**: True Positive

**FP**: False Positive

**FN**: False Negative

**DVH**: Dose-Volume Histogram

**EANN**: Evolutionary Artificial Neural Networ

# Overview

The first chapter shows the background, the problem, and the objectives of this research, and from these two hypotheses are established regarding the use of Neural Networks and the Monte Carlo Model for the planning and prediction of radiation doses for patients with cancer. mother.

In the second chapter, we talk about breast cancer and its implications, and statistics worldwide. As a very important point, radiotherapy and the equipment used for it are discussed. In addition, important aspects of artificial intelligence are delved into, such as the type of learning, and the types of neural networks. In the case of the Monte Carlo Model, the statistical and physical relationship related to radiotherapy and the behavior of the particles is established. In this section, the resources are also shown the computational resources such as the software, hardware, and applications that were required for the research.

The third chapter is one of the most important, here the construction of the general model based on the ResNet50 and U-Net neural networks is explained in addition to the modifications to the Monte Carlo model code for the dose prediction and optimization process.

The fourth chapter shows the results obtained by the convolutional Neural Network model, where the learning plots, the volume variation, the emitted dose, and the absorbed dose were obtained. The Monte Carlo Model on the other hand indicates more variables as a result such as the maximum dose, minimum dose, standard deviation, optimization graphs, dose-volume, and the longitudinal and axial profiles of the beams.

In the discussion section, a comparison of the models used for this thesis is established, and they are reflected in a mustache table where the average of the doses, and the quintiles for both models, are established.

In the last chapter, we talk about the conclusions reached in this work, as well as its future perspectives. The use of three-dimensional images is proposed that allow us to observe the nodules of the breast where the cancer is located.

# Chapter 1

## Introduction

### 1.1 Background

Cancer is characterized by the uncontrolled growth of malignant cells forming tumors. One of the most common types of cancer is breast cancer, and it is the second that cause of most women deaths per year around the world (Hong & Xu, 2022). In Latin America, 13% of deaths caused by breast cancer occur in women less than 45 years old, which represents a significant problem for the region (American Cancer Society, 2019a). Over the years, significant strides have been made in diagnosing and treating this complex disease (American Cancer Society, 2019b).

The usual course of treatment for localized breast cancer consists of either a mastectomy in cases where a big tumor prevents breast-conserving treatment or a lumpectomy, followed by radiation therapy to the breast, sometimes in conjunction with a tumor bed boost. This method increases overall patient survival while lowering the chance of a local recurrence (Jornet et al., 2021).

For patients that are in the early stages of cancer radiotherapy and chemotherapy the best option is treatment (National Cancer Institute (NIH), 2022). Radiotherapy has remarkably improved local control and survival rates (Hausmann et al., 2020). However, delivering precise and tailored radiotherapy to individual patients requires sophisticated tools and techniques (Hausmann et al., 2020). In the case of chemotherapy is the oldest and most frequently used unfortunately it is not efficient in eradicating the cancer cells as expected (Behranvand et al., 2022).

On the other hand, in recent years, artificial intelligence and machine learning have revolutionized various fields, including medical imaging and cancer treatment (Abbass, 2002). Among these techniques, neural networks have emerged as a powerful tool for image analysis and pattern recognition (Chougrad et al., 2018). Their ability to learn from data and make accurate predictions holds tremendous promise in radiotherapy for breast cancer (Yamashita et al., 2018) Developing a neural network specifically tailored for analyzing

radiotherapy treatment in breast cancer represents a cutting-edge endeavor with immense potential to improve treatment outcomes and patient care. (Barragán-Montero et al., 2021)

We will begin by reviewing the current state of breast cancer treatment and radiotherapy techniques. An in-depth examination of the challenges and limitations faced in current radiotherapy planning will be presented, emphasizing the need for innovative solutions to improve treatment efficacy while minimizing side effects. An overview of artificial intelligence, neural networks, and their applications in medical image analysis and cancer treatment will also be provided.

The subsequent sections will delve into the development and implementation of the neural network described in this project. The data used for training and validation will be carefully selected, and the neural network's architecture will be tailored to suit the specific requirements of breast cancer radiotherapy analysis. Key features and parameters will be identified to optimize the network's performance, ensuring its ability to accurately analyze treatment plans and deliver precise dose distributions.

The evaluation of the neural network will be a crucial aspect of this research. Comparisons will be made with existing radiotherapy planning methods, including manual contouring and other computer-based algorithms. The accuracy, efficiency, and clinical relevance of the developed neural network will be thoroughly assessed using a dataset of patient treatment plans.

The implications of successful implementation and integration of the neural network into clinical practice will be discussed. The potential benefits in terms of treatment efficiency, cost-effectiveness, and improved patient outcomes will be highlighted. Moreover, the challenges and ethical considerations associated with incorporating artificial intelligence into healthcare will be addressed.

## **1.2 Problem statement**

Breast cancer is one of the most common incidents in the world, however, in Ecuador, it is unknown which is the best treatment for each specific type of cancer, in addition to the fact that there is no exhaustive analysis of the patient's radiation dosage.

### 1.3 General Objective

This research aims to address several critical aspects of radiotherapy planning and delivery, compare different types of treatments, and ultimately improve accuracy and outcomes for patients by leveraging the power of artificial intelligence, particularly Neural Networks, and the Monte Carlo method.

### 1.4 Specific Objectives

- To determine which type of therapy is best between chemotherapy and radiotherapy to treat breast cancer.
- To analyze dose distribution and angles using Monte Carlo simulation.
- To improve the accuracy in the dose calculation, using current computer capabilities, allows us to perform Monte Carlo Model (MCM) simulations and work with machine learning.
- To interpret the results obtained by the Convolutional Neural Network (CNN) to provide relevant clinical information, such as the probability of treatment success, identification of risk factors, and recommendations for clinical decision-making.
- To evaluate the performance of the neural network on an independent test data set, using performance metrics such as accuracy, sensitivity, and specificity.
- To select relevant clinical variables to be used as inputs to the neural network.
- To validate the clinical utility of the neural network by comparing results with traditional approaches for the evaluation of radiotherapy treatments.

### 1.5 Hypothesis

**H1:**Based on the findings of Sande, Sharabiani, Bluemink, Kneepkens, Bakx, Hagelaar, Sangen, Theuws, and Hurkmans (2021) on the automatic generation of treatment plans for patients with locally advanced breast cancer using a neural network model convolutional (CNN) combined with a dose imitation algorithm, it is postulated that the implementation of advanced machine learning techniques will result in a significant improvement in the accuracy and applicability of dose treatment plan generation (van de Sande et al., 2021).

**H2:** Given the impressive performance of rapid Monte simulation compared to conventional methods in estimating dose distribution in radiotherapy, it is postulated that its implementation in clinical settings will significantly improve the efficiency of the treatment planning process according to Franciosini (2023). It is hypothesized that its application will result in an improvement in the results of dose prediction in the present thesis (Franciosini et al., 2023).

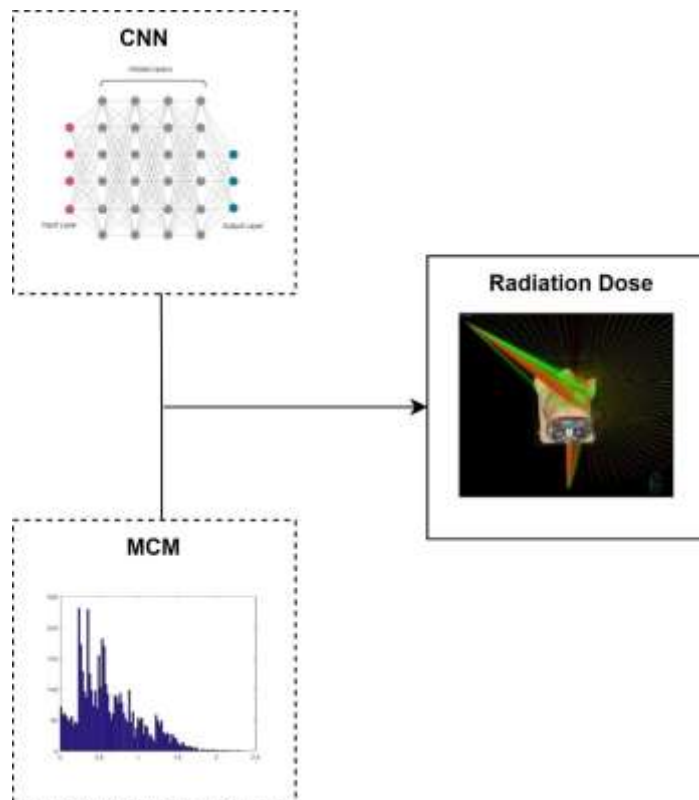


**Fig 1.1.** H1 and H2 representatio

## Chapter 2

### Literature Review

#### 2.1 Basics of Breast Cancer

Breast cancer is a complex disease that can develop when abnormal cells in the breast begin to grow uncontrollably (Center for Disease Control and Prevention, 2019). It is one of the most common types of cancer in women. The exact causes of breast cancer are not fully understood, but it is believed to result from a combination of genetic, hormonal, environmental, and lifestyle factors. The development of breast cancer begins with genetic mutations in the DNA of breast cells (Center for Disease Control and Prevention, 2019). These mutations can be inherited or acquired during a person's lifetime

Hormonal factors also play a significant role in breast cancer development (Drăgănescu & Carmocan, 2017). Estrogen and progesterone, two female hormones, can promote the growth of breast cells (Rastelli & Crispino, 2008). Prolonged exposure to these hormones, either naturally (early onset of menstruation, late menopause) or through hormone replacement therapies, may increase the risk of breast cancer (NCI, 2022). Environmental and lifestyle factors have been linked to breast cancer risk as well as high-fat diets, lack of physical activity, alcohol consumption, and smoking (Burguin et al., 2021)

Furthermore, exposure to certain environmental toxins and radiation has also been linked to breast cancer development (American Cancer Society, 2019a). For instance, ionizing radiation, such as that used in previous medical treatments like radiation therapy, can increase the risk of breast cancer, especially in women who were treated at a young age.

It is essential to note that not all individuals with risk factors will develop breast cancer, and some individuals without identifiable risk factors may still develop the disease (Foidart et al., 2007). Therefore, breast cancer is a multifactorial disease with complex interactions between genetic, hormonal, environmental, and lifestyle factors (American Cancer Society, 2019b).

### 2.1.1 Types of breast cancer

There are different types of breast cancer, and the differences between them are related to where they are located (Figure 2.1).

- **Ductal Invasive Breast Cancer:** Invasive cancer, in which malignant cells that start in the milk ducts have moved into other areas of the breast tissue (National Cancer Institute (NIH), 2022).
- **Lobular Breast Cancer:** Begins on the lobules and then cancer cells break out of the lobule and spread to the lymph nodes and other areas of the body (Wasif et al., 2010).
- **Mixed Tumor Breast Cancer:** Comprises two types of histotypes such as ductal and lobular carcinoma, it coexists in a single mass (Zhang et al., 2017).
- **Inflammatory Breast Cancer:** Cancer cells block lymph vessels in the skin of the breast. Because its breast looks swollen and red or inflamed (National Cancer Institute (NIH), 2022).
- **Mucinous Breast Cancer:** It starts on the main cells of mucus called mucin; this type of cancer can develop in any part of the body but is commonly developed in the breast (Marrazzo et al., 2020).

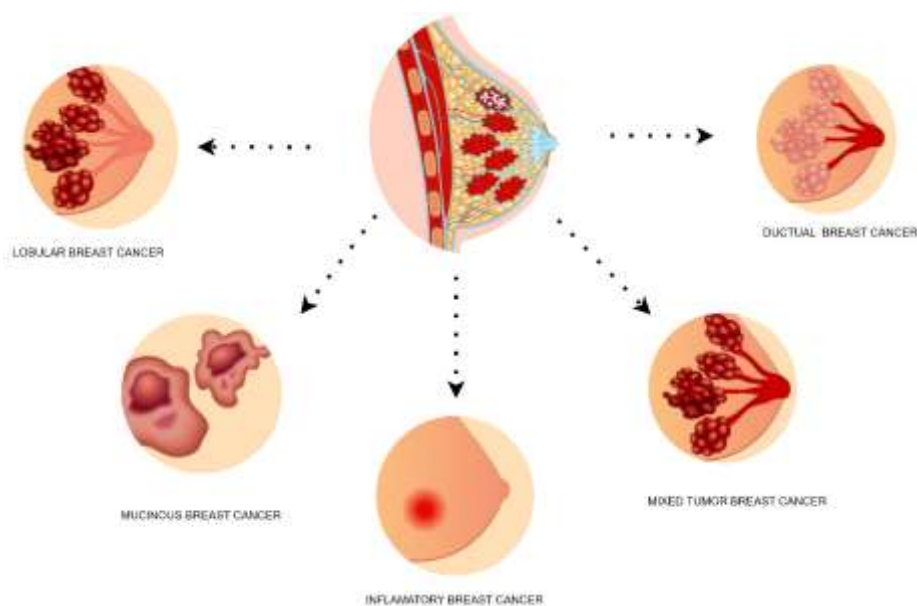


**Figure 2.1.** Types of Breast Cancer

### 2.1.2 Stages of Breast Cancer

Breast cancer staging is based on the TNM classification system, which evaluates the Tumor size and invasiveness, Lymph Node involvement, and the presence of Metastasis. Tumor size ranges from carcinoma in situ (Tis) to invasive tumors (T1-T4) that may involve nearby structures (Figure.2.3). Lymph Node involvement (N) signifies the extent of regional spread, while Metastasis (M) indicates the presence of distant spread. The integration of these parameters facilitates the categorization of breast cancer into different stages, with lower stages generally indicating localized disease and higher stages reflecting more advanced disease with potential metastatic involvement.

#### Propagation and Metastasis:

Metastasis is a complex multistep process involving tumor cell invasion, intravasation into blood or lymphatic vessels, dissemination through the circulation, extravasation into distant tissues, and colonization of distant organs. The tumor microenvironment, angiogenesis, immune responses, and molecular factors play pivotal roles in facilitating or inhibiting the metastatic cascade. The understanding of these mechanisms holds promise for targeted therapies aimed at disrupting the metastatic process and improving patient outcomes. (Burguin et al., 2021)

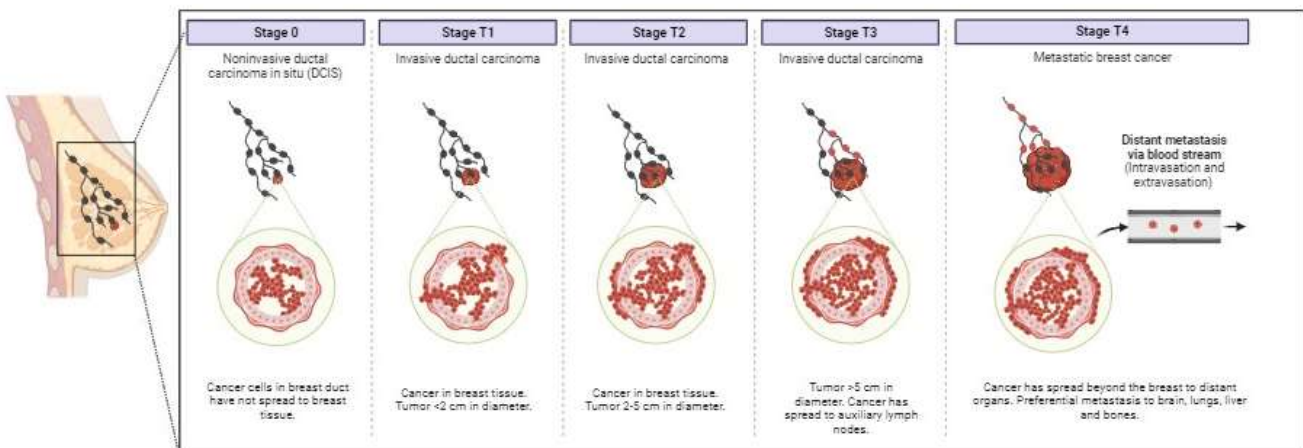


**Figure 2.2.** Stages of Breast Cancer

### 2.1.3 Types of Treatment

Nowadays, there are different ways to treat breast cancer and all of them have been described below.

- **Surgery**

It is the removal of a breast tumor with healthy tissue around it and the sentinel lymph node. This sentinel lymph refers to the lymph node within a cluster to obtain lymphatic drainage from the main tumor. This procedure starts by injecting a colored substance near a lump, which works as a biomarker to detect the lymph nodes that are directly connected (NCI, 2022). Therefore, a doctor analyzed if there were malignant cells inside the conducts. Then, extract only the first lymph node and the tumor or remove the whole breast with the total number of lymph that contains cancerous cells (G. N. Sharma et al., 2010). Thus, there are three kinds of surgeries such as breast-conserving surgery, total mastectomy, and modified radical mastectomy.

- **Radiation:** It is another way to treat cancer that always uses high radiation doses to kill the malignant cells. This therapy uses X-rays to prevent the cells from growing up. Besides, it classifies into two types of methods internal and external therapies. External radiation uses a machine that uses X-rays to destroy the DNA of cancer cells (Castaneda & Strasser, 2017). Meanwhile, internal therapy injects a tube or some device close to the tumor to release the radioactive substance to relieve the pain of the patient (NCI, 2022). This treatment eliminates cancer progressively. It is due to it avoiding cellular division (Abbas & Rehman, 2018). Therefore, the body removes these dead cells over a long period.

- **Chemotherapy:** It uses drugs for medical treatment. Thus, there are a lot of medicines or chemical substances that inhibit the growth of killing cells. Its compounds are supplied using injection or oral administration (NCI, 2022). Also, this treatment is delivered at various time intervals. It is also usually complementary to other techniques for treating cancer, such as after surgery to remove the tumor. Hence, it decreases the size of the cancer to apply other therapies or only to relieve the patient's pain (Hassan et al., 2010). It happens intending to avoid mastectomy.

- **Hormone therapy:** Endocrine therapy stops the spread of lumps and is related to the production of hormones, which can increase or decrease this production to retain the development of cancer. The goal of breast cancer is to block the connection between estrogen and the mechanisms that stimulate cancerous cells when they are dependent on estrogen (Drăgănescu & Carmocan, 2017). Then, there are two forms of hormone therapy, which are blocking ovarian function and blocking estrogen production. The first of these tries to normalize the function of the ovaries, which are the main organ that produces estrogen. Therefore, surgery is performed to remove the ovaries, or through radiotherapy, the production of estrogens necessary to control the cancer is used (Foidart et al., 2007). Meanwhile, the second uses medications that inhibit the aromatase enzyme, which is the main producer of estrogen in the ovaries and tissue (Rastelli & Crispino, 2008). It causes alterations in the growth of breast cancer.
- **Targeted:** The targets treated usually use drugs to identify and attack cancerous cells. As a result, physicians may recommend biomarker testing to gauge your likelihood of responding to specific targeted treatment medications (NCI, 2022). The drug development for the treatment of breast cancer has mostly focused on two well-established therapeutic targets: the estrogen receptor (ER) and the human epidermal growth factor receptor 2 (HER2) (Mohamed et al., 2013).
- **Immunotherapy:** Immunotherapy works with drugs that help the immune system of the patients to combat by themselves defense mechanisms counter cancer. In this case, The HER2+ and TNBC subtypes are thought to be the most immunogenic subtypes, whereas breast cancer is categorized typically as a moderately immunogenic malignancy (Henriques et al., 2021). Immune cells are essential for both the early detection and elimination of carcinoma as well as the advancement of tumors. Immunoediting is the term for the three-phase process that explains the interactions between the immune system of the host and the cells forming the tumor: elimination, equilibrium, and escape (Sternschuss et al., 2021).

The following table establishes a comparison between the two most used types of treatment.

<i>Characteristic</i>	<b>Chemotherapy</b>	<b>Radiotherapy</b>
<i>Mechanism of action</i>	Chemotherapeutic agents to destroy cancer cells	Ionizing radiation damages the DNA of cancer cells
<i>Treatment Area</i>	Entire body	Specific areas of the body
<i>Type of cancer treated</i>	Localized or disseminated tumor	Localized tumor
<i>Treatment Frequency</i>	Administered in cycles	Daily session on a period
<i>Side Effects</i>	Affect the entire body including healthy cells	Affect the treated area and nearby tissues
<i>Therapeutic Approach</i>	Systematic, act throughout the entire body	Localized, acts in a specific area

**Table 2.1.** Comparison between Chemotherapy and Radiotherapy. Modified from (Hassan et al., 2010; Haussmann et al., 2020)

## 2.2 Techniques to Obtain Medical Images

Medical images are visual representations of the inside of the human body, used for diagnostics, treatment, and research in the medical field (Contreras et al., 2022). Also, it allows one to obtain detailed information about internal anatomy, organ, and tissue functions, as well as anomalies, injuries, or illnesses.

There are several types of images and each one has its applications and advantages the most common to detect breast cancer are:

- **Radiography:** This is a quick test that generates images on a plate of internal structures. It is obtained by exposing the patient to a radiation source, commonly X-ray or gamma radiation. At the moment of interposing an object between the radiation source and the receptor, the densest parts appear with different tones in a grayscale (Roberts & Graham, 2001). In the case of breast cancer mammography is

commonly used, because is used in routine controls when no symptoms or signs appear.

- **Computerized Tomography (CT):** It is a scan that uses an X-ray to make images in a cross-sectional way. Instead of taking a few images as normal radiography, it takes several images and joins these images to show a portion of the chest and surrounding organs and tissues (Roberts & Graham, 2001)
- **Magnetic Resonance Imaging (MRI):** This is a diagnostic imaging technique that uses radio waves and strong magnets to generate images (Radhakrishna et al., 2018)
- **Positron Emission Tomography (PET):** This is an imaging test that uses a radioactive substance called a tracer. This substance is administered by the vein, the tracer travels around the body and collects in organs and tissues. This tracer gives off a signal, then the patient slides into a large tunnel-shaped scanner. The PET detects the signal given by the tracer after a computer converts the results into a 3d picture, this process takes 90 minutes (Tabouret-Viaud et al., 2015)(Hadebe et al., 2023).
- **Ultrasound:** This is a technique non-invasive that generates images through sound waves. First, a gel is applied on the breast skin surface, and then the transducer moves over the skin sending sound waves and picking up echoes as they bounce off deeper body tissues beneath the skin. These echoes are converted into images (Sood et al., 2019).

### 2.2.1 Magnetic Resonance Imaging

MRI uses magnetic fields and radio waves to obtain detailed images, it is especially useful for visualizing soft tissues and provides 3-dimensional images with high resolution (Varela et al., 2022). The magnetic resonator components are (Figure 2.3):

- **Radiofrequency coils:** These coils are designed to emit the radiofrequency pulse and receive the signals generated by the protons in the breast tissue. The coils are strategically placed around the breast to obtain detailed images(Serai et al., 2021)
- **Examination table:** This is the surface on which the patient lies during the procedure. It can be moved in and out of the resonator to facilitate obtaining images from different angles (Varela et al., 2022)
- **Main Magnet:** This magnet creates the strong magnetic field necessary to align the protons in the breast tissue (Serai et al., 2021).
- **Control console:** From here, the technician or radiologist controls and monitors the procedure, adjusting parameters as necessary to obtain the desired images (Varela et al., 2022).

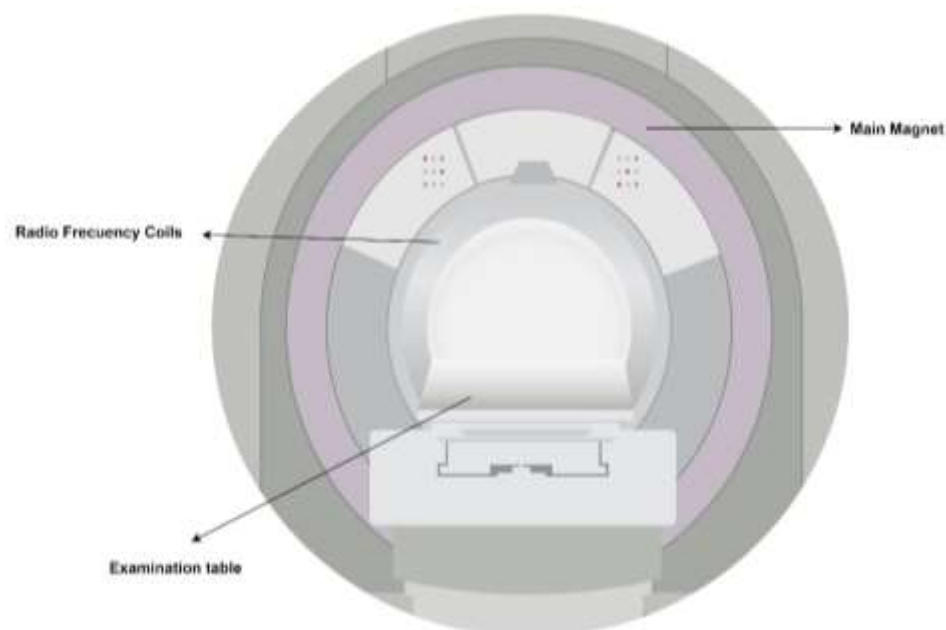


**Figure 2.3** MRI Components

Figure 2.4 explains the principal steps of the process to create an image on the MRI considering the physics and chemical principles.

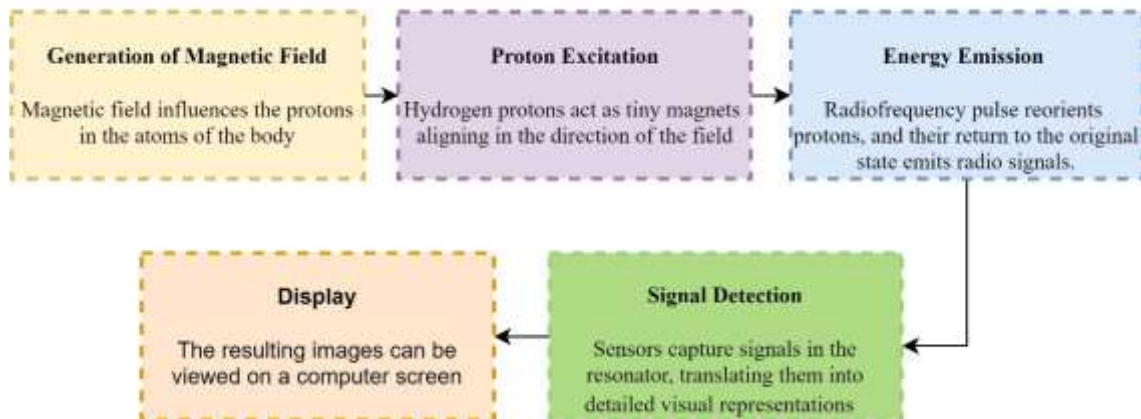


**Figure 2.4.** Process of obtaining an image from a MRI

MRI plays a crucial role in characterizing breast lesions and distinguishing between benign and malignant lesions, particularly when mammography and ultrasound findings are inconclusive. Also, some techniques improve the quality of it, such as:

- **Dynamic contrast-enhanced MRI (DCE-MRI):** It allows the assessment of lesion vascularity, which aids in differentiating malignant tumors from benign lesions. Malignant tumors typically demonstrate rapid and intense enhancement, whereas benign lesions exhibit slower and less intense enhancement (Gordon et al., 2014). Then, evaluate blood perfusion and contrast uptake in real-time in breast tissues by observing how certain areas retain or eliminate contrast over time in sequential images (Thawani et al., 2022).
- **Diffusion-weighted imaging (DWI)** is another MRI technique that can provide valuable information for breast cancer diagnosis. DWI assesses the random motion of water molecules within tissues, and it is sensitive to tissue cellularity (Partridge et al., 2010). Malignant breast tumors often demonstrate restricted diffusion due to increased cellular density, leading to higher apparent diffusion coefficient (ADC) values in benign lesions (Deike-Hofmann et al., 2018).

The combination of DCE-MRI and DWI, known as multiparametric MRI, has shown promising results in improving diagnostic accuracy. A meta-analysis by Youk et al. (2017)

reported that the combination of DCE-MRI and DWI had a higher sensitivity (90%) and specificity (84%) for breast cancer diagnosis compared to either technique alone.

### 2.2.2 Computerized Tomography

Computerized tomography is also known as computed axial tomography (CAT). CT scan is a medical imaging technique that uses X-rays to obtain detailed images of the body's internal structures. Here is an overview of the main parts of a CT scanner:

- **Gantry (Ring):** It is the structure that contains the X-ray tube and the detectors. It can rotate around the patient during the scan (Zhu et al., 2022b).
- **X-ray Tube:** Emits X-rays into the patient's body.
- **Detector:** A series of detectors located on the opposite side of the X-ray tube that collect information after the X-rays pass through the body (Zhu et al., 2022a).
- **Motorized patient bed:** Where the patient lies during the scan. It can move in and out of the ring to allow the acquisition of images of different parts of the body (Zhu et al., 2022a).
- **Cooling System:** Due to the amount of heat produced by the x-ray tube, CT scanners are equipped with cooling systems to maintain the proper temperature(Zhu et al., 2022b).

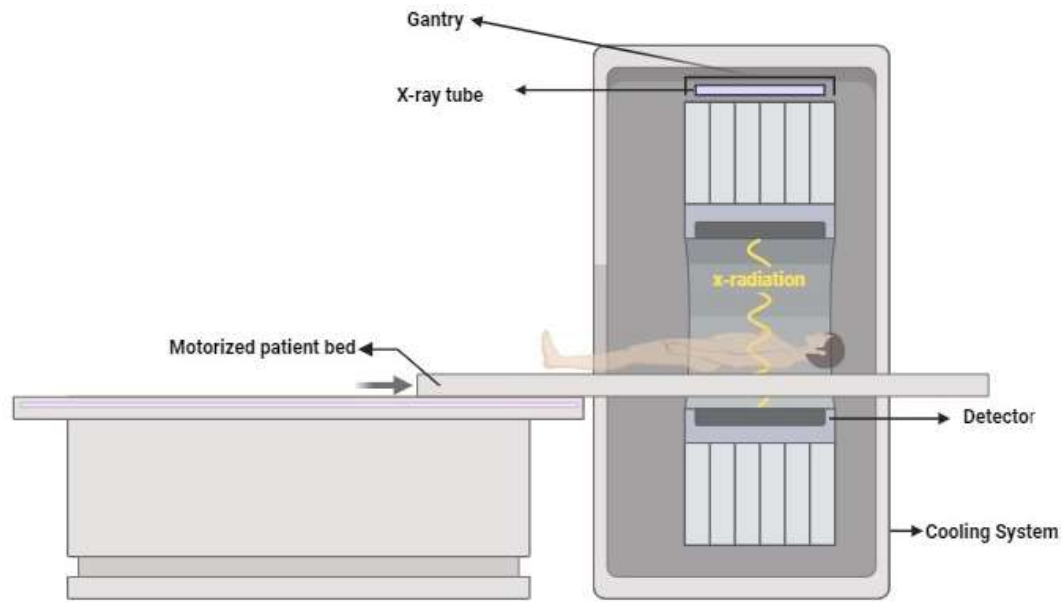


**Figure 2.5** CT Components

CT works as seen in the following Figure 2.6

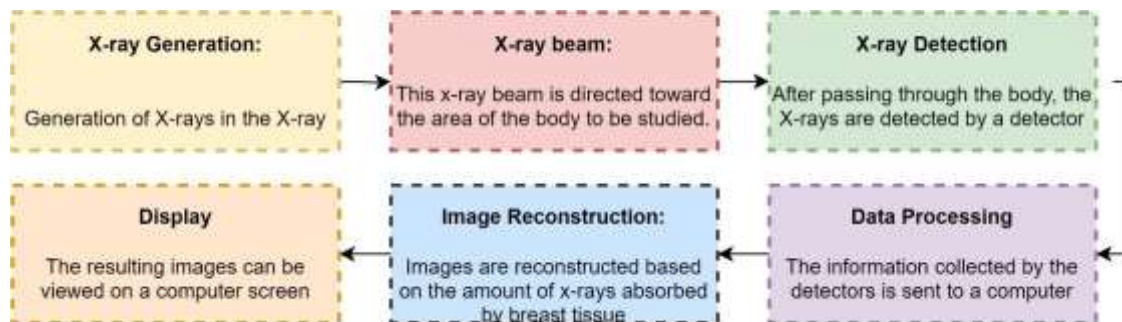


**Figure 2.6** Process of obtaining an image from CT.

### 2.2.3 Contrast between MRI and CT

Magnetic resonance imaging (MRI) and computed tomography (CT) are two imaging techniques with different approaches to evaluating breast cancer. MRI uses magnetic fields and radio waves to generate detailed images of soft tissue, given superior sensitivity in detecting tumors, especially in women with dense breast tissue. In contrast, CT uses X-rays and, although it can detect tumors, it has lower sensitivity in soft tissues and involves exposure to ionizing radiation (Lothar et al., 2023).

Each modality has advantages and considerations. MRI is notable for its high sensitivity and ability to highlight anatomical details but can be more expensive and time-consuming (Lothar et al., 2023; Radhakrishna et al., 2018). On the other hand, CT is faster and more accessible but has lower sensitivity in identifying subtle soft tissue changes and uses ionizing radiation (Zhu et al., 2022b). The choice between MRI and CT for breast cancer diagnosis depends on factors such as the specific clinical situation, equipment availability, and patient and physician preferences. They are often used in a complementary manner to obtain a complete evaluation of the disease. The following table represents the differences between both.

	<b>MRI</b>	<b>CT</b>
<i>Technique</i>	X-Ray	Radio waves and magnetic field
<i>Resolution</i>	Contrast	Spatial
<i>Depth</i>	Different types of tissue	Bone and Soft tissue
<i>Radiation</i>	None	Minimum dose of ionizing radiation
<i>Time</i>	1h-2h	10 minutes

**Table 2.2** Comparison between MRI and CT. Modified from (Roberts & Graham, 2001; Serai et al., 2021; Varela et al., 2022)

## 2.3 Radiotherapy

Is a medical treatment that uses ionizing radiation, and it is used to damage cancerous cells, interrupting their growth and division (NIH National Cancer Institute, 2019). Before radiation therapy begins, careful planning is done to determine the exact amount of radiation and the precise location of the area to be treated (Castaneda & Strasser, 2017). Treatment is applied daily for several weeks or in shorter sessions, depending on the type and extent of the cancer (Martins & Azevedo, 2021).

### 2.3.1 Types of Radiotherapy

As mentioned in the chapter above, there are two types of radiotherapy to treat breast cancer: internal and external beam radiation therapy.

- **Internal Beam Therapy**

This therapeutic approach involves the direct insertion of radiation sources into the body. It is categorized into two types. Firstly, brachytherapy entails the insertion of a solid radiation source within the body. Enclosed within a solid container, this radiation source emits radiation over a specific period to target breast cancer directly (NCI, 2022). Presently, various types of capsules are employed to deliver the radiation source substance into the body, such as multi-catheter interstitial brachytherapy, balloon catheter brachytherapy, conformal external beam radiation therapy, and intra-operative radiation therapy (Njeh et al., 2012). Additionally, the second type involves the insertion of a liquid radiation source, known as systemic therapy. This liquid circulates through the veins until it reaches malignant cells and eradicates them. An example of a liquid radiation source is strontium-89, often injected to alleviate pain when breast cancer metastasizes to the bones (Pons et al., 1997).

- **External Beam Radiation Therapy**

This treatment modality utilizes a machine to generate an external beam for delivering radiation to a specific area where cancer is located. The machine employs three types of radiation sources: photons, protons, and electrons (Njeh et al., 2012). Recent advancements have introduced techniques utilizing these radiation sources for treating breast cancer, such as 3D-conformational radiation, intensity-modulated radiation therapy, tomotherapy, volumetric arc therapy, and proton beam therapy (Kozak et al., 2006). Among these techniques, 3D conformational therapy has emerged as the most effective. It involves the utilization of multiple stationary photon or electron fields, minimizing the impact on surrounding healthy tissue compared to whole breast radiotherapy (Jain et al., 2009). Consequently, this radiation treatment method has a lower impact on the patient's health.

### 2.3.2 Equipment of Radiotherapy

There are many equipment that are usually used to treat cancer. However, in this project, we focus on machines whose operating principle is that of a linear accelerator (LINAC). These machines work with an external beam source of radiation. It releases high energy in the area where the tumor appears(cite). These are classified according to the type of technique to launch the radiation, such as Volumetric Modulated Arc, Image Guided, Stereotactic Radiosurgery, Stereotactic Body Radio Therapy, and Intensity-Modulated Radiation Therapy (Lennox, 2001).

- **Volumetric Radiation Arc**

It works using a radiation source that has a continuous rotation. It allows treatment of the tumor in all 360 beam angles (Teoh et al., 2011). Overall, this technique shows three main parameters that can be changed, such as dose rate, gantry rotation speed, and treatment aperture shape via Multi-leaf collimator movement (Otto, 2008).

- **Image Guided**

The principle of work is with a cyclotron to irradiate the tumor. Besides, it uses technology to obtain images to scan the lump with techniques such as magnetic resonance, ultrasound, and X-rays. Fiducial markers or electromagnetic transponders are inserted into or close to the tumor (DiMaio et al., 2007). It identifies the treated area and is irradiated using a beam with high energy.

- **Stereotactic Radiosurgery and Stereotactic Body Radio Therapy**

It is a non-surgical treatment to hit and destroy cancer. Both stereotactic radiosurgery and stereotactic body techniques work with the same principle. First, this device determines the coordinates of the tumor using 3D images. Second, it uses a system to immobilize and irradiate the lump using gamma or X-rays as the radiation.

- **Intensity-Modulated Therapy**

The intensity-modulated therapy (IMT) works with linear accelerators as the radiation source. Its machines are controlled with software that delivers and precisely calculates radiation dose. Therefore, this device considers the volume, the state, and the region where the tumor appears. It is the most used technique to treat cancer with radiation

(Kooy & Grassberger, 2015) . Thus, in the present work, the dose quantification is done using an intensity-modulated photon device.

The working principle starts with defining the volume of the tumor region. Then, these are obtained using images before starting the IMRT. After, the doctor puts these images inside IMRT and uses the information on tumor dimensions to determine the correct quantity of multiple energy beams or a beam that rotates at entire angles. Besides, these multiple beams divide with different intensities that can build a unique pattern for each shape and size (Lomax et al., 2019). This feature allows radiation to reach with enough strength to each part of the tumor that contains cancerous cells and avoid damage to healthy tissues. Finally, it is evaluated with a histogram volume dose that shows the quantity of radiation per volume(Taylor & Powell, 2004).

This device has some important parts to make a correct function. This is composed of a linear accelerator that creates an electron beam that hits a bending magnet that changes the direction of the beam. Then, it reaches a beam filter to classify the quantity of radiation dose passed. Later, it enters a beam shaping to divide the beam into multiple beams with different strengths to treat breast cancer (Lomax et al., 1999) . All these parts are classified in the next figure to understand better how they work and their main parts of equipment.

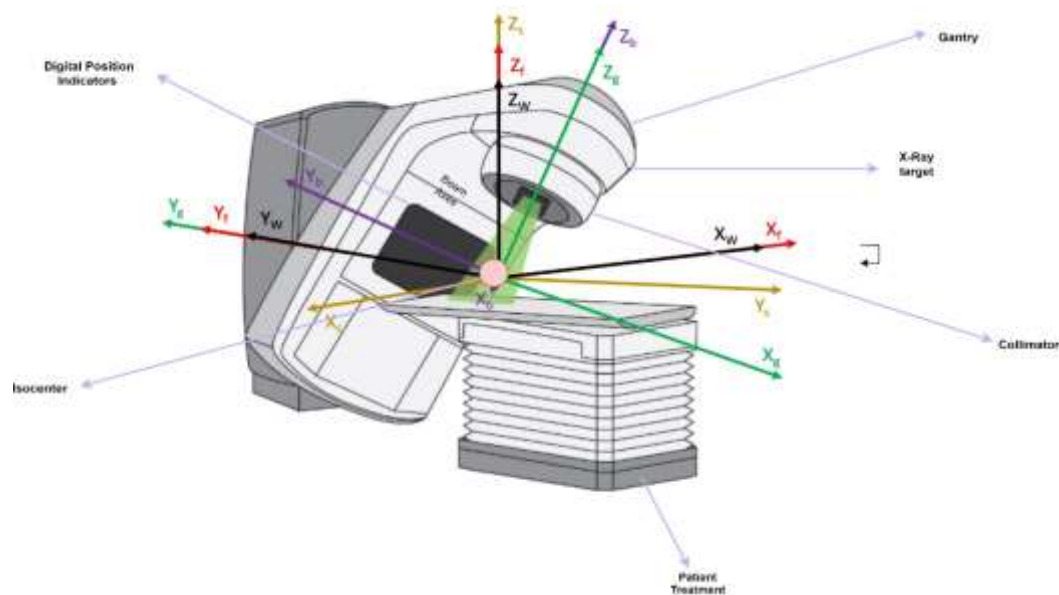


**Figure 2.7** Components of LINAC for IMRT. Own development is taken from TOPAS MC

## 2.4 Artificial Intelligence

Artificial intelligence (AI) is considered the ability of computers to solve complex problems by using algorithms so that they learn from data and make decisions just as humans would. That is, automating intellectual tasks that we normally perform (Rouhiainen, 2018). Currently, artificial intelligence has grown in various areas of daily life. Some of the applications of AI are:

- Recognition of static images, classification, and labeling.
- Efficient and stable processing of patient data.
- Performance improvements of the algorithmic strategy.
- Distribution of content on social networks.
- Predictive maintenance

The following figure shows the different fields of AI.

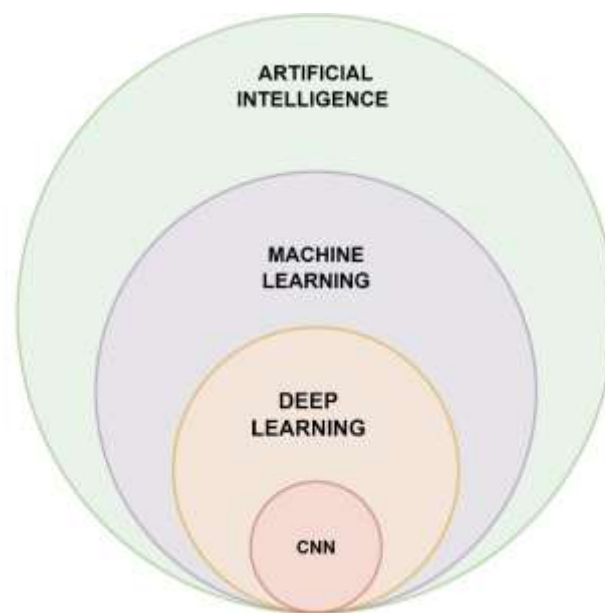


**Figure 2.8** Learning hierarchies in artificial intelligence. Own elaboration from (A. K. Sharma et al., 2022)

### 2.4.1 Types of Learnings

Some types of learning are used to train models depending on the task that it has. Starting from the basis that would be artificial intelligence, there is machine learning followed by deep learning, which allows the design of all types of neural networks .

**Machine learning**

Analyze data, learn from that data, and ultimately apply what they learn to make informed decisions (Cavalcanti et al., 2021).

- **Supervised Learning:** The name refers to the idea of a ‘supervisor’ that instructs the learning system from training (Cunningham et al., 2008). The model is trained using a labeled data set, which consists of inputs and expected outputs. The objective is to establish a relationship between inputs and outputs to make accurate predictions on new data. During training, the model adjusts its parameters to minimize the difference between predictions and actual outputs (Tiwari, 2022).
- **Unsupervised Learning:** It is a class of algorithms, where the goal is to find patterns, structures, or representations in a dataset with no labels (Sen & Das, 2023). Clustering and dimensionality reduction are common examples of unsupervised learning tasks. In clustering, the model groups similar data, while in dimensionality reduction, the objective is to simplify the representation of the data while preserving the most relevant information (Sen & Das, 2023).
- **Reinforcement Learning:** the model interacts with an environment and receives feedback in the form of rewards or penalties. Reinforcement learning models make sequential decisions and learn through experience, exploring different actions and adjusting their behavior based on the consequences.

**Deep learning**

Deep learning models are designed to analyze data with a logical structure that draws human-like conclusions. To achieve this analysis, deep learning applications use a layered algorithmic structure called a deep neural network (DNN) (Figure 2.9), which is made up of layers, and these in turn neurons, include 3 or more hidden layers (Microsoft, 2022). The input information is processed by different layers until the desired results. The disadvantage is It needs a large amount of data to be trained. Currently, it is used in the field of computer vision, thanks to the increase in computational capacity of the processors.

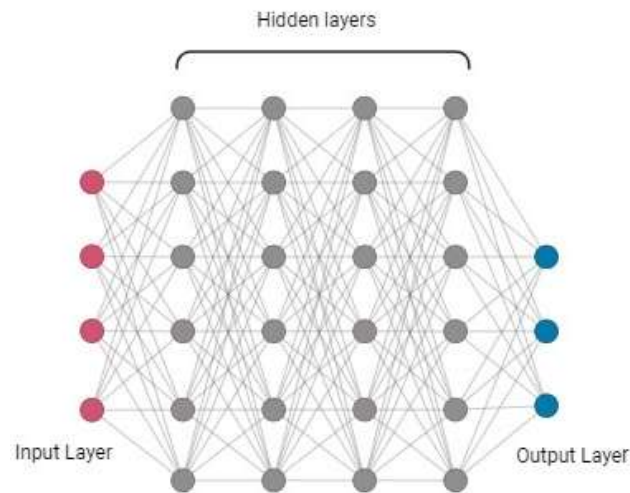


**Figure 2.9** Deep learning Neural Network

## 2.4 Neural Networks

Neural Networks (NN) are computational models inspired by human brain function. These are part of AI and Deep Learning fields to perform specific tasks. A Neural Network has many interconnected processing elements known as nodes. These nodes relate to other nodes using a connection link. The connection link contains weights, which contain information about the input signal or image(Choi et al., 2020).

### Types of Neural Networks

- **Artificial Neural Network (ANN):** This is a feedforward neural network because the inputs are sent in the forward direction. It can also contain hidden layers which can make the model even denser, it is used for textual data and is the simplest red(Islam et al., 2019).
- **Recurrent neural networks (RNNs):** A class of computational models that are designed to handle sequential data and model temporal dependencies. Unlike feedforward neural networks, RNNs have feedforward connections, allowing them to maintain an internal state or memory that can remember information from previous inputs.

- Convolutional Neural Network (CNN):** This kind of network was designed to process grid data such as images, they have proven effective in a variety of tasks, from object recognition to semantic segmentation. CNN learns in an automatic and adaptative form through backpropagation by using multiple building blocks such as convolutional layers, pooling layers, and fully connected layers (Yamashita et al., 2018). Convolutional layers apply filters to local regions of the input to extract relevant features while pooling layers reduce the spatial dimension of the representation.

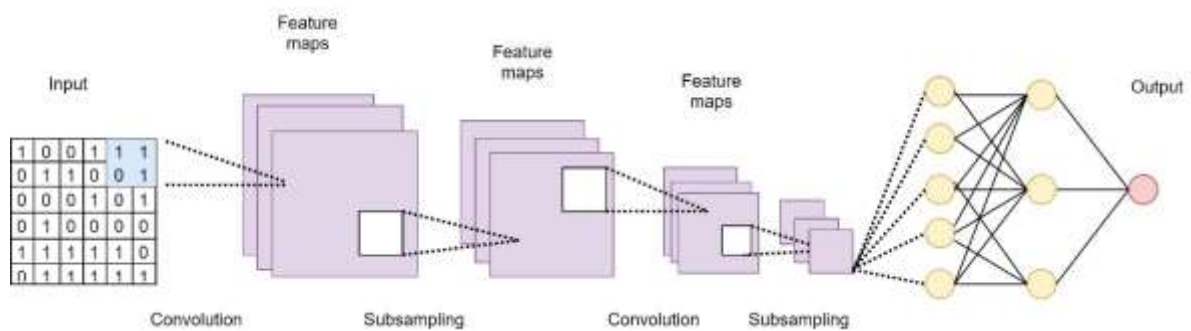


**Figure 2.10** Convolutional Neural Network. Own elaboration from (Krizhevsky et al., 2017)

### 2.4.3 ResNet50

It has an architecture of 50 layers and uses a bottleneck design for the building block. This allows for much faster training of each layer. Use a three-layer stack instead of two two-layers. The key innovation in ResNet is the introduction of residual blocks, which use skip connections also known as identity mappings to skip one or more layers during the forward pass. This helps mitigate the vanishing gradient problem and makes it easier to train (Mascarenhas & Agarwal, 2021). Besides ResNet50 layers consisting of multiple convolutional layers, batch normalization (BN), rectified linear unit (ReLU) activation functions, and shortcuts (A. K. Sharma et al., 2022). In mathematical terms, it would mean *Eq 2.1*  $y = x + F(x)$  where  $F$  is the residual,  $x$  is the input, and  $y$  is the final output of the layer, (Figure. 2.11).

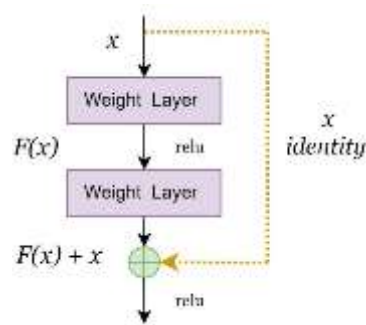


**Figure 2.11** Residual Learning: Building blocks ResNet50. Own elaboration from (A. K. Sharma et al., 2022)

The residual network is composed of the initial convolutional layers and multiple basic blocks. ResNet-50 features 49 convolutional layers, a  $3 \times 3$  max-pooling layer, an intermediate pool layer, a ReLU nonlinearity fully connected layer, and batch normalization applied to all convolutional layers (as illustrated in Figure.x). The SoftMax function is utilized in the final layer. Additionally, ResNet employs transfer learning (TL), which refers to the reuse of knowledge gained from solving one problem to tackle a related but distinct problem. This includes utilizing the weight and bias values from prior similar problems that have required considerable time and computational resources (Mascarenhas & Agarwal, 2021).

#### 2.4.4 U-Net

It is a convolutional neuronal network. The main goal of it is to classify the images with a unique label (Krizhevsky et al., 2017). In recent years, it has developed to apply this network in biomedical images. It is used to localize a region in dataset collected images. These regions are localized. It means assigning a label to each pixel in the processed image. Hence, this network complements the acquiring network because these additional layers improve the resolution to find the characteristics using the high-resolution image (Cireşan et al., 2012). The convolutional layer learns to identify these features to give a more precise output.

The architecture network is based on two sides that have a U form. In the left part, it has a contractive way. Meanwhile, on the right side, it has an expansive way. Thus, the left side follows the design of a convolutional network. Its part employs two convolutions  $3 \times 3$ . Per each convolution, there is a rectified linear unit. Then, the  $2 \times 2$  max pooling down-sampling

procedure using stride 2. Every step of the down-sampling process doubles the amount of feature channels. Then, on the right side, enhance the feature map's quality by continuing with 2x2 ascendent convolution, which reduces the number of channels in equal parts. It has a concatenation with the cropped left side and two 3x3 convolutions, each with a rectified linear unit (Ronneberger et al., 2015). Finally, the convolution 1x1 works to assign the vector with 64 components to the required number of classes. All of the entire process works until getting the output image.

## 2.5 Monte Carlo Method

In simplified form, the Monte Carlo method is a stochastic simulation technique in which multiple independent results are obtained from a modeled system by repeatedly solving the model for randomly sampled (input) values of the input variables and events (Koch, 2018). Unlike a normal forecasting model, Monte Carlo simulation predicts a set of outcomes based on an estimated range of values against a set of fixed input values (Fielding, 2023). In other words, a Monte Carlo simulation creates a model of possible outcomes by taking advantage of a probability distribution, for example, a uniform or normal distribution, for any variable that has inherent uncertainty. It then recalculates the results repeatedly, each time using a different set of random numbers between the minimum and maximum values (Gentle, 2009).

### 2.5.1 Boltzmann Transport Equation (BTE)

This is the equation system of Boltzmann Transport Equation.

$$\begin{aligned}
 Q_1(x, E, \Omega) &= \Omega \cdot \Delta \psi_1 + \Sigma_1 \psi - K_1 \psi \\
 Q_2(x, E, \Omega) &= \Omega \cdot \Delta \psi_2 + \Sigma_2 \psi - K_2 \psi \\
 Q_3(x, E, \Omega) &= \Omega \cdot \Delta \psi_3 + \Sigma_3 \psi - K_3 \psi
 \end{aligned}$$

Eq 2.2)

- $Q_N(x, E, \Omega)$  Represents the neutron source in the angular direction  $\Omega$  at spatial point  $x$  for the  $N$  number of repetition
- $\psi_1, \psi_2, \psi_3$  Represents the rate of change of neutron flux in the angular directions  $\Omega$  and energy.

- $K_1, K_2, K_3$  Represents the macroscopic absorption cross-section at spatial point  $x$  for the three energies.

It describes the preservation of the radiation source during the transfer of this source across the medium. Thus, the flow of particles travels at a specific point directly to the patient tissue, where this flow depends on the increase or decrease of the net particles due to the dispersive events (Bedford, 2019). This model has an approach to non-homogeneous materials such as tissues. Therefore, it is necessary to have the total and differential cross sections, which rely on how particles interact (Tervo et al., 2008). Then, the BTE solution gives the exact dose distribution for the patient.

This model has three partial differential-integral equations system. The stationary solution is obtained from the following function with these three terms:  $\psi_1, \psi_2, \psi_3$ . This solution works in six-dimension space, such as position, energy, and velocity direction (Tervo, 2007). Hence, these three components explain particulate phase space number densities. Then, for radiation therapy, a derived equation Eq 2.3), where a multigroup approach is used for energy discretization and, more recently, the finite element method for spatial discretization (St. Aubin et al., 2015).

$$Eq\ 2.3) \quad Q = \frac{1}{N} \sum_{i=1}^N q_i^{\sigma}$$

- $Q$  indicates the dose.
- $q_i$  indicates the irradiated dose.
- $N$  Position particle Matrix
- $\sigma$  independent histories

## 2.5.2 Monte Carlos simulation in Radiotherapy treatment

In the context of radiotherapy treatment, the Monte Carlo method is used to simulate the interaction of radiation with biological tissue (Fielding, 2023). To begin, the Monte Carlo model uses information about the shape of the linear accelerator head to measure the distribution of photons and electrons entering the patient in terms of energy, angle, and location. This information is crucial to understanding how radiation interacts with the patient

(DeMarco et al., 2022) The simulation also considers the depth at which the target tissue is located, as this significantly affects how the radiation dose is distributed in the tissue. The linear accelerator (LINAC) equipment and the specific geometry of the patient's treated region are combined with the Monte Carlo code to accurately calculate the radiation dose (Rogers, 2021). This involves simulating how photons and electrons interact with tissues, depositing energy as they travel through the body. Accuracy in simulating these interactions is critical to ensuring that the correct radiation dose is delivered to the cancerous tissue while minimizing exposure to surrounding tissues (Franciosini et al., 2023).

## 2.6 Computational Sources

**MATLAB** is a high-level programming language and interactive environment widely used in engineering, mathematics, and applied science. It is known for its ease of use and wide range of tools and functions for numerical analysis, data visualization, algorithm development, and model creation. It allows you to perform complex numerical calculations, manipulate matrices and vectors efficiently, and visualize the results interactively. In addition, it has numerous tools for solving problems in a variety of fields, such as signal processing, image processing, automatic control, artificial intelligence, simulation, modeling, and more (Mathworks, 2022).

The MATLAB integrated development environment (IDE) provides a code editor, debugger, and tools for interactively executing and testing code. In addition, MATLAB supports the creation of graphical user interfaces (GUIs) and integration with other programming languages, such as C/C++, Java, and Python (Mathworks, 2022). In this research were used to special software and toolkits of MATLAB like:

- **MatRad:** is an open-source software for radiation treatment planning for photon, proton, and carbon ion therapy. MatRad comprises MATLAB functions to model the entire treatment planning workflow, physically and biologically based data for all required calculations. It comprises functions to model treatment planning, for example, patient data, and physical and biological base data. Also, this software provides (H. P. Wieser et al., 2017):
  - Ray tracing
  - Photon dose calculation

- Proton dose calculation
- Carbon ion dose calculation (including 3D RBE modeling)
- Inverse planning (based on physical dose and biological effect)
- Multileaf collimator sequencing
- Basic treatment plan visualization and evaluation

## 2.7 Related Works

In the field of dose prediction in radiotherapy, there are various research studies employing different approaches and techniques. The relationship between these works and the current thesis lies in their shared objective of enhancing accuracy and efficiency in the administration of radiotherapy treatments. However, it is crucial to highlight the differences in the methods and approaches utilized, as well as the specific contributions of each study. For this reason, the following table establishes a relationship with different authors in the field of NN in the treatment of cancer.

<b>Type of Neural Network</b>	<b>Application</b>	<b>Data Set</b>	<b>Type of leads</b>	<b>Reference</b>
<i>CNN</i>	Breast Cancer Screening	DDSM	Multichannel	(Chougrad et al., 2018)
<i>EANN</i>	Breast Cancer Diagnosis	Mammography	Multichannel	(Abbass, 2002)
<i>CNN</i>	Breast Cancer Histology Image Analysis	Biopsy Images	Multichannel	(Rakhlin et al., 2018)
<i>CNN</i>	Improve Radiologist's Performance in Breast Cancer	ELMDS	22 Channels	(Wu et al., 2020)
<i>PPN</i>	Breast Cancer classification	FDMS	Multichannel	(Azar & El-Said, 2013)
<i>DCNN</i>	Breast cancer diagnosis in digital breast tomosynthesis	Tomosynthesis	Multichannel	(Samala et al., 2018)

**Table 2.3** Summary of the literature referring to CCN on breast cancer.

When comparing work related to Monte Carlo modelling in radiotherapy, it is essential to evaluate various factors in different studies to understand their contributions and limitations. The following table provides a comparative overview of several studies conducted by different authors in this field. Each study aims to evaluate the effectiveness or accuracy of the Monte Carlo model in different aspects of radiotherapy planning and delivery.

<b>Autor</b>	<b>Year</b>	<b>Application</b>	<b>Methodology</b>	<b>Type of particle</b>
Lagdijk et al.	2008	Evaluate precision of MC in IMRT	Utilization of MC to simulate IMRT in a water phantom; validation with measurements.	Photons
Adamson et al.	2023	Investigate the efficacy of MC in SRS (Stereotactic Radiosurgery)	Employing MC to simulate SRS in a head phantom; validation with measurements.	Photons
Boylan et al.	2013	Analyze VMAT (Volumetric Modulated Arc Therapy) on prostate cancer.	Compare MC with other methods in VMAT	Photons
Rosenstrom et al.	2023	Assess MC in FLASH treatments	MC to simulate FLASH treatments; comparison with conventional techniques.	Photons

**Table 2.4** Summary of the literature referring to MCMC on radiotherapy treatment.

# Chapter 3

## Methodology

The development project in the present thesis has two parts: first, the prediction of radiation dose using CNN of MRI images based on tumor sizes. In the next step, a DICOM database of CT images is used to implement MatRad, a software extension of MATLAB for radiation treatment planning of intensity-modulated photon therapy. The goal is to compare the dose radiation prediction of both methods in contrast with real dose and set the best treatment for breast cancer. The following Block diagram shows the main structure of the methodology (Figure 3.1).

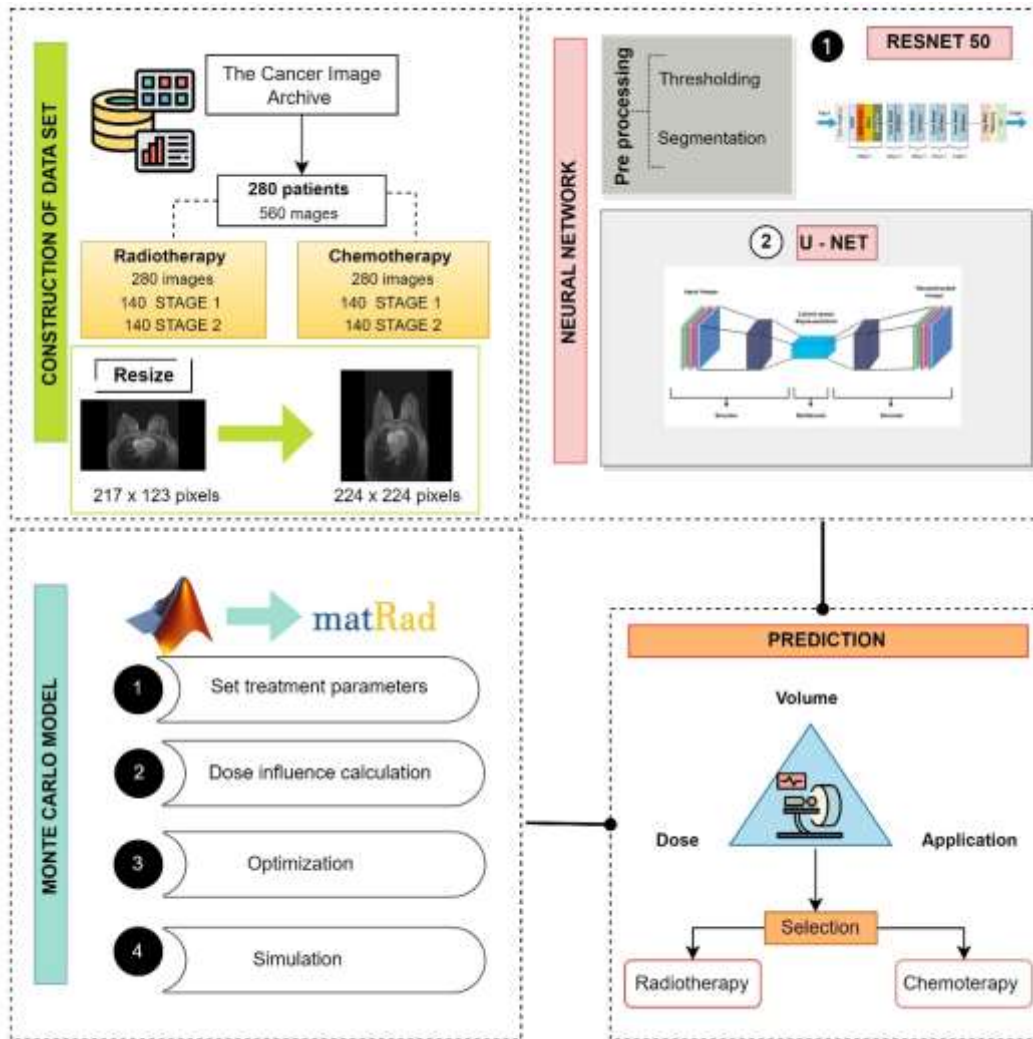


**Figure 3.1** Block diagram of the research methodology

### 3.1 Data Set

- **MRI Data Set**

Data set **Duke-Breast-Cancer-MRI** (Dynamic contrast-enhanced magnetic resonance images of breast cancer patients with tumor locations) were obtained from The Cancer Imaging Archive. The dataset is a collection of 922 patients with invasive breast cancer, it contains the following data components: clinical notes, radiology reports, pathological reports, and the type of scanner, of these data, 280 patients were taken (Saha, et al.2021).

The MRI images and clinical notes were classified as follows: on the one hand, the information of the patient as code, cancer stage, and tumor size, and in some of these cases if patients went to surgery, and on another the radiological information provided such as dose, type of scanner (1.5T or 3.0T) and type of therapy. In the case of images, 560 medical images were extracted and divided into two groups according to the treatment in Chemotherapy (280 images and 140 patients) and Radiotherapy (280 images and 140 patients), which in turn, were classified into early stage 1 and medium early stage 2. For the entire set of images, the information before (initial) and after (final) applying the radiotherapy and chemotherapy treatment plan was considered to analyze the tumor size and therapy treatment.

Therapy	Number of patients	Stage	Case	Number of images
Radiotherapy	140	1	Initial	70
			Final	70
		2	Initial	70
			Final	70
Chemotherapy	140	1	Initial	70
			Final	70
		2	Initial	70
			Final	70

**Table 3.1** Descriptions for classes and subclasses of Data Distribution

- **CT Data Set**

Data Set **ACRIN-FLT-Breast (ACRIN 6688)** is a DICOM collection of multi-center trials that measure cellular proliferation in the primary early tumor stages. The trial examines pre-therapy and post-therapy through the association of F-FLT uptake with the tissue proliferative marker Ki-67 to compare F-FLT/CT. In this study, 90 patients were enrolled of which 140 images were selected for NN and 1000 for MC (Acs et al., 2019).

CT images were used at this stage due to MatRad's capability for only reading DICOM-CT scans. In addition,, the DICOM format allows communication between information systems and at the same time with medical image storage format that generates interoperability between different types of devices (Cisternas et al., 2015; H. P. Wieser et al., 2017)

Both data sets are used in the development of the neural network, however, the **Duke-Breast-Cancer-MRI** is used in the training of CNN and **ACRIN-FLT-Breast (ACRIN 6688)** in the validation of CNN.

## 3.2 Preprocessing

In Image acquisition, some factors influence the quality of images like contrast, lightning, size, and noise. In general, CNN needs some readjustments in the quality and size of the image, therefore the following scheme (Figure 3.2) indicates the first step of the image where it resizes from a value of 223x217 pixels to 224x224, followed by process of thresholding and segmentation.

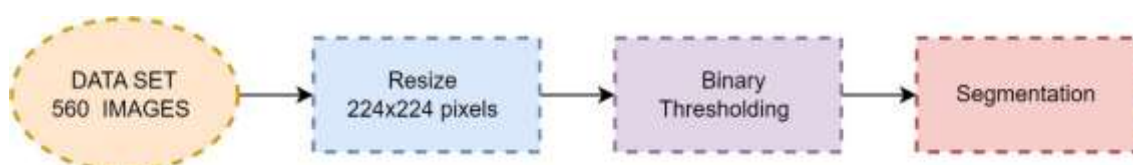
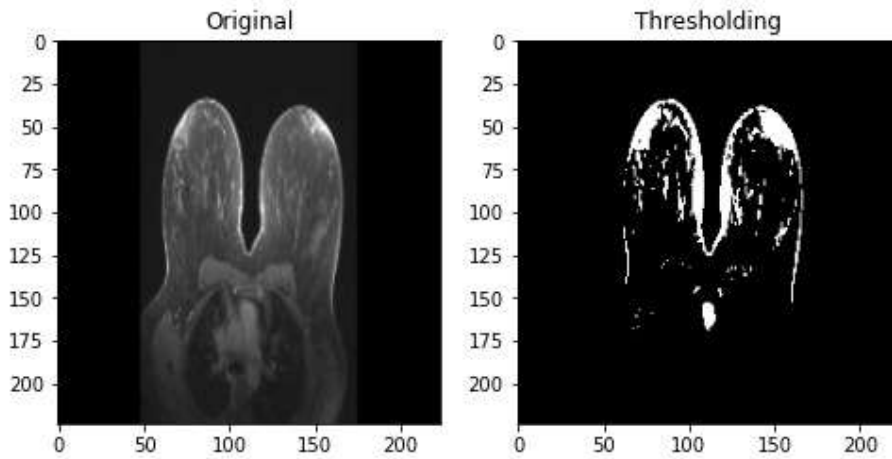


**Figure 3.2** Preprocessing of Data

### 3.2.1 Thresholding

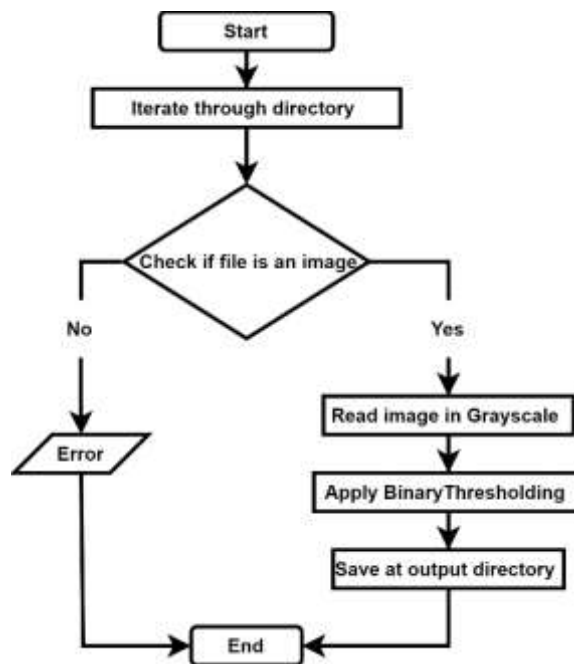
Thresholding is a technique widely used in different applications, in the medical field it is used to identify anatomic structures, types of tissues, and pathologies. In this case, the binary thresholding was applied using the function `cv2.threshold` from the OpenCV library, it converts images to grayscale, where each pixel is classified into two categories: black or white. This process is done by selecting a threshold value, and the original image pixels are

assigned white if their intensity is greater than the threshold, and black if it is less than or equal to the threshold. The threshold value set was 100 and a maximum value of 255 was assigned to pixels that exceed the threshold. All pixels with intensity greater than 100 are converted to white (255) and those with intensity equal to or less than 100 are converted to black (0), thus creating a binary image that highlights regions of the original image that exceed the intensity threshold (Figure 3.3).



**Figure 3.3** Original and Threshold images

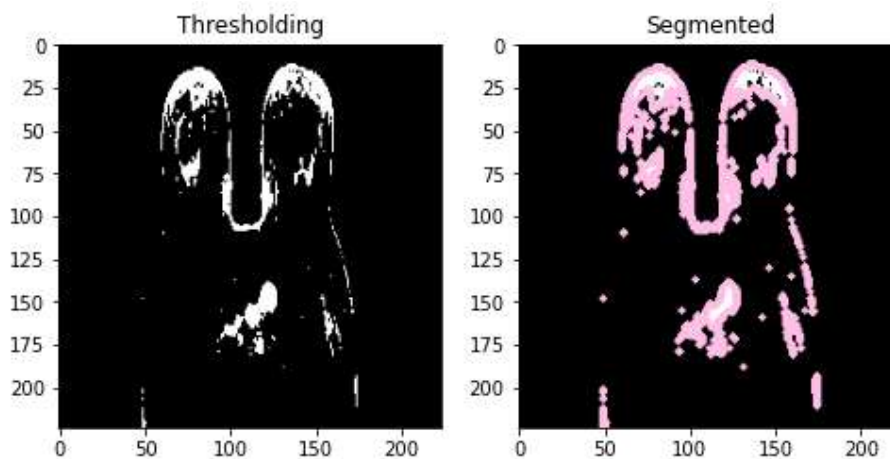
Figure 3.4 shows the algorithm process for executing thresholding starting from the original images until the threshold images are obtained (Figure 3.4)



**Figure 3.4** Block diagram of the thresholding process.

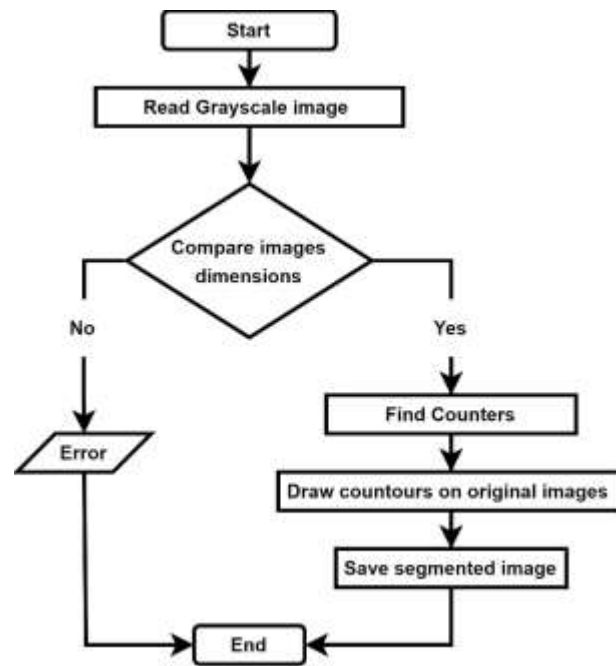
### 3.2.2 Segmentation

Image segmentation is defined as the semantic extraction or division of images, that is, into shapes or areas that have a direct relationship with a real object or shape, in this case with an organ or tissue. Segmentation algorithms try to look for relationships of homogeneity (regions) or heterogeneity (contours) within the images to classify and determine the parts that compose them (Chen et al., 2010). In this segmentation process with the function *cv2.findContours* from threshold images, the detected contours are drawn on a copy of the original image, thus creating a visual representation of the identified areas of interest. This contour-based segmentation approach is commonly used to extract features and delineate regions of interest in this area peripheral to the tumor (Figure 3.5)



**Figure 3.5** Threshold and Segmented images

Figure 3.6 shows the process for executing segmentation starting from the thresholding images until the segmented images are obtained.



**Figure 3.6** Segmentation process

### 3.3 Neural Network

The models were built in Spyder in the Python language. GPU and High RAM functions were used because of the large amount of data to train. The first model is based on ResNet 50, and the second model is on U-Net. Both are deep neural network models, in the first case, this is a network that allows us to create 50 layers of depth in addition to helping us with characteristic extraction, on the other hand, the U-Net allows us to identify structures through semantic segmentation.

In general, to develop the process of these models, some types of libraries were imported, such as:

- *TensorFlow* for training and inference with the deep neural network.
- *Matplotlib* generates the graphics of loss and training and allows visualization of breast images.
- *Os* for reading the files and path directions.
- *OpenCv* allows the manipulation of python images.
- *Panda* provides data structure.
- *Numpy* provides support to multidimensional arrays.

### 3.3.1 Construction of CNN based on ResNet 50

Based on a previously created model from ResNet50, certain parameters are modified that are required to extract features from breast cancer images. As was mentioned in section 3.1 there are 700 images (560 are for training and 140 for validation). Then these images are loaded from the directory where each folder is located. The input layer of the ResNet50 model is arranged to receive data from the data set as 224,224,1, this means that the dimensions of the input image are 224x224 pixels and a channel size of 1 corresponding to the grayscale (A. K. Sharma et al., 2022).

Then through '*cv2.imread* function' images are read from a specific path. A pre-trained neural network architecture (ResNet50) is used, and custom layers are added to fit the categorical classification problem. The model is compiled with the '*categorical\_crossentropy*' loss function and the '*adam*' optimizer (Figure 3.7)

The neural network is made up of an initial layer, max pooling, and four main blocks. Each of these blocks contains residual layers, followed by custom layers continuing with a flattening layer that converts the base neural network's three-dimensional output into a one-dimensional vector. Then, there is a dense layer with a ReLU activation function, a dropout (0.5) layer that randomly turns off 50% of neurons to prevent overfitting during training. Finally, there is a connected dense layer with as many units as there are classes in the problem, and an activation softmax function for categorical classification (Choi et al., 2020; Islam et al., 2019; Yamashita et al., 2018).

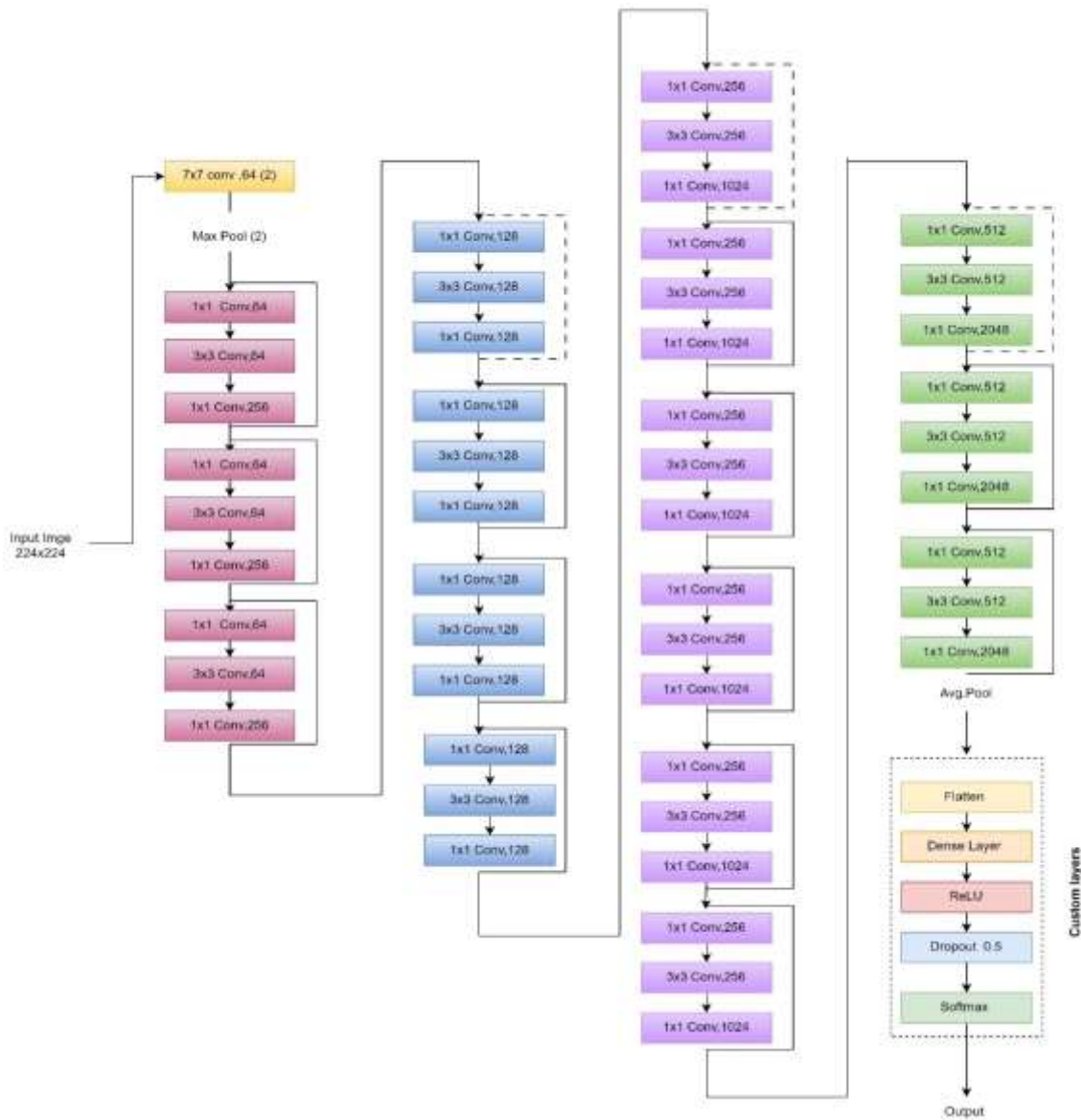


**Figure 3.7** Network architecture and parameters at each layer based on ResNet50.

### 3.3.2 Construction of CNN based on U-Net

Taking as input the global average pooling layer of ResNet 50 and the dose information that was specified in section 3.1. This layer takes the higher-level features extracted by ResNet-50 and uses them as input for the next part of the network images here have 224x224 pixels and a channel size of 3 corresponding to RGB (red, green, blue). As mentioned in section 2.4.4, the u-net network works with an encoder-decoder system where the image is reduced through convolutional filters, then this feature vector follows the opposite path, increasing

its dimensions up to the size of the original image, where at the same time output a mask is created. As in the previous section, a U-net network previously trained with Application Programming Interface (API) 'Keras' is used as a base, since the problem, in this case, is related to the value of the volume extracted by the network and the prediction, the following modifications are made:

- Modify the Output Layer by placing an additional layer for dosage prediction. Using an appropriate activation function such as '*linear*' to generate a regression.
- Adjust the Loss Function, using the '*mean\_squared\_error*' to avoid dosage regression problems.
- Modify the Data Generator so that it generates batches of images and their respective associated dosages. The following image represents the architecture of this section of NN .

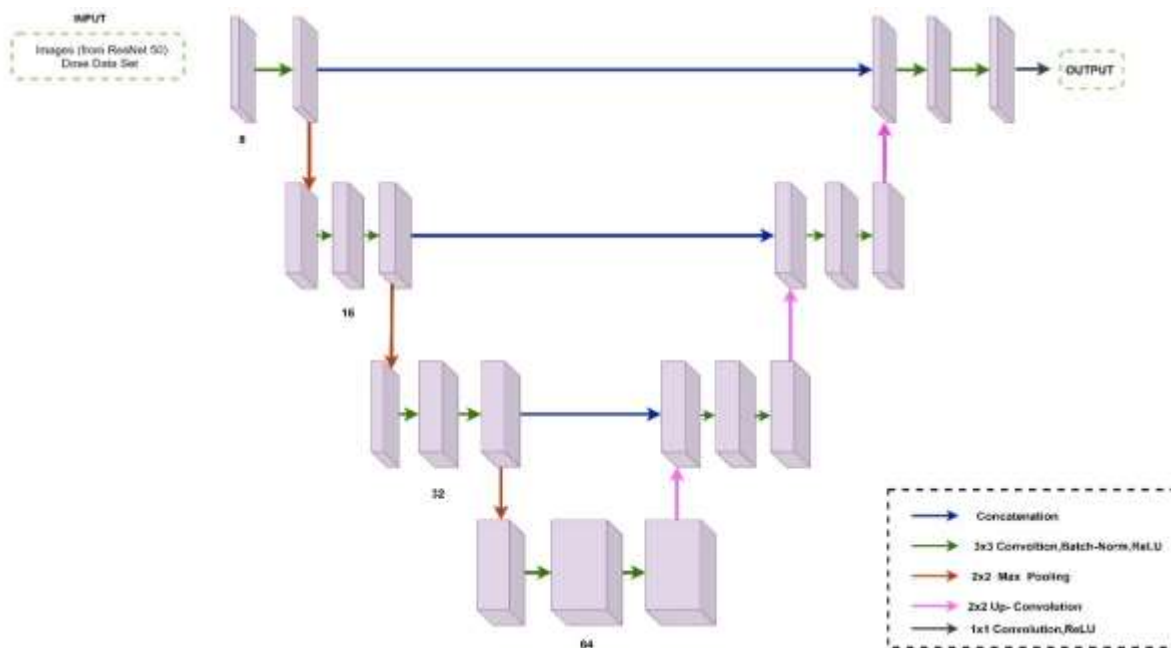


**Figure 3.8** Network architecture and parameters at each layer based on U-Net

The global architecture (Figure 3.9) operates by applying convolutions and pooling operations to extract features, followed by the integration of the U-Net layer that performs the tumor segmentation task. Regarding dose, the architecture is extended to address the differentiation between two groups of images based on the treatment dose. The total tumor volume in each group is calculated using segmented images and the difference in volume is compared between the groups. This is achieved through functions that calculate the area and volume of the tumor in segmented images, considering the thickness of the slices to obtain

the volume in units of cubic millimeters ( $mm^3$ ). It is necessary to emphasize that during training, the model adjusts its parameters based on the established images and doses to make accurate predictions about the dose and tumor volume in new medical images in the validation section.

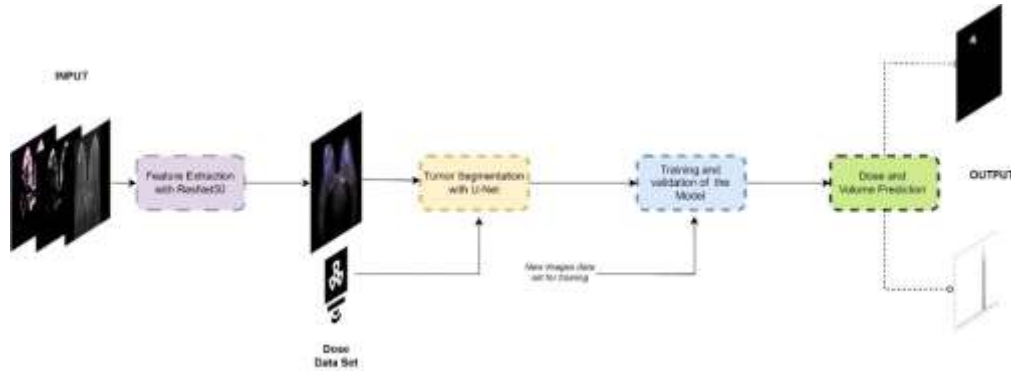


**Figure 3.9** CNN Final Model

### 3.3.3 Strategies of Training and Validation

In this section, the strategy for the training and validation process is based on Pareto’s principle, where a division of training data and evaluation of 80 and 20. According to this principle, a statistical phenomenon is described by which in any population that contributes to a common effect, a small proportion contributes most of the effect. The 80/20 rule suggests that, in any example, a few (20%) are vital, and many (80%) are trivial (Kheybari et al., 2019).

As explained in the previous paragraph and the reviewed state-of-the-art articles, it is considered a division of 80% of the total number of images, for the training process, leaving 20% of the total amount for the evaluation process of the trained modules classification (see Figure 3.10). Both partitions will be duly represented with the two classifications: MRI and CT.

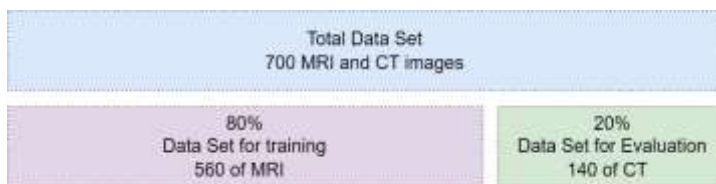


**Figure 3.10** Distribution of Data Set

## 3.4 Monte Carlo Simulation

### 3.4.1 MatRad

As it was mentioned before, the Monte Carlo Model is a stochastic technique in which multiple independent results are obtained from a modeled system by repeatedly solving the model for randomly sampled (input) values and events (Koch, 2018). To develop this simulation, MatRad was used, it comprises MATLAB functions to model the entire treatment planning workflow, physically and biologically based data for all required calculations.

MatRad is a cloud-based treatment planning software that enables conformal radiotherapy and radiosurgery treatment planning. It relies on advanced optimization algorithms to calculate the radiation doses needed to effectively treat tumors while minimizing adverse effects on surrounding tissues (H.-P. Wieser et al., 2018).

- **Graphical User Interface**

The GUI has some sections :

- **Workflow:** In the Workflow section, the patient data is initially loaded. Also here starts the dicom import data previously segmented . After the adjustment of all parameters, the dose calculation and the fluence optimization can be started from here.

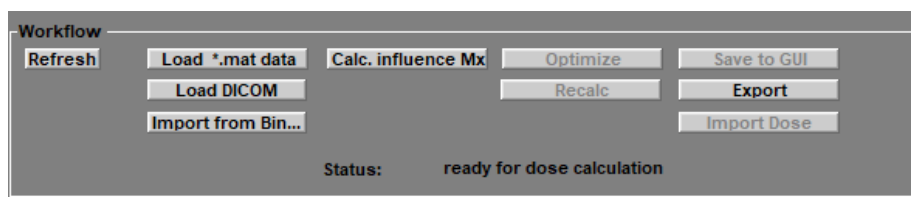


**Figure 3.11** GUI of Workflow

- **Adjustment of plan parameters**

The plan parameters are adjusted before to calculate the dose-influence-matrix

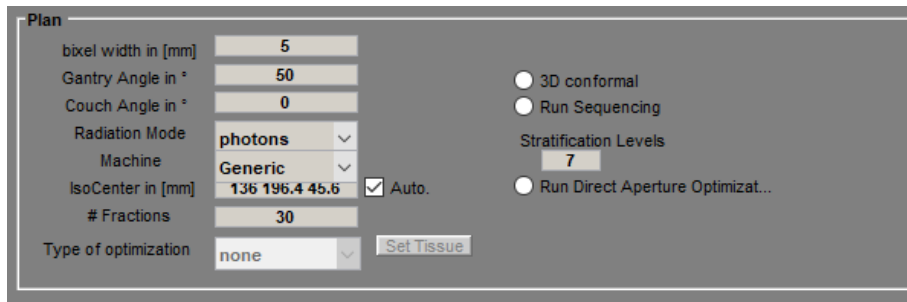


**Figure 3.12** GUI of Plan Parameters

○ **Adjustment of optimization parameters**

The optimization parameters regarding the volumes of interest (VOIs) are stored in the variable *cst* which is configurated from MATLAB-matrad code

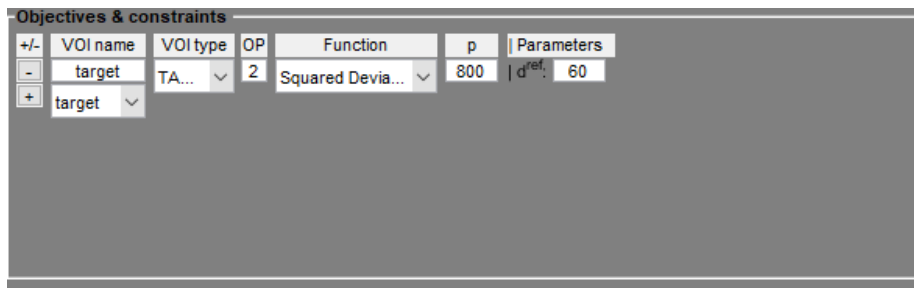


**Figure 3.13** GUI of Optimization parameters

○ **Visualization of plan treatment**

Using the visualization parameters, you can change the view. The radio buttons can be used to turn off/on, among others, the plotting of contours, dose (isolines) and isoline labels.



**Figure 3.14** GUI of Visualization

### 3.4.2 Development of MCM

For this part of the methodology, as mentioned in section 3.1, a CT DICOM database is used following the following steps.

- **Tumor delimitation**

The first step in radiotherapy treatment planning involves the precise delineation of the tumor on the patient's medical images, because is necessary to determinate the isocenter of tumor an surrounding area. This is achieved by using the Volume Segmenter tool in MATLAB, which provides an interactive interface for the segmentation of anatomical structures in three-dimensional images. Using this tool, the tumor is visually identified and accurately delineated by semi-automatic and manual methods. Subsequently, the contours of the segmentation are refined and verified to ensure accuracy. Finally, the resulting segmentation is exported for further processing and analysis in the context of radiotherapy treatment planning, while all steps and adjustments made during the process are documented and recorded. In the following images is shown the delimitation of tumor.

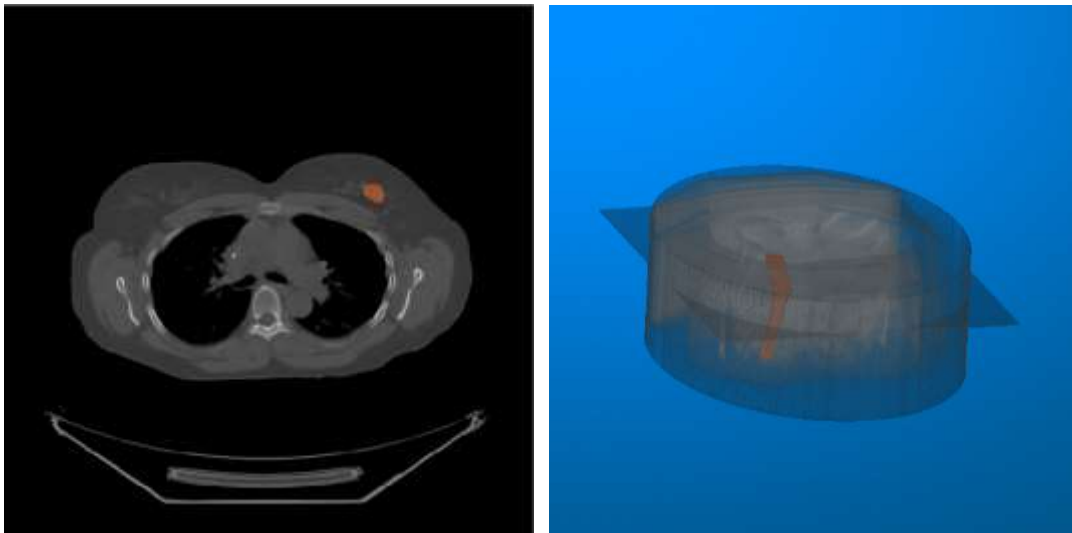


**Figure 3.15** Tumor segmentation

- **Set treatment plan parameters**

**Plan parameters:** First, the patient data is imported in the native matRad format, the desired configuration is specified in the structure plan where the maximum and minimum values of emitted doses are established, which were between 20 and 50 Gy according to the bibliography (H.-P. Wieser et al., 2018), the type of tissue, in this case, soft and photons as the radiation mode. The intensity-modulated radiation treatment plan comprised seven coplanar beams with angles of gantry:  $0^\circ$ ,  $50^\circ$ ,  $114^\circ$ ,  $206^\circ$ ,  $257^\circ$ , and  $309^\circ$ . The corresponding sofa angles were set to  $0^\circ$  (Cisternas, et al., 2015)

**Optimization parameters:** Parameter optimization in matRad is performed taking into account several factors and using specific tools within the software interface. First, patient data, including medical images and segmentation of relevant anatomical structures, such as tumor and organs at risk (OAR), are taken into consideration. This segmentation is performed beforehand using tools such as Volume Segmenter in MATLAB (Koch, 2018).

Once the patient geometry has been defined and the structures of interest have been specified, parameter optimization proceeds. This involves adjusting the optimization parameters to achieve an optimal radiation dose distribution that meets the established clinical objectives (Koch, 2018).

Within the matRad interface, users can modify the optimization parameters by editing the source code in MATLAB using specific fields, such as the objective function, penalty and parameters associated with each structure of interest. For example, they can select the desired objective function, which can include criteria such as average dose, maximum or minimum dose, and dose uniformity within the structure. In addition, they can adjust the penalty for each objective, allowing certain constraints to be prioritized over others (Koch, 2018).

For parameter optimization, an optimization approach is used based on algorithms that seek to minimize a global objective function that takes into account all specified constraints and objectives. This is done iteratively, adjusting the planning parameters until an optimal solution is reached that meets the established criteria (H.-P. Wieser et al., 2018).

- **Dose influence matrix calculation.**

The calculation of the dose influence matrix in matRad is divided into two parts: the irradiation geometry and the generation of dosimetric information through the pre-computation of dose influence matrices for inverse planning. In the irradiation geometry, a beam and bixel concept is used, where the beams cover the target volume, such as the tumor, with a series of discrete bixels forming a two-dimensional slice. These bixels, which represent rectangular fluence elements, cover the entire target volume (Figure 3.16) .

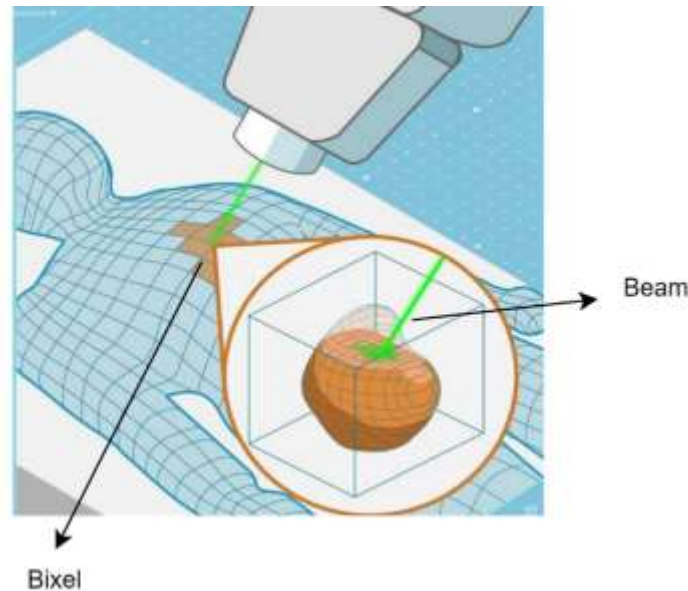


**Figure 3.16** Schematic visualization of the concept of beam and bixel.

For dose generation, Monte Carlo sampling is employed where a dose influence matrix is generated. The dose in a voxel is calculated as the weighted sum of the bixel contributions using a matrix-vector multiplication.

$$d_i = \sum_j D_{ij} w_j \quad \text{or} \quad \vec{d} = D \vec{w}$$

Here, the matrix  $D$  stores the dose contribution to a given voxel by each bixel-pencil beam in unit intensity, and  $w_j$  represents the weight of the corresponding bixel-pencil

beam. This dose influence matrix is stored in double precision sparse matrix format and is realized through the IPOPT tool.

- **Fluence optimization**

It focuses on projecting the patient geometry onto the beam view plane for each beam orientation. The patient geometry is transformed into beam view coordinates and the target volume is projected onto the isocenter plane perpendicular to the connection of the virtual radiation source and the isocenter. Since this isocenter was not reflected in the database, adjustments were made to the base code to adapt the measurements according to the depth of the tumor volume(H.-P. Wieser et al., 2018). During optimization, one seeks to find the optimal fluence distribution that maximizes the dose in the target volume while minimizing the dose in the surrounding tissues. This is achieved by adjusting the bixel weights iteratively to meet predefined dose targets. The mathematical formulation of fluence optimization involves solving a convex optimization problem that seeks to minimize an objective function subject to constraints, where the objective function can be either minimization of dose to healthy tissues or maximization of dose to the target volume. This process is repeated over multiple optimization cycles, the duration of which may vary according to the patient's evolution. Although the exact tumor-killing dose cannot be calculated, the average target dose is sought during these cycles to achieve the desired therapeutic effect.

- **Visualization**

Through the GUI the workspace is automatically verified, and the result data is shown according to the defined plan.

## Chapter 4

### Results

#### 4.1. Results of CNN

##### 4.1.1 Hyperparameters

To describe the model is essential to mention the hyperparameters used. This term refers to configuration variables external to the model itself and whose value. In general, the data cannot be estimated, and the programmer adjusts the learning algorithms. First, the hyperparameters of the two base models used are related to the algorithm learning level: ResNet was trained with 50 epochs in about 2.5 hours, using a batch size of 32 and a learning rate of 0.001. U-net was trained on 50 epochs in about 4 hours, using a batch size of 32 and a learning rate of 0.001. Secondly, the hyperparameters related to structure and topology were the layers. The ResNet50 model consists of fifty layers, and U-Net has 23 layers. Figures x and x show the architecture of the neural network networks. The Activation layer is the most critical because it determines the output of one or more nodes through a function. For the first model, was used an output layer activation that is *softmax*. The reason is that the NN fulfills the classification function, and at the same time, it is a multiclass classification; that is, each input can be a single output value. In other words, one node per class. The second model used a hidden layer activation function that was selected depending on the type of NN that is CNN therefore, a *ReLU* activation function was chosen. An Adam-type optimizer is then used in both models. Use the first and second-moment gradient estimates to dynamically adjust the learning rate of each parameter. In other words, after correcting the deviation, each iteration of the learning rate has a specific range, which makes the parameters stable. Furthermore, to select the loss function, both models are multiclass classification, and the cross-entropy function is selected. The two base models are considered to avoid overfitting in one of the architectures, however, the results of the metrics represent the values resulting from the model in general. Table 4.1 shows all parameters used on time.

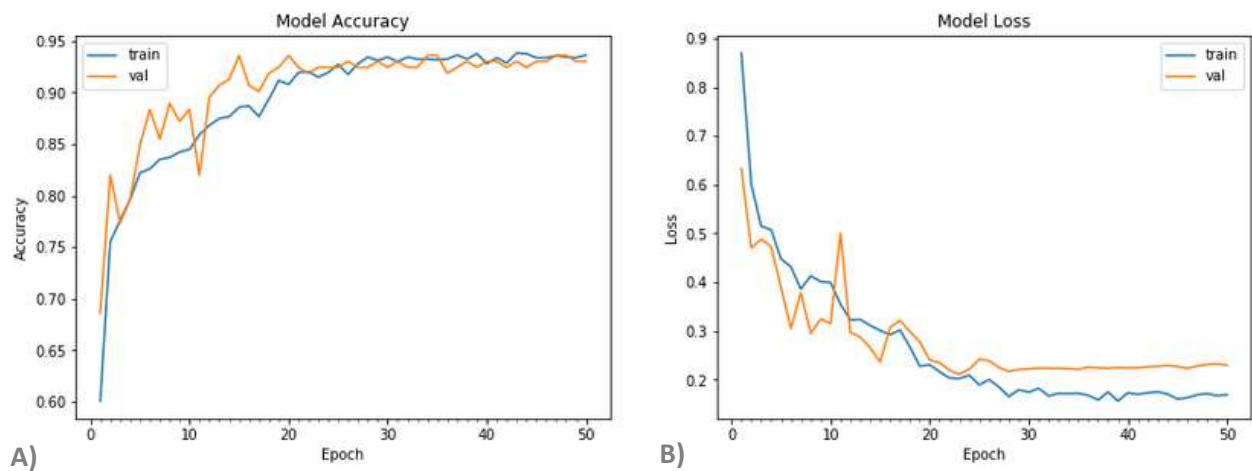
<i>Hyperparameters</i>	<b>ResNet50</b>	<b>U-Net</b>
<i>Epoch number</i>	50	50
<i>Time of training</i>	2.5 hours	4 hours
<i>Batch size</i>	32	32
<i>Learning rate</i>	0,001	0,001
<i>Number of layers</i>	50	23
<i>Activation function</i>	Soft Max ReLU	ReLU
<i>Optimizer</i>	Adam	Adam
<i>Loss function</i>	Categorical Cross-Entropy	Categorical Cross- Entropy

**Table 4.1** Hyperparameters used in the training of neural networks.

#### 4.1.2 Plots of Learning

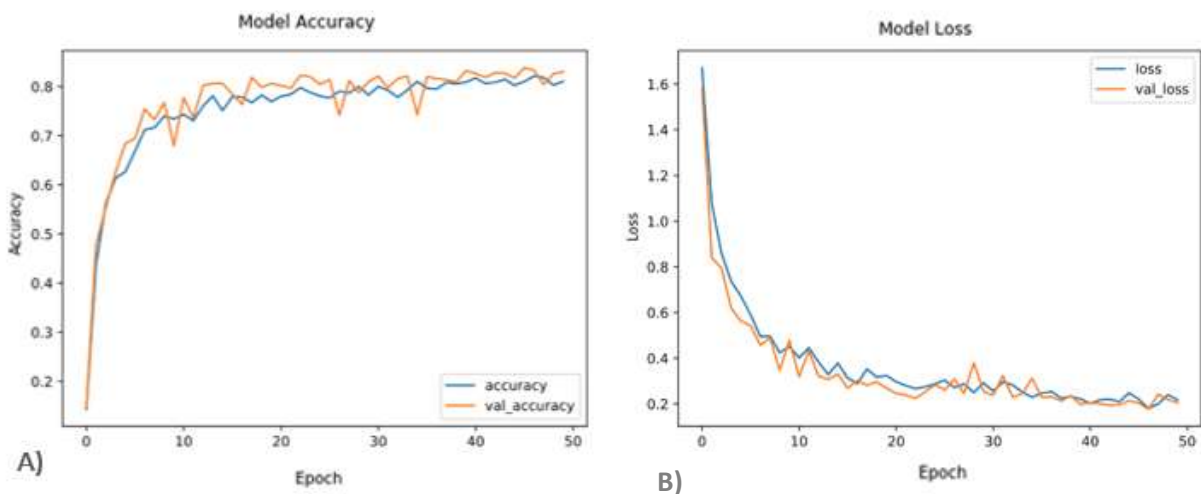
As mentioned in section x, for this model, two pre-trained neural networks were applied, and these were subsequently combined to generate a general convolutional network model. Thus, in Figure x we can see how ResNet 50 evolves in terms of precision and loss. A clear correlation is observed between the blue line that represents training and the orange line that represents validation. In the case of precision Figure 4.1a shows this tends to a percentage of 95%. On the other hand, in the case of loss, it is necessary to consider the use of a loss function: Categorical Cross-Entropy that is defined like Equation, the lower the value of the function, the more similar both distributions will be and the better the model. Taking this into account in Figure 4.1b, the training and validation loss tend to 0.

$$L(y, y') = \sum_{j=0}^M \sum_{i=0}^N (y_{ij} \times \log(y'_{ij}))$$



**Figure 4.1** Plots of training and validation accuracy and loss of ResNet50

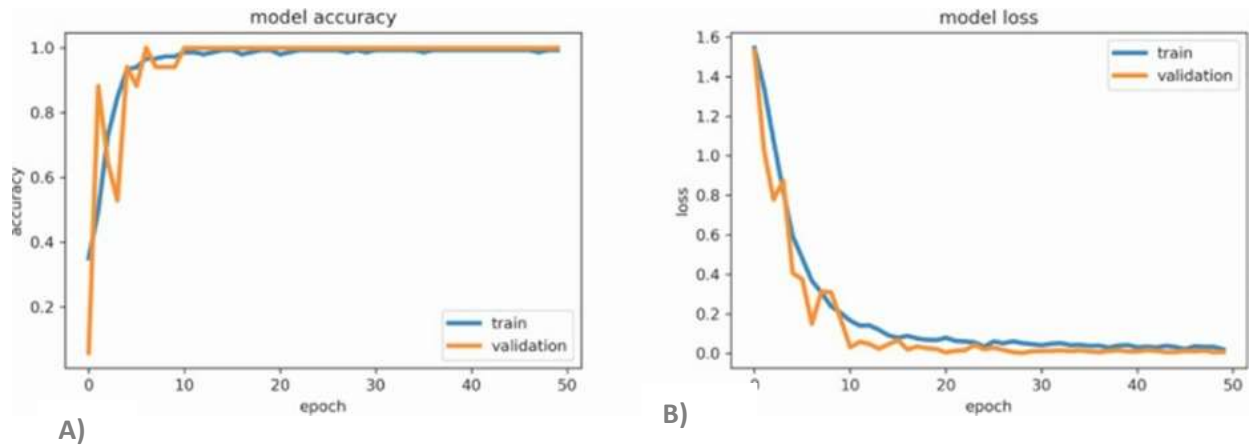
Now in Figure 4.2 shows how U-net evolves in terms of precision and loss. As in the previous network there is a clear correlation between the blue line and the orange line. In the case of precision, Figure 4.2a shows that it tends to a percentage of 86%. On the other hand, in the case of loss, it is necessary to consider that the Categorical cross entropy function is also used and has a low value, in Figure 4.2b, the training and validation loss tends to 0. This model shows excellent precision; however, it is not better than the previous network.



**Figure 4.2.** Plots of training and validation accuracy and loss of U-Net

This last Figure 4.3 represents the final development of the model in general, the accuracy percentage is greater than 97% (Figure 4.3a) and the loss function is low, tending to 0 (Figure 4.3b). In addition, there is a clear correlation between training and validation. Unlike the results provided by each network separately, we see that the general model is better, this

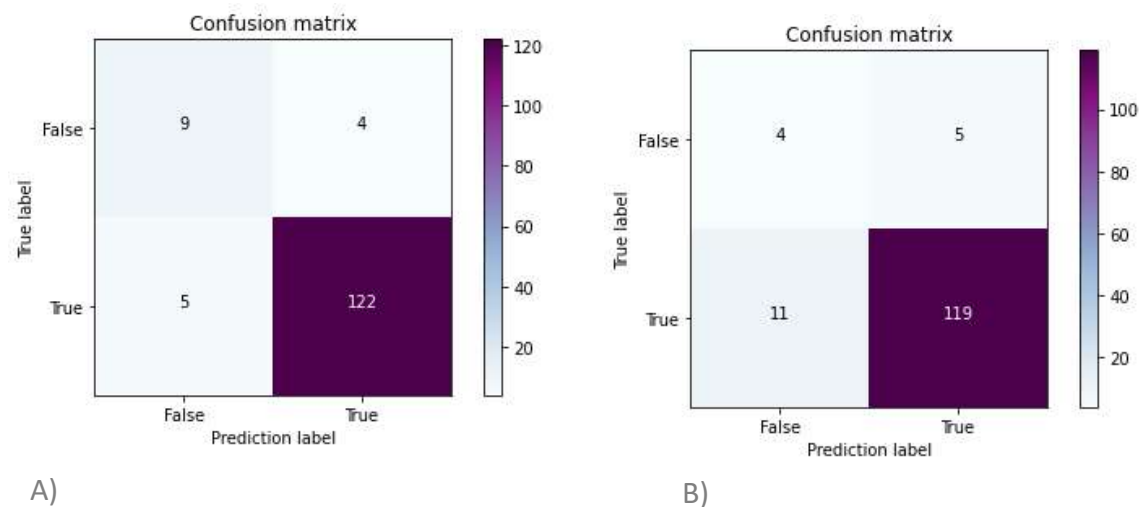
is because it combines the most important functions of each one to work around the problem that we want to solve in this case, the delimitation of the tumor volume and dose prediction.



**Figure 4.3** Plots of training and validation accuracy and loss of the General CNN Model

**Confusion Matrix**

The confusion matrix allows visualization of the performance of the algorithm. Each row of the matrix represents the real classes, while columns represent the predicted classes by the model. On the other hand, each cell of the matrix shows the count of instances classified correctly or incorrectly (Xu et al., 2020). In the following figures indicate the confusion matrices of the ResNet50 (Figure 4.4 a), U-net (Figure 4.4b) and the General Model (Figure 4.4c). The cell in the diagonal corresponds to true negatives (TN) and true positives (TP) (dark purple) and the two leftovers are false positives (FP) and false negatives (FN).



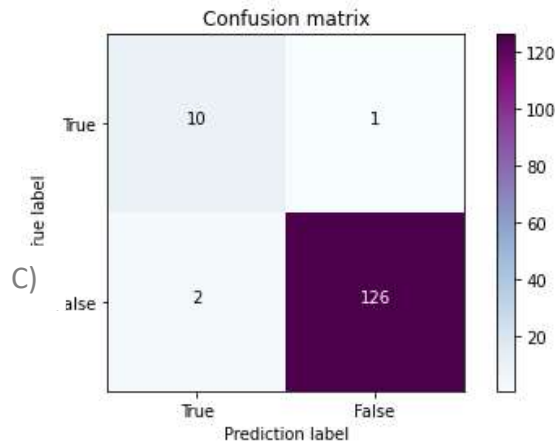


**Figure 4.4** Confusion Matrix A) ResNet50 B) U-net C) General CNN Model

Based on the information in the confusion matrix, the evaluation metrics can be calculated, given by the following formulas:

$$Eq\ 4.1) Acc = \frac{TP+TN}{TP+TN+FP+FN}$$

$$Eq\ 4.2) Precision = \frac{TP}{TP+FP}$$

$$Eq\ 4.2) Recall = \frac{TP}{TP+FN}$$

$$Eq\ 4.4) F1\ Score = 2 \frac{Precision \times Recall}{Precision + Recall}$$

Below are the values obtained for each metric as a result calculated with the values of each confusion matrix related to each type of neural network in this study.

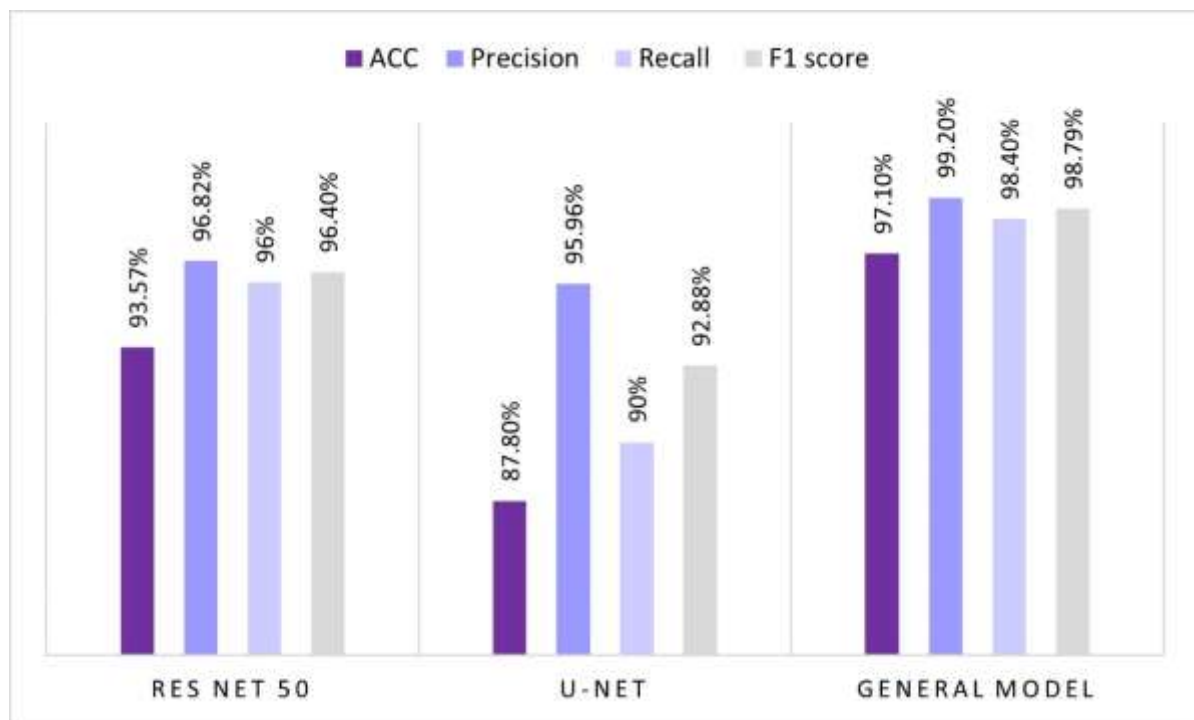


**Figure 4.5** Accuracy, Precision, Recall, and F1 score of different models.

Recovery or sensitivity values focus on type II errors (FN). A type II error occurs when a false null hypothesis is accepted. This is when the model states that the dose has not been correctly predicted when it has. For all models, the recovery is greater than 90% but we focus especially on the general model in which this value was greater than 98%. Specificity values focus on type I errors (TF). A type I error occurs when a false null hypothesis is accepted. This is when the prediction says that a disease has been detected but is not present. For the U-net model, we see that the accuracy value is the lowest of all, reaching 87%, however, we see that this generally has no impact on the general model where it reaches an excellent value greater than 97%. Finally, precision indicates how close the result of a measurement is to the real value, this being greater than 95%. The last thing to evaluate is the F1 score, it is an estimator of the classification capacity of a diagnostic test, in this case, the dosage where, as in other metrics, the general model exceeds 98%.

## 4.2 Volume Analysis

The model of NN also calculates the volume of the tumor, starting from the results of the delimitation area obtained from the modified ResNet50, while the definition of the entire volume of the tumor was done by modified U-Net. The resulting images are shown below.

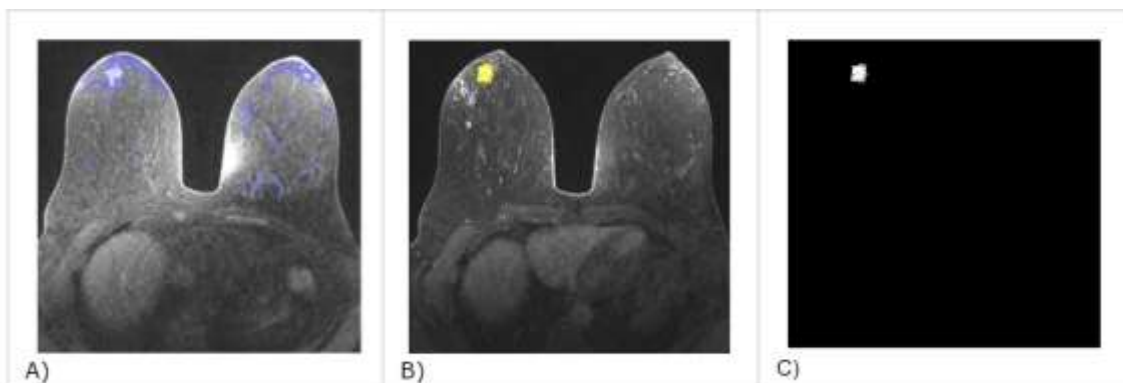


**Figure 4.6** Segmentation of Volume a) Surrounding area b) y c) Tumor.

### 4.2.1 Difference between Chemotherapy and Radiotherapy

One of the objectives of this research was to demonstrate the effectiveness of Radiotherapy compared with other techniques. This section shows the difference in tumor volume before (purple) and after (blue) each therapy.

Figures 4.7 and 4.8 show the graph of early state 1 of chemotherapy and radiotherapy correspondingly.

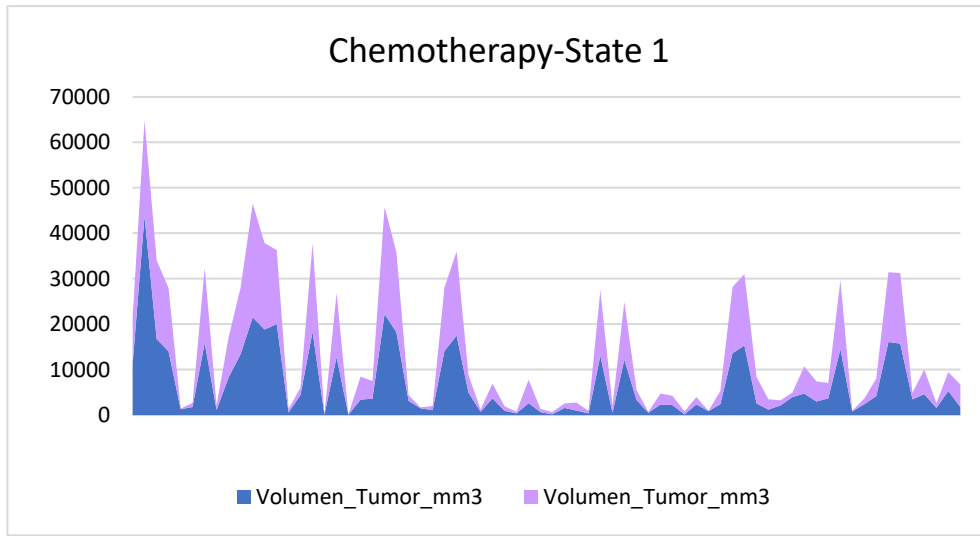


**Figure 4.7** Difference in tumor size before and after Chemotherapy state 1

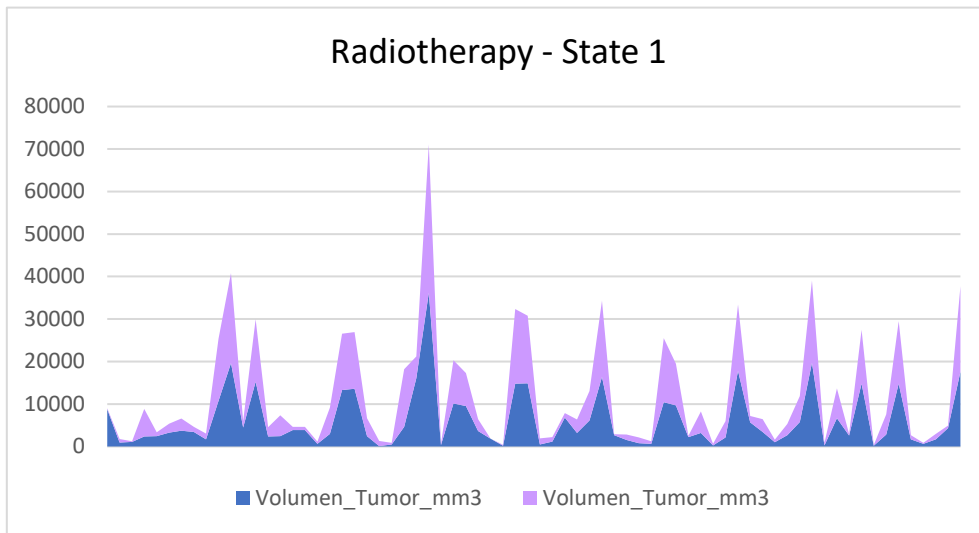


**Figure 4.8** Difference in tumor size before and after Radiotherapy state 1

The results obtained from the comparison of tumor volumes in patients undergoing chemotherapy and radiotherapy in medium early stage 2 are presented below.

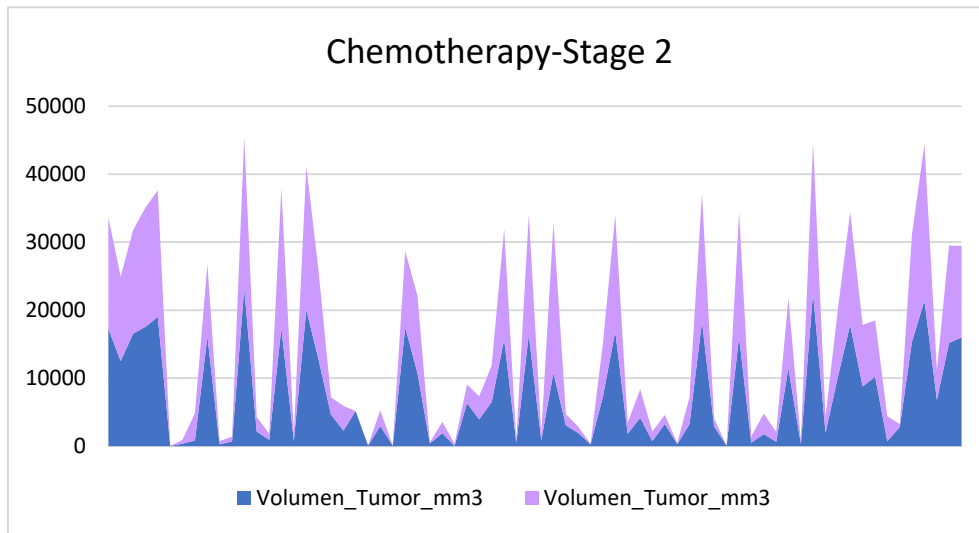


**Figure 4.9** Difference in tumor size before and after Chemotherapy stage 2

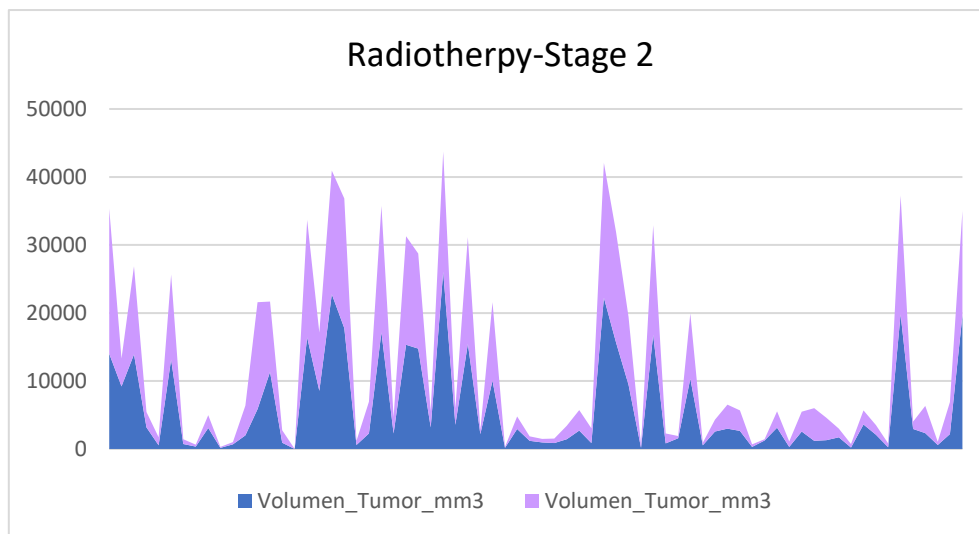


**Figure 4.10** Difference in tumor size before and after Radiotherapy stage 2

During the analysis of the results, a significant finding related to the effectiveness of radiotherapy in reducing tumor size was observed. It was found that radiotherapy demonstrated a 20% greater reduction in tumor size than chemotherapy at the same time. This finding suggests that radiotherapy may be a more effective therapeutic option in terms of tumor size reduction compared to chemotherapy.

## 4.3 Radiation Dose

### 4.3.1 Results of CNN on dosage prediction

The CNN-based dose calculation model provided detailed results. It should be noted that in the network results, the calculated dose was the emitted dose. Therefore, using the information on the volume calculated in the previous section, the next equation (Antolak, 2015) was used:

$$\text{Absorbed dose} = \text{Emitted dose} \times \text{Attenuation Factor}$$

The attenuation factor was provided on dataset clinical information, Figure 4.11 depicts radiation dose distributions across axial, coronal, and sagittal planes. Each color gradient represents absorbed doses ranging from 1.5 to 2.5 Gy.

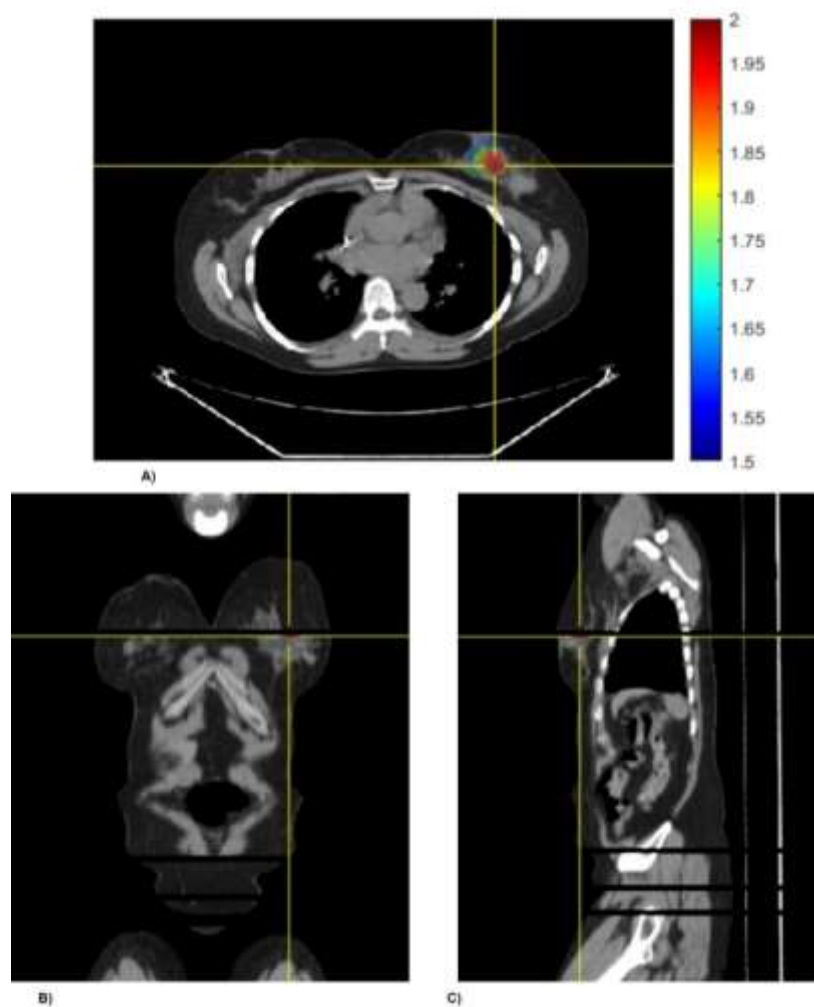


**Figure 4.11** Patient ACRIN-FLT-005 CNN-Dose distribution a) Axial Cort b) Coronal Cort c) Sagittal Cort

The neural network model generates an output that indicates the maximum absorbed dose in a specific treatment point based on the breast volume of each patient. This result is obtained by adjusting the weights and parameters during the model training process to minimize the error between the actual and predicted absorbed doses. Since the model was trained with maximum emitted dose data, the predicted absorbed dose matches this maximum dose at the treatment point, and its value is multiplied by the attenuation factor.

Overall, the output of the neural network model provides an accurate prediction of the maximum absorbed dose at a treatment point, using breast volume as input. This prediction is based on the model's learning during training and is consistent with the maximum emitted dose used for its training. Table 4.2 illustrates the result of the dose of a sample of 25 patients out of the total, which was 90.

<b><i>ID PATIENT</i></b>	<b>Emitted Dose</b>	<b>Absorbed dose</b>
<i>ACRIN-FLRT-Breast_001</i>	23.813	2.286048
<i>ACRIN-FLRT-Breast_002</i>	23.238	2.230848
<i>ACRIN-FLRT-Breast_003</i>	24.766	2.377536
<i>ACRIN-FLRT-Breast_004</i>	22.295	2.14032
<i>ACRIN-FLRT-Breast_005</i>	22.759	2.184864
<i>ACRIN-FLRT-Breast_006</i>	20.577	1.975392
<i>ACRIN-FLRT-Breast_007</i>	22.996	2.207616
<i>ACRIN-FLRT-Breast_008</i>	24.447	2.346912
<i>ACRIN-FLRT-Breast_009</i>	20.43	1.96128
<i>ACRIN-FLRT-Breast_010</i>	20.747	1.991712
<i>ACRIN-FLRT-Breast_011</i>	20.686	1.985856
<i>ACRIN-FLRT-Breast_012</i>	23.786	2.283456
<i>ACRIN-FLRT-Breast_013</i>	22.743	2.183328
<i>ACRIN-FLRT-Breast_014</i>	22.075	2.1192
<i>ACRIN-FLRT-Breast_015</i>	23.28	2.23488
<i>ACRIN-FLRT-Breast_016</i>	24.463	2.348448
<i>ACRIN-FLRT-Breast_017</i>	24.001	2.304096
<i>ACRIN-FLRT-Breast_018</i>	23.067	2.214432
<i>ACRIN-FLRT-Breast_019</i>	23.115	2.21904
<i>ACRIN-FLRT-Breast_020</i>	20.345	1.95312
<i>ACRIN-FLRT-Breast_021</i>	20.129	1.932384
<i>ACRIN-FLRT-Breast_022</i>	22.725	2.1816
<i>ACRIN-FLRT-Breast_023</i>	24.974	2.397504
<i>ACRIN-FLRT-Breast_024</i>	23.619	2.267424
<i>ACRIN-FLRT-Breast_025</i>	23.053	2.213088

**Table 4.2** Dose Prediction Results of CNN

### 4.3.2 Results of MC on dosage prediction

In this section, the radiation dose distribution in the axial, sagittal, and coronal planes is shown with values ranging from 0 to 2.5 Gy. It is important to note that, unlike the neural network, here the isocenter is set to the LPS (Left, Posterior, Superior) coordinates of the area to be treated. In this case, this is called "target."

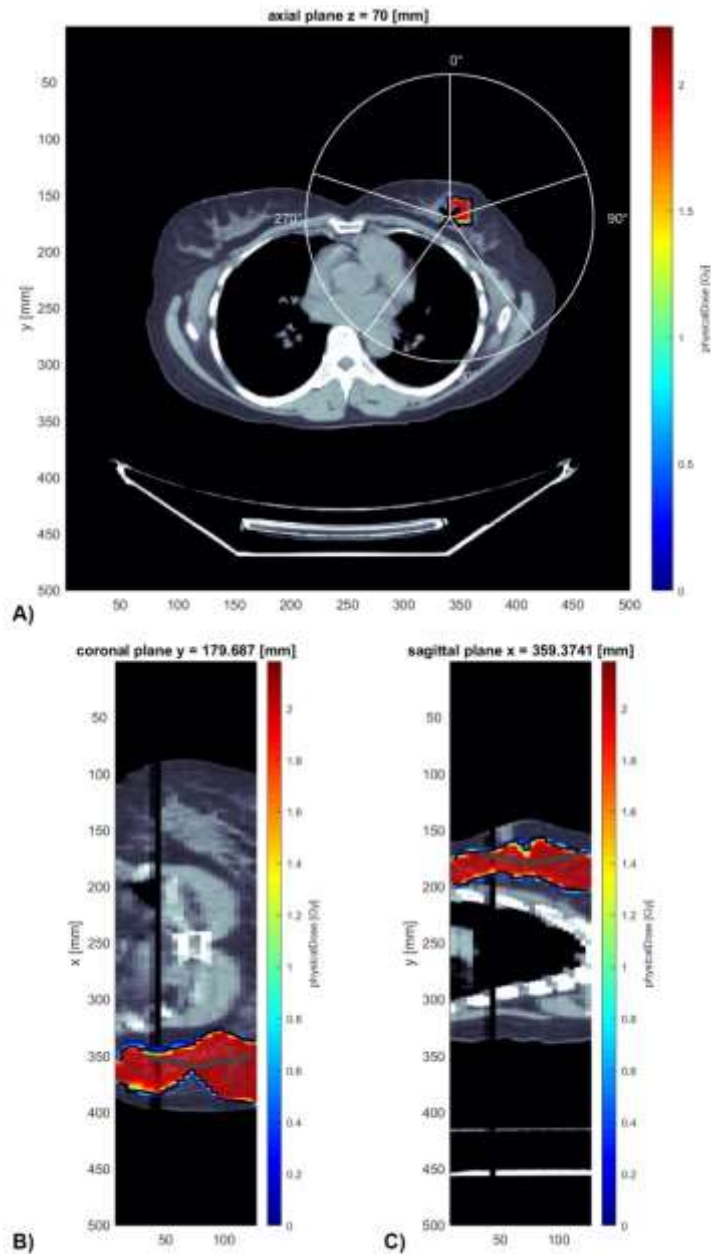


**Figure 4.12** Patient ACRIN-FLT-005 MC-Dose distribution a) Axial Cort b) Coronal Cort c) Sagittal Cort

Taking into consideration that the area of interest is the 'target', the model enables us to extract dosage information solely for the segmented tumor (Figure 4.13). Consequently, it's observed that within this region, the dosage values range from 1.8Gy and upwards. This precision in dosage within the tumor area is crucial for ensuring effective treatment and minimizing side effects on surrounding tissues.

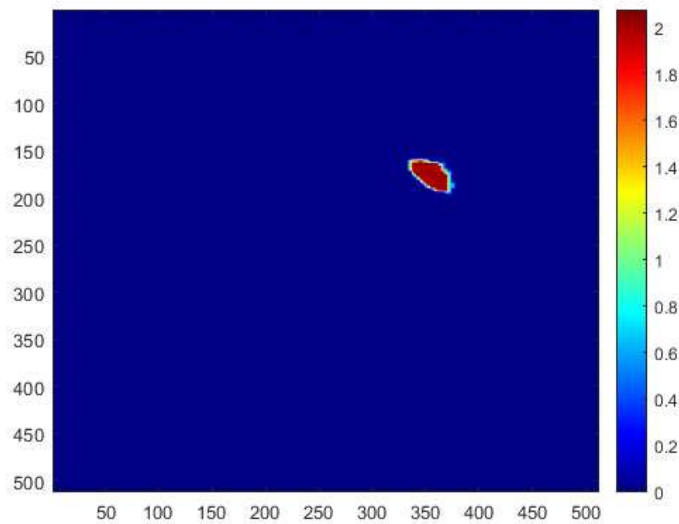


**Figure 4.13** Tumor dose distribution.

### **Dose Optimization**

Next, figure 4.14 shows the dose optimization of one of the 50 patients (ACRIN-FLT-005), where it is seen that as the iterations increase, the value of the objective function tends to zero. Fluence optimization aims to determine the best set of bixel or spot weights that can produce an optimal dose distribution based on the clinical goals and limitations of radiation treatment (H. P. Wieser et al., 2017). To achieve mathematical optimization, the clinical objectives and restrictions should be converted into mathematical objectives and constraints (Yoon et al., 2023). matRad provides support for the mathematical optimization of a weighted sum of targets. This helps in finding an optimal balance between adequate target coverage and preservation of normal tissue for each patient. Additionally, matRad also facilitates the formulation of constraints.

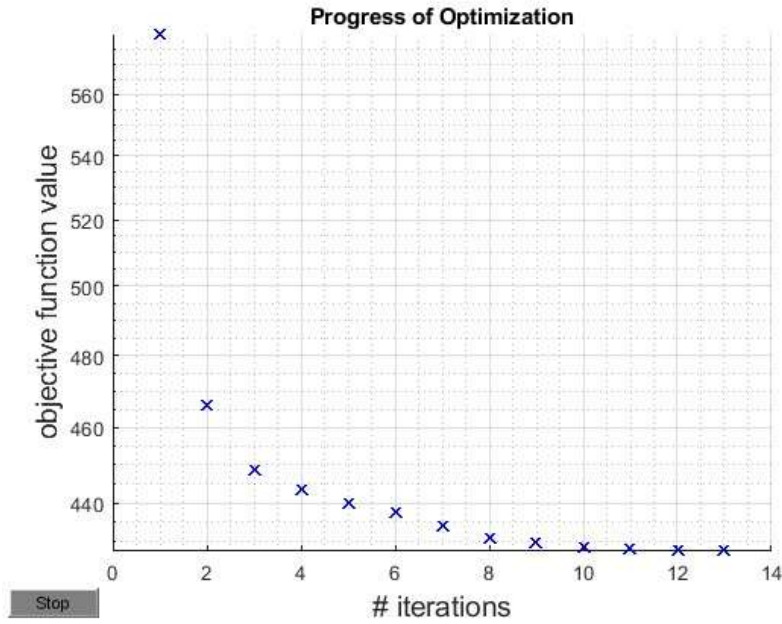


**Figure 4.14** Progress of Fluence Optimization (ACRIN-FLT-005)

**Dose-Volume Histogram**

The dose-volume histogram (DVH) shows the distribution of radiation dose concerning the volume of the breast tissue being targeted. The horizontal axis of the histogram represents the different radiation dose levels, while the vertical axis shows the percentage of the tissue volume that receives that dose or less. Each point on the DVH indicates what percentage of the total tissue volume receives a specific dose or less.

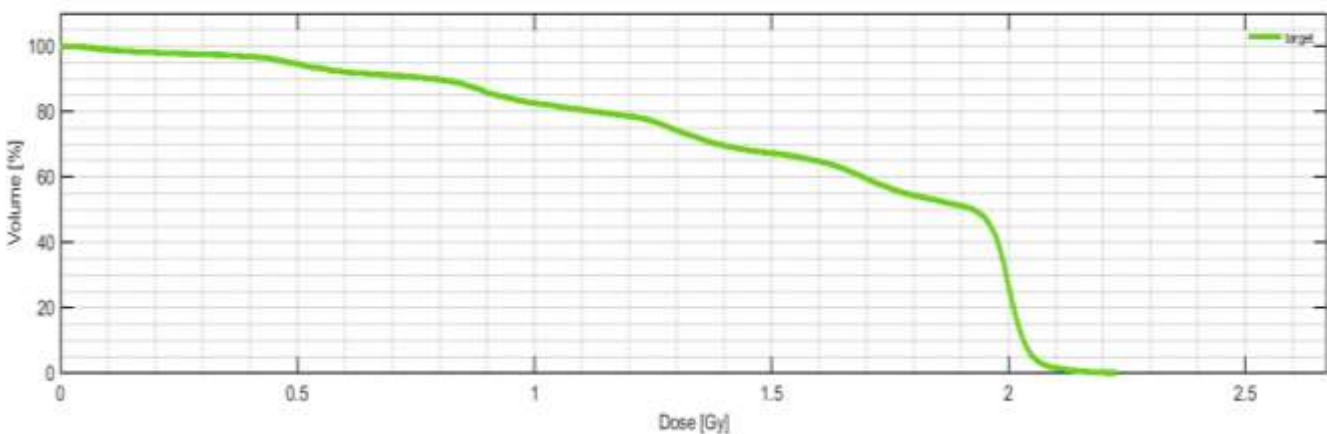


**Figure 4.15** DVH of ACRIN-FLT-005 patient.

From this graphic, some metrics were calculated:

- **Mean (Mean dose):** It is the average radiation dose received by the tissue or anatomical structure of interest.
- **Std (Standard Deviation):** It is the standard deviation of the radiation dose, which indicates the dispersion of the dose values around the mean.
- **Max (Maximum dose):** It is the highest radiation dose received by the tissue.
- **Min (Minimum dose):** It is the lowest radiation dose received by the tissue.
- **D2, D5, D50, D95, D98:** Represent the dose percentiles, that is, the doses corresponding to 2%, 5%, 50% (median), 95%, and 98% of the tissue volume.
- **V<sub>0Gy</sub>, V<sub>0.4Gy</sub>, V<sub>0.8Gy</sub>, V<sub>1.3Gy</sub>, V<sub>1.7Gy</sub>, V<sub>2.2 Gy</sub>:** These metrics represent the volume of tissue that receives at least a specific dose of radiation. For example, V<sub>0Gy</sub> indicates the volume of tissue that receives no dose (0 Gy), V<sub>2.2 Gy</sub> while indicates the volume of tissue that receives at least 2.2 Gy.
- **Cl<sub>2Gy</sub>:** This is the Coverage Index for a 2 Gy dose, indicating the proportion of the target volume that receives at least 2 Gy (Cisternas et al., 2015).
- **HI<sub>2Gy</sub>:** It is the homogeneity index (Homogeneity Index) for a dose of 2 Gy, which evaluates the uniformity of the dose within the target (Cisternas et al., 2015).

<i>Metric</i>	<b>ID-Patient</b>					
	Patient 003	Patient 004	Patient 005	Patient 006	Patient 007	Patient 008
<i>mean</i>	1.4585	1.6912	1.6027	1.6646	1.5802	1.7476
<i>std</i>	0.5636	0.4746	0.5363	0.4943	0.5568	0.5235
<i>max</i>	2.1075	2.1598	2.229	2.2599	2.3777	2.2407
<i>min</i>	0	0	0	0	0	0
<i>D2</i>	2.0291	2.0426	2.0852	2.107	2.0674	2.0735
<i>D5</i>	2.0159	2.0285	2.0515	2.0806	2.0464	2.0536
<i>D50</i>	1.6113	1.9662	1.9235	1.9466	1.9018	1.9939
<i>D95</i>	0.362	0.6463	0.4769	0.5926	0.3982	0.3402
<i>D98</i>	0.1582	0.3178	0.1717	0.3549	0.2055	0.2722
<i>V<sub>0Gy</sub></i>	1	1	1	1	1	1
<i>V<sub>0.4Gy</sub></i>	0.9436	0.9727	0.9661	0.9755	0.9484	0.9386
<i>V<sub>0.8Gy</sub></i>	0.8375	0.9166	0.8961	0.8917	0.8409	0.8962
<i>V<sub>1.3Gy</sub></i>	0.6881	0.8229	0.7407	0.7791	0.6975	0.8371
<i>V<sub>1.7Gy</sub></i>	0.5055	0.6797	0.5943	0.5886	0.5013	0.7793
<i>V<sub>2.2 Gy</sub></i>	1.21E-04	5.67E-04	6.73E-04	3.72E-04	1.71E-04	9.91E-05
<i>Cl<sub>2Gy</sub></i>	0.3594	0.5953	0.5105	0.5399	0.5013	0.7418
<i>HI<sub>2Gy</sub></i>	82.6958	69.1075	78.7288	74.4019	82.4072	85.6733

**Table 4.3** Results of metrics of MCM simulation for dose Calculation

## Beams Geometry

In radiotherapy, a "beam" refers to a flow of charged particles (such as electrons or protons) or photons (x-rays or gamma rays), in this case, photons that are directed toward the target (Bedford, 2019). These beams are used to deliver focused, controlled doses of radiation to cancerous tissue (Njeh et al., 2012). These beams were generated theoretically using software that simulates particle accelerators.

In this part of the results, the interaction of the 5 radiation beams with the tissue anatomy is analyzed. Below is a three-dimensional (3D) image that represents the distribution of voxels of tissues and anatomical structures in the treatment area. These voxels are constructed through interpolation of a series of CT images and represent discrete volumetric elements within the patient's anatomy, offering a comprehensive depiction of tissue composition and density variations. This 3D image provides a detailed representation of the anatomical environment in which the radiotherapy treatment is administered, allowing to study how the radiation beams affect the tissues and structures in this area.

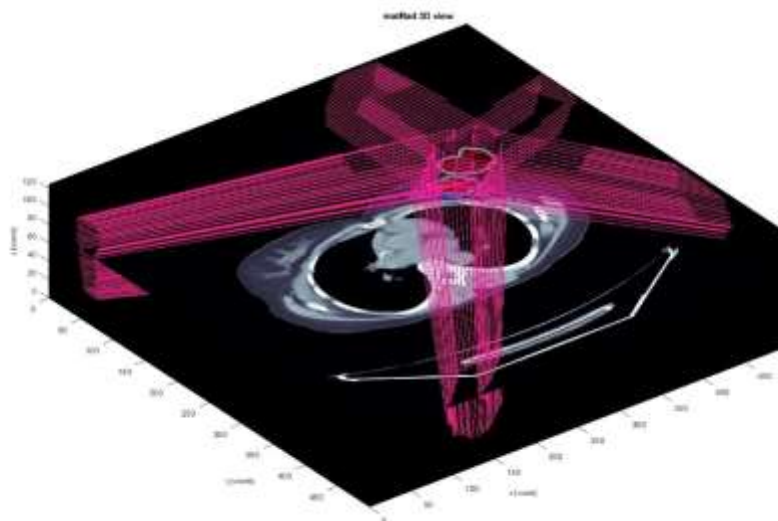


**Figure 4.16** 3D representation of dose and beam distribution

Another way to analyze the behavior of the particles is to examine their interaction with the tissue. The simulation was made on 5 to 10 cycles with the interaction of five X-ray beams in most cases, in each cycle the depth of beams change. Figure 4.17 shows the longitudinal and lateral profiles of five beams in the last cycle of the physical dose of the patient ACRIN-FLT-005.

For each beam, a specific angle was set, in the case of the gantry angle it's  $0^\circ, 72^\circ, 144^\circ, 216^\circ, 288^\circ$  (Figure 4.17) respectively, while the couch angle was  $0^\circ$  for all, as the couch in this case did not move and remained static while the beams radiated.

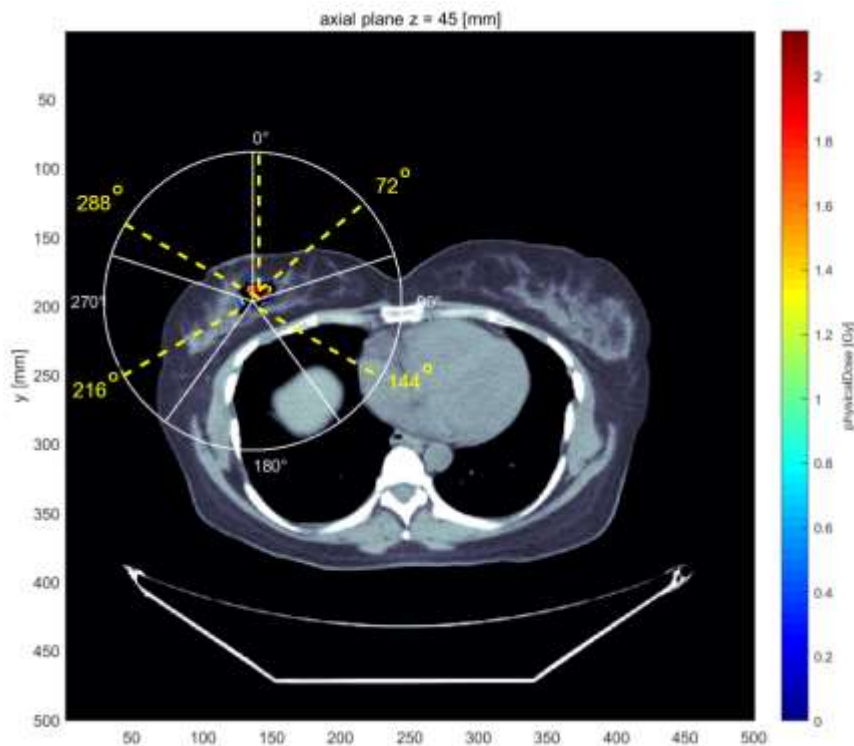


**Figure 4.17** Angles of beams

The next figures show the longitudinal and lateral profiles of each of the five beams in the last cycle. The y-axis shows the dose value, while the x-axis shows the radiological depth which is also known as the radiation length or radiation attenuation length, is a measure used in radiation physics to quantify the amount of material that a high-energy photon or electron traverses before its intensity is reduced (Hussain et al., 2012), red line represents the physical dose, the purple line is the target boundary, and the light blue line is the data.

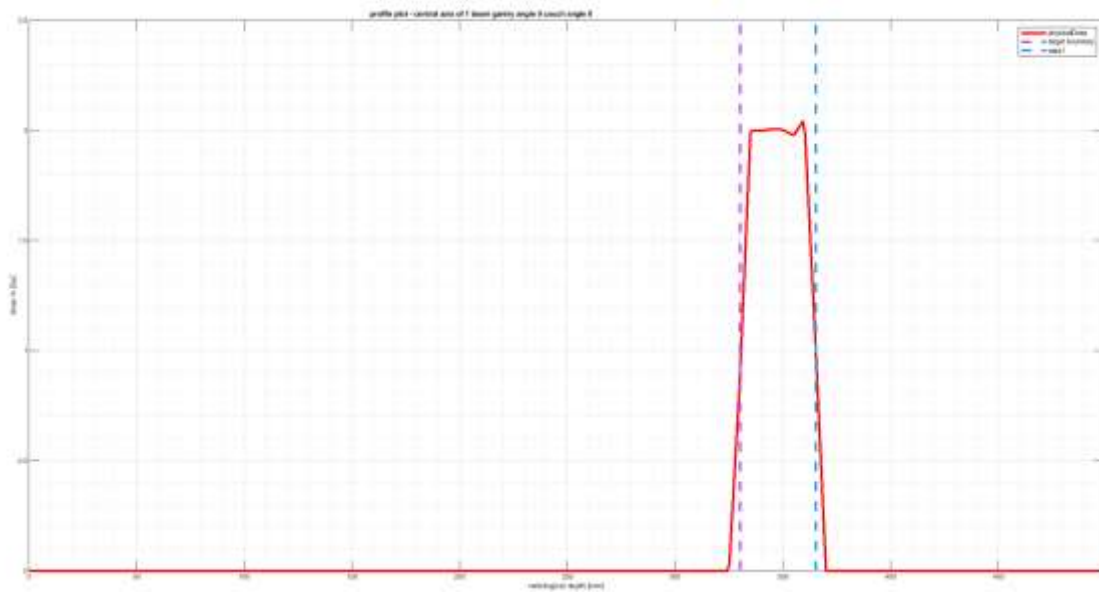


**Figure 4.18** Longitudinal profile beam 1

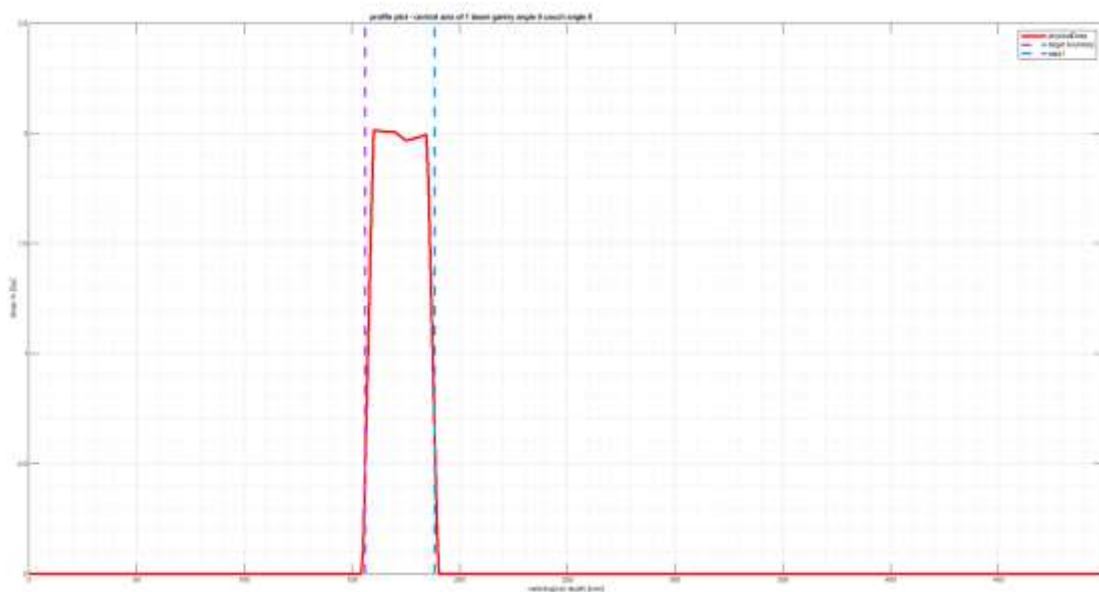


**Figure 4.19** Lateral profile beam 1

Now analyzing the graphs, the following was obtained.

The first beam at a radiological depth between 325mm and 370mm it reached a higher physical dose of 2Gy in the longitudinal plane (Figure 4.18), in the case of the lateral profile it reached a value a little less than 2Gy at a depth of 155mm and 190mm (Figure 4.19). For the case of beam 2,3 and 4 shows a similar behavior as this, just the last beam has differences.

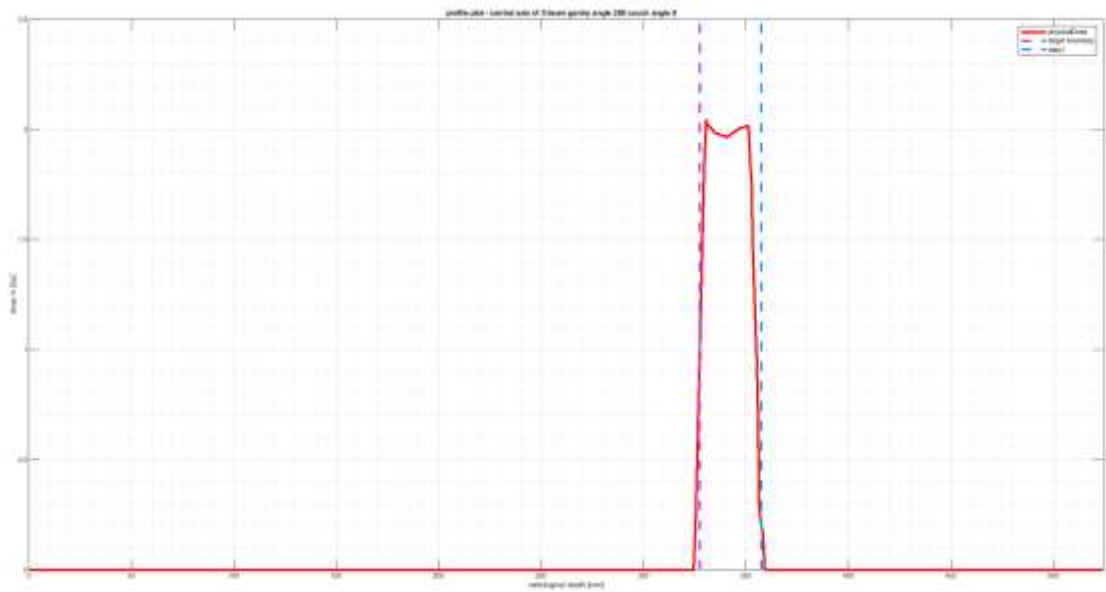


**Figure 4.20** Longitudinal profile beam 5

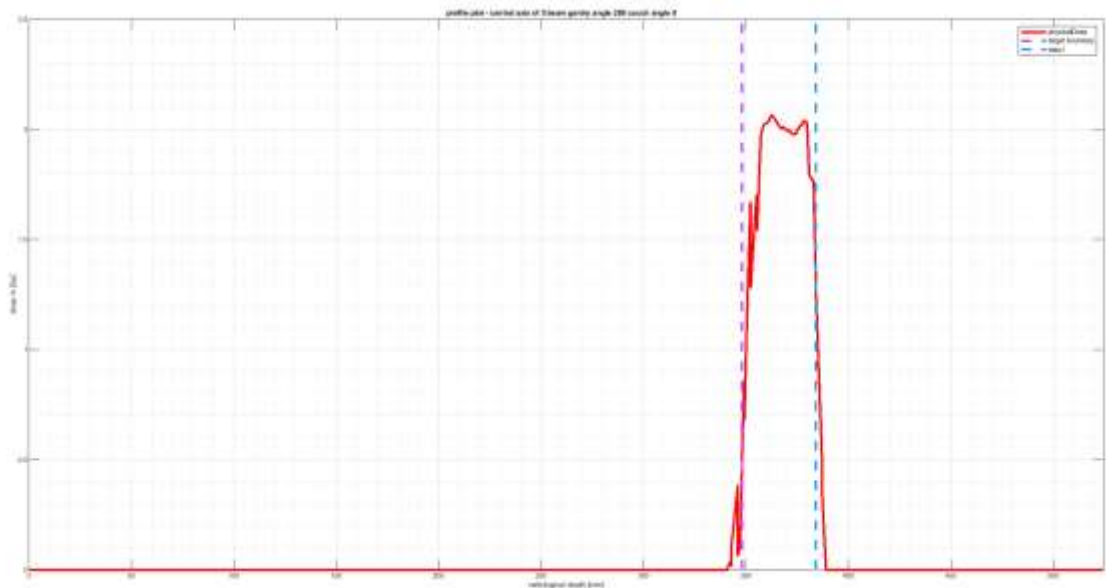


**Figure 4.21** Lateral profile beam 5

For the last beam the longitudinal profile, the physical dose range reaches 2Gy between 315mm and 360mm radiological depth values. In the case of the lateral profile, something different occurs with the rest of the beams since in this graph some peaks are observed, and the lowest reaches a value of 0.4 Gy and the highest 2.05 Gy, between 340mm and 380mm of radiological depth, however, it is important to point out that these

values are slightly outside the delimitation lines that marked by target boundary limit and the data provided.

In the context of radiotherapy, it is important to know the behavior of the particle. The following graphs provide information on the specific characteristics of the first radiation beam in the treatment plan, including its shape, width and the configuration of the collimator leaves used to form the beam.

- **Beam:** Indicates the beam in the treatment plan of Radiotherapy.
- **Shape:** refers to the type of beam shape or profile. Radiation beams may have different shapes or profiles depending on how the collimators or beam-shaping devices are configured.
- **W:** This value could represent the width of the beam in millimeters. Indicates the measurement of the beam in the horizontal direction.
- **Leaf Pair number:** Refers to the number of pairs of leaves of the multi-leaf collimator used to shape the beam. These leaves are moved to modify the beam shape and adjust the radiation dose distribution.
- **Horizontal Position (mm):** Indicates the horizontal position of the collimator leaves in millimeters. This position can influence the shape and size of the radiation delivered to the tissue or tumor.

Examining the characteristics of the first beam, a discernible pattern emerges regarding the collimator position. It initiates at -40mm and steadily traverses horizontally, reaching a maximum value of 20mm as the complexity of the shapes being formed increases. Correspondingly, the collimator blades expand incrementally up to shape 9, aligning with the evolving contours of the beam. However, an intriguing observation arises in the final two shapes, where there is a noticeable reduction in the number of blades. This phenomenon suggests a possible correlation with the imminent conclusion of the beam's duration, hinting at an adaptive mechanism to optimize efficiency or accommodate specific requirements. Furthermore, it's noteworthy that the width of the beam remains consistent throughout, measuring at a precise 0.2mm.

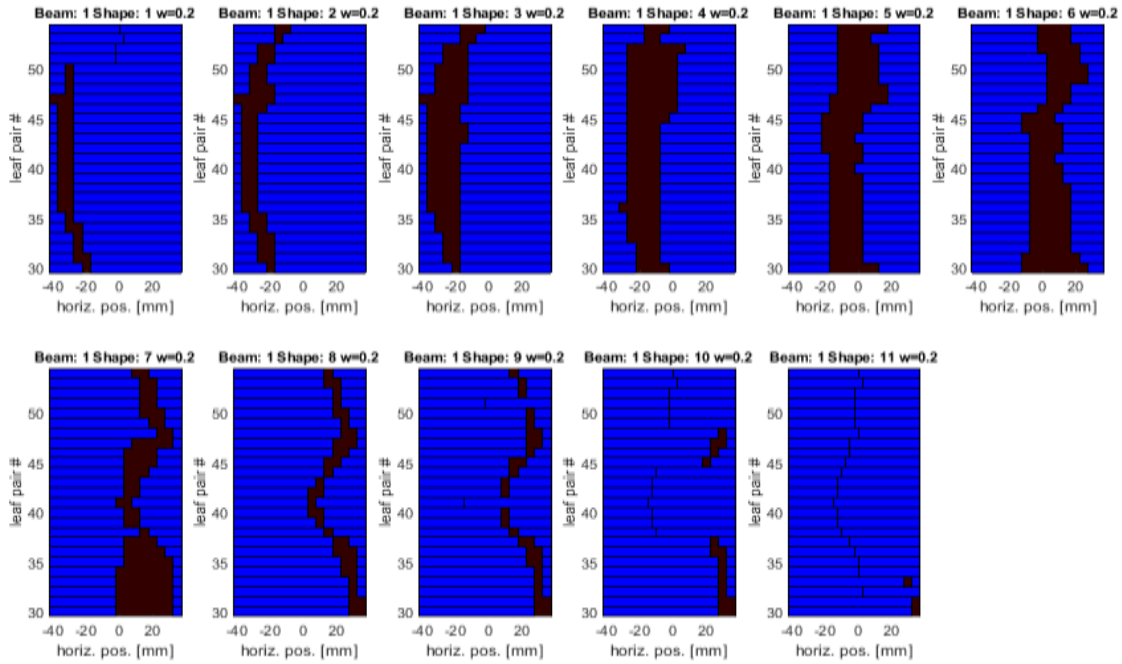


Figure 4.22 Shapes of beam 1

In this last beam it can be noticed that the duration time was shorter than all the other beams, because the number of shapes is only 9, as well as the shape does not vary so much, the horizontal position range goes from -40mm to 40mm as well as some beams.

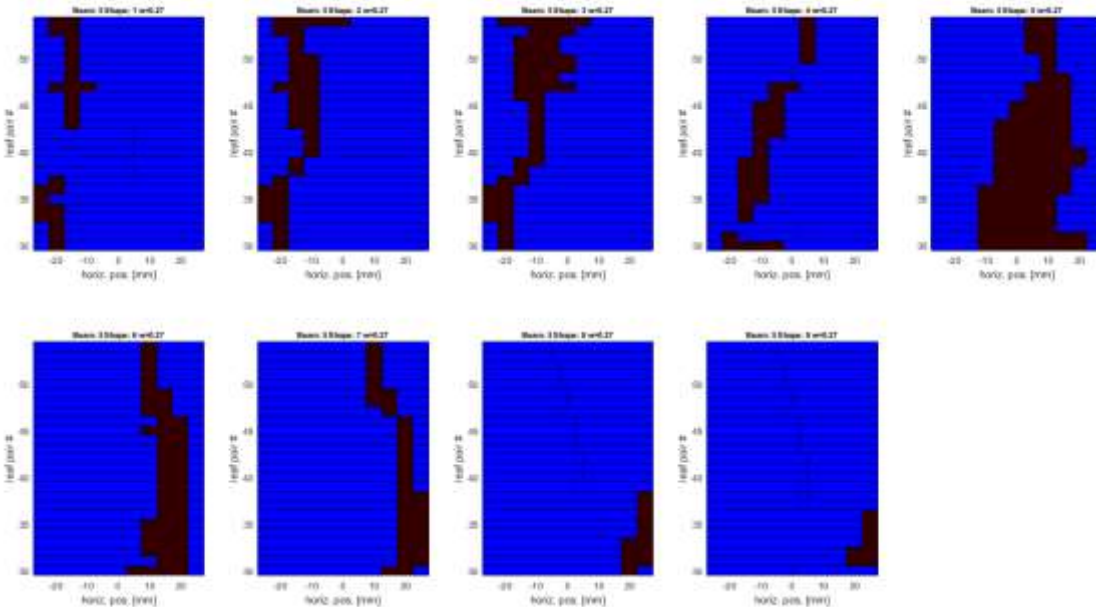


Figure 4.23 Shapes of beam 5

In this last beam it can be noticed that the duration time was shorter than all the other beams, because the number of shapes is only 9, as well as the shape does not vary so much, the horizontal position range goes from -40mm to 40mm as well as some beams.

### **4.3 T-test**

The comparison between the doses obtained by the neural network and the Monte Carlo model yielded a p value of 0.4649 when a statistical analysis was performed using a t-test. This value indicates that there is not enough evidence to reject the null hypothesis that there is no significant difference between the doses calculated by both methods.

Consequently, according to the results of the statistical test performed, the doses obtained by the neural network and the Monte Carlo model are comparable in terms of their effect on the results obtained. It is important to note that this conclusion is based solely on the p-value obtained and the significance level used, which was 0.05.

## Chapter 5

### Discussion

#### 5.1 Analysis between MCM and CNN

In this thesis, two models were implemented to simulate radiotherapeutic treatments: the convolutional neural network (CNN) and the Monte Carlo Model. Both models offer significant potential for improving the accuracy and efficacy of treatments, however, their approaches and applications differ in several key aspects.

CNN has demonstrated remarkable accuracy and efficiency in dose prediction, making it a valuable tool in radiotherapeutic treatment planning. When trained on a data set, the CNN can generalize patterns and predict doses with a considerable accuracy of 97.10%. In our study, CNN showed high agreement with actual dose values in the 90 patients analyzed, suggesting its clinical utility in daily practice on an extensive and automatic dataset.

However, it is crucial to keep in mind the inherent limitations of CNN. Despite its accuracy, CNN cannot provide detailed information on the spatial distribution of dose on the shape and propagation of the radiation beam. In addition, CNN relies on prior training and cannot easily adapt to changes in treatment conditions or patient anatomy during radiation therapy. This can be especially problematic in situations where anatomical variability or patient response to treatment is significant.

On the other hand, the Monte Carlo Model offers a more complete and detailed view of radiotherapeutic dosimetry. By simulating the interaction of radiation particles with matter the Monte Carlo Model can accurately predict the dose distribution in specific tissues and organs. Our study revealed that the Monte Carlo Model provided crucial clinical and physical information, such as collimator shape, patient position, and radiation beam distribution, which facilitates more accurate and personalized treatment planning.

In addition, MCM allows detailed visualization of dose optimization through histograms and dose maps, which facilitates the identification of critical areas and assessment of surrounding tissue toxicity. However, if multiple patients need to be analyzed, as in the present case which addressed more than 50 cases, the analysis with the Monte Carlo Model

is more time-consuming, as it can only be performed after all individual treatments have been completed. This temporal limitation should be considered when planning large studies or in clinical settings with high patient demand.

It is important to note that, although our study focused on a group of 90 patients (validation group) for the network and 50 patients for the model, since the number of images per patient was approximately 30 images, it was too large to take the same number of images as for the network. The results obtained are consistent with previous studies that have demonstrated the efficacy of both models in the optimization of radiotherapeutic treatments. The high agreement between the predicted doses and the actual doses observed in our patients supports the validity and clinical utility of these advanced approaches.

The following table summarizes the advantages and disadvantages of these models and the joining of both.

	<b>CNN</b>	<b>MCM</b>	<b>Both</b>
<i>Advantages</i>	High precision in dose prediction.	Precise simulation of radiation-matter interaction.	Complementary precision and detail
	Automatization of CT image analysis.	Detailed radiotherapy dosimetry.	Efficiency in analysis.
	Generalization of patterns.	Optimal visualization of dose optimization.	Automation and detail in planning.
<i>Disadvantages</i>	Lack of spatial distribution detail in doses.	Time and resource-intensive patient-by-patient analysis.	Requires exhaustive validation between both models.
	Limitations in adapting to treatment conditions	Higher computational complexity and technical requirements.	Limitations in adaptability
	Dependence on prior training.	Prerequisites of the plan depend on tissue or organ	

**Table 5.1** Advantages and Disadvantages of Models

Finally, the following image shows the distribution of the dose data, where the mean values of both MCM and CNN are almost similar, and concerning the predicted dose, both models show similar values of dose, their small differences may be due to the attenuation factor.

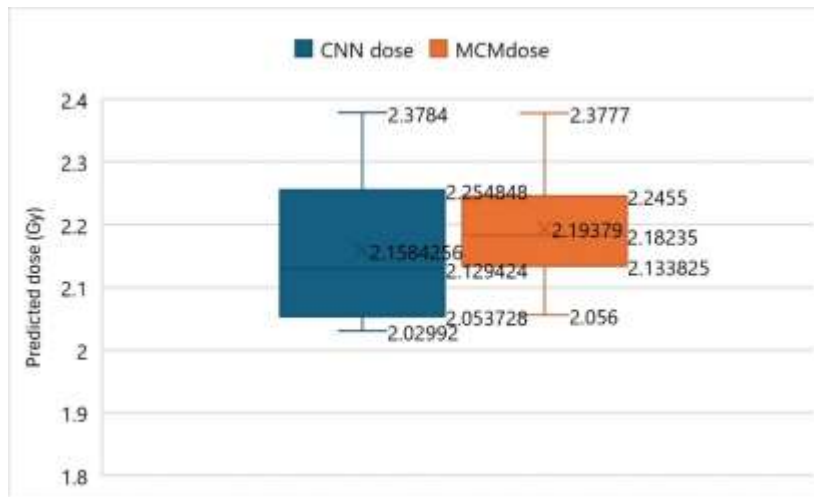


**Figure 5.1** Distribution of dose data of CNN and MCM

## 5.2 Comparison with Other Studies

Another way to analyze this thesis is to compare it with other studies related to the same topic and verify the values obtained in their metrics.

<i>Autor</i>	<b>Method</b>	<b>Metric</b>		<b>Reference</b>
		Acc	Precision	
----	Our Method	97.10	99.2	
<i>Chougrad et al.,</i>	DCNN	96.67	97.1	(Chougrad et al., 2018)
<i>Abbass</i>	EANN	97.5	98.05	(Abbass, 2002)
<i>Rakhlin et al.,</i>	CNN	87.2	88	(Rakhlin et al., 2018)
<i>Wu et al.,</i>	CNN	90	92.03	(Wu et al., 2020)
<i>Azar &amp; El-Said</i>	PPN	92.46	---	(Azar & El-Said, 2013)
<i>Samala et al.,</i>	DCNN	95	97.8	(Samala et al., 2018)

**Table 5.2** Comparison of different methods

## Chapter 6

# Conclusions and Future Works

### 6.1 Conclusions

The convergence between convolutional neural network (CNN) and Monte Carlo Model (MMC) in the optimization of radiotherapeutic treatments poses a promising prospect, with the potential to elevate the reliability and accuracy of results. Delving into the specific advantages of ResNet50 and U-Net-based CNN, together with the IMRT-focused Monte Carlo Model approach, highlights their unique capabilities and the synergy that could be achieved through their integration.

CNN, particularly based on architectures such as ResNet50 and U-Net, excels at efficiently handling large data sets and accurately predicting radiation dose. This makes it an invaluable tool in the initial treatment planning phase, where it provides a quick and reliable estimate of the initial dose distribution. Its ability to discern general patterns and trends in dose distribution is essential for accurate and timely preliminary decision-making by the medical team.

On the other hand, the IMRT-based Monte Carlo Model provides a detailed and accurate assessment of radiation dose at each tissue site, considering critical factors such as collimator shape, patient position, and tissue composition. By simulating the interaction of radioactive particles at the subatomic level, MCM provides thorough validation at the physical level, increasing confidence in the accuracy of the final treatment plan.

The combination of these methodologies establishes a synergy that leverages the strengths of each approach and mitigates their respective limitations. While CNN provides a quick and reliable initial estimate, the Monte Carlo Model refines and validates this initial distribution, thereby improving the reliability and accuracy of the final treatment plan. This strategic integration not only improves the reliability of the results but also increases confidence in the accuracy of the final treatment plan.

However, this convergence faces technical and computational challenges, such as interoperability between the two systems and efficient management of large volumes of data. Moreover, additional validation and verification methods will be required to ensure the consistency and accuracy of the results obtained through this integration.

In summary, the marriage of the ResNet50 and U-Net-based convolutional neural network with the IMRT-centric Monte Carlo Model could significantly improve radiotherapy treatment planning and delivery if applied together, rather than separately. This strategic integration represents a move towards more sophisticated and effective approaches, with the final goal of improving clinical outcomes based on previous studies such as this one and the quality of life of patients.

## 6.2 Future Works

It is proposed to develop a model that integrates neural networks and the Monte Carlo Model for radiation analysis, extending its application beyond radiotherapy to other therapies. In addition, a more detailed analysis considering the mammary anatomy is contemplated, providing a three-dimensional representation of the intramammary nodes, arteries, and the location of the tumor. The figure below shows the breast structure, although for the moment the tumor has not been located.



**Figure 6.1** Breast Anatomical Structure including intramammary nodes .

## References

- Dynamic Contrast-Enhanced Magnetic Resonance Images of Breast Cancer Patients with Tumor Locations[Data Set] (2021).
- Abbas, Z., & Rehman, S. (2018). An Overview of Cancer Treatment Modalities. In *Neoplasms*. <https://doi.org/10.5772/intechopen.76558>
- Abbass, H. A. (2002). An evolutionary artificial neural networks approach for breast cancer diagnosis. *Artificial Intelligence in Medicine*, 25(3). [https://doi.org/10.1016/S0933-3657\(02\)00028-3](https://doi.org/10.1016/S0933-3657(02)00028-3)
- Acs, B., Pelekanou, V., Bai, Y., Martinez-Morilla, S., Toki, M., Leung, S. C. Y., Nielsen, T. O., & Rimm, D. L. (2019). Ki67 reproducibility using digital image analysis: an inter-platform and inter-operator study. *Laboratory Investigation*, 99(1). <https://doi.org/10.1038/s41374-018-0123-7>
- Adamson, J., Erickson, B. G., Wang, C., Cui, Y., Alber, M., Kirkpatrick, J., & Yin, F. F. (2023). Generation, validation, and benchmarking of a commercial independent Monte Carlo calculation beam model for multi-target SRS. *Zeitschrift Fur Medizinische Physik*. <https://doi.org/10.1016/j.zemedi.2023.08.004>
- American Cancer Society. (2019a). *Survival Rates for Breast Cancer*. American Cancer Society.
- American Cancer Society. (2019b). *What Is Breast Cancer? | Breast Cancer Definition*. 18 September.
- Antolak, J. (2015). The Physics of Radiation Therapy. *Medical Physics*, 42(8). <https://doi.org/10.1118/1.4927276>
- Azar, A. T., & El-Said, S. A. (2013). Probabilistic neural network for breast cancer classification. *Neural Computing and Applications*, 23(6). <https://doi.org/10.1007/s00521-012-1134-8>
- Barragán-Montero, A., Javaid, U., Valdés, G., Nguyen, D., Desbordes, P., Macq, B., Willems, S., Vandewinckele, L., Holmström, M., Löfman, F., Michiels, S., Souris, K., Sterpin, E., & Lee, J. A. (2021). Artificial intelligence and machine learning for medical imaging: A technology review. In *Physica Medica* (Vol. 83). <https://doi.org/10.1016/j.ejmp.2021.04.016>
- Bedford, J. L. (2019). Calculation of absorbed dose in radiotherapy by solution of the linear Boltzmann transport equations. In *Physics in Medicine and Biology* (Vol. 64, Issue 2). <https://doi.org/10.1088/1361-6560/aaf0e2>
- Behranvand, N., Nasri, F., Zolfaghari Emameh, R., Khani, P., Hosseini, A., Garssen, J., & Falak, R. (2022). Chemotherapy: a double-edged sword in cancer treatment. In *Cancer Immunology, Immunotherapy* (Vol. 71, Issue 3). <https://doi.org/10.1007/s00262-021-03013-3>
- Boylan, C. J., Aitkenhead, A. H., Rowbottom, C. G., & Mackay, R. I. (2013). Simulation of realistic linac motion improves the accuracy of a Monte Carlo based VMAT plan QA system. *Radiotherapy and Oncology*, 109(3). <https://doi.org/10.1016/j.radonc.2013.08.046>

- Burguin, A., Diorio, C., & Durocher, F. (2021). Breast cancer treatments: Updates and new challenges. *Journal of Personalized Medicine*, 11(8).  
<https://doi.org/10.3390/jpm11080808>
- Castaneda, S. A., & Strasser, J. (2017). Updates in the Treatment of Breast Cancer with Radiotherapy. In *Surgical Oncology Clinics of North America* (Vol. 26, Issue 3).  
<https://doi.org/10.1016/j.soc.2017.01.013>
- Cavalcanti, A. P., Barbosa, A., Carvalho, R., Freitas, F., Tsai, Y. S., Gašević, D., & Mello, R. F. (2021). Automatic feedback in online learning environments: A systematic literature review. In *Computers and Education: Artificial Intelligence* (Vol. 2).  
<https://doi.org/10.1016/j.caeai.2021.100027>
- Center for Disease Control and Prevention. (2019). *Basic Information About Breast Cancer*. Center for Disease Control and Prevention.
- Chen, L., Lu, M., & Chen, C. L. P. (2010). Multiple kernel fuzzy c-means based image segmentation. *Conference Proceedings - IEEE International Conference on Systems, Man and Cybernetics*. <https://doi.org/10.1109/ICSMC.2010.5641782>
- Choi, R. Y., Coyner, A. S., Kalpathy-Cramer, J., Chiang, M. F., & Peter Campbell, J. (2020). Introduction to machine learning, neural networks, and deep learning. *Translational Vision Science and Technology*, 9(2). <https://doi.org/10.1167/tvst.9.2.14>
- Chougrad, H., Zouaki, H., & Alheyane, O. (2018). Deep Convolutional Neural Networks for breast cancer screening. *Computer Methods and Programs in Biomedicine*, 157.  
<https://doi.org/10.1016/j.cmpb.2018.01.011>
- Cireşan, D. C., Giusti, A., Gambardella, L. M., & Schmidhuber, J. (2012). Deep neural networks segment neuronal membranes in electron microscopy images. *Advances in Neural Information Processing Systems*, 4.
- Cisternas, E., Mairani, A., Ziegenhein, P., Jäkel, O., & Bangert, M. (2015). matRad – a multi-modality open source 3D treatment planning toolkit. *IFMBE Proceedings*, 51.  
[https://doi.org/10.1007/978-3-319-19387-8\\_391](https://doi.org/10.1007/978-3-319-19387-8_391)
- Contreras, J. S., Jiménez- Rodríguez, L. A., & Gamboa-Suárez, R. (2022). Contribución de la radiología digital al mejoramiento de la calidad en el servicio de imagenología. *Nova*, 20(39). <https://doi.org/10.22490/24629448.6576>
- Cunningham, P., Cord, M., & Delany, S. J. (2008). Supervised learning. *Cognitive Technologies*.  
[https://doi.org/10.1007/978-3-540-75171-7\\_2](https://doi.org/10.1007/978-3-540-75171-7_2)
- Deike-Hofmann, K., Kuder, T., König, F., Paech, D., Dreher, C., Delorme, S., Schlemmer, H. P., & Bickelhaupt, S. (2018). Diffusion-weighted breast imaging. In *Radiologe* (Vol. 58).  
<https://doi.org/10.1007/s00117-018-0423-3>
- DiMaio, S., Kapur, T., Cleary, K., Aylward, S., Kazanzides, P., Vosburgh, K., Ellis, R., Duncan, J., Farahani, K., Lemke, H., Peters, T., Lorensen, W. (Bill), Gobbi, D., Haller, J., Clarke, L. (Larry), Pizer, S., Taylor, R., Galloway, R., Fichtinger, G., ... Jolesz, F. (2007). Challenges in image-guided therapy system design. *NeuroImage*, 37(SUPPL. 1).  
<https://doi.org/10.1016/j.neuroimage.2007.04.026>

- Drăgănescu, M., & Carmocan, C. (2017). Hormone therapy in breast cancer. In *Chirurgia (Romania)* (Vol. 112, Issue 4). <https://doi.org/10.21614/chirurgia.112.4.413>
- Fielding, A. L. (2023). Monte-Carlo techniques for radiotherapy applications I: introduction and overview of the different Monte-Carlo codes. In *Journal of Radiotherapy in Practice* (Vol. 22, Issue 247). <https://doi.org/10.1017/S1460396923000079>
- Foidart, J. M., Desreux, J., Pintiaux, A., & Gompel, A. (2007). Hormone therapy and breast cancer risk. *Climacteric*, 10(SUPPL. 2). <https://doi.org/10.1080/13697130701598324>
- Franciosini, G., Battistoni, G., Cerqua, A., De Gregorio, A., De Maria, P., De Simoni, M., Dong, Y., Fischetti, M., Marafini, M., Mirabelli, R., Muscato, A., Patera, V., Salvati, F., Sarti, A., Sciubba, A., Toppi, M., Traini, G., Trigilio, A., & Schiavi, A. (2023). GPU-accelerated Monte Carlo simulation of electron and photon interactions for radiotherapy applications. *Physics in Medicine and Biology*, 68(4). <https://doi.org/10.1088/1361-6560/aca1f2>
- Gentle, J. E. (2009). Computational Statistics. In *International Encyclopedia of Education, Third Edition*. <https://doi.org/10.1016/B978-0-08-044894-7.01316-6>
- Gordon, Y., Partovi, S., Müller-Eschner, M., Amarteifio, E., Bäuerle, T., Weber, M.-A., Kauczor, H.-U., & Rengier, F. (2014). Dynamic contrast-enhanced magnetic resonance imaging: fundamentals and application to the evaluation of the peripheral perfusion. *Cardiovascular Diagnosis and Therapy*, 4(2). <https://doi.org/10.3978/j.issn.2223-3652.2014.03.01>
- Hadebe, B., Harry, L., Ebrahim, T., Pillay, V., & Vorster, M. (2023). The Role of PET/CT in Breast Cancer. In *Diagnostics* (Vol. 13, Issue 4). <https://doi.org/10.3390/diagnostics13040597>
- Hassan, M. S. U., Ansari, J., Spooner, D., & Hussain, S. A. (2010). Chemotherapy for breast cancer (review). In *Oncology Reports* (Vol. 24, Issue 5). [https://doi.org/10.3892/or\\_00000963](https://doi.org/10.3892/or_00000963)
- Hausmann, J., Corradini, S., Nestle-Kraemling, C., Bölke, E., Njanang, F. J. D., Tamaskovics, B., Orth, K., Ruckhaeberle, E., Fehm, T., Mohrmann, S., Simiantonakis, I., Budach, W., & Matuschek, C. (2020). Recent advances in radiotherapy of breast cancer. In *Radiation Oncology* (Vol. 15, Issue 1). <https://doi.org/10.1186/s13014-020-01501-x>
- Henriques, B., Mendes, F., & Martins, D. (2021). Immunotherapy in breast cancer: When, how, and what challenges? In *Biomedicines* (Vol. 9, Issue 11). <https://doi.org/10.3390/biomedicines9111687>
- Hong, R., & Xu, B. (2022). Breast cancer: an up-to-date review and future perspectives. In *Cancer Communications* (Vol. 42, Issue 10). <https://doi.org/10.1002/cac2.12358>
- Hussain, A., Dunscombe, P., Villarreal-Barajas, J. E., & Brown, D. (2012). Total body irradiation dose optimization based on radiological depth. *Journal of Applied Clinical Medical Physics*, 13(3). <https://doi.org/10.1120/jacmp.v13i3.3767>
- Islam, M., Chen, G., & Jin, S. (2019). An Overview of Neural Network. *American Journal of Neural Networks and Applications*, 5(1). <https://doi.org/10.11648/j.ajjna.20190501.12>
- Jornet, D., Loap, P., Pierga, J. Y., Laki, F., Vincent-salomon, A., Kirova, Y. M., & Fourquet, A. (2021). Neoadjuvant concurrent radiotherapy and chemotherapy in early breast cancer

- patients: Long-term results of a prospective phase II trial. *Cancers*, 13(20).  
<https://doi.org/10.3390/cancers13205107>
- Kheybari, S., Naji, S. A., Rezaie, F. M., & Salehpour, R. (2019). ABC classification according to Pareto's principle: a hybrid methodology. *OPSEARCH*, 56(2).  
<https://doi.org/10.1007/s12597-019-00365-4>
- Koch, K. R. (2018). Monte Carlo methods. *GEM - International Journal on Geomathematics*, 9(1). <https://doi.org/10.1007/s13137-017-0101-z>
- Kooy, H. M., & Grassberger, C. (2015). Intensity modulated proton therapy. In *British Journal of Radiology* (Vol. 88, Issue 1051). <https://doi.org/10.1259/bjr.20150195>
- Krizhevsky, A., Sutskever, I., & Hinton, G. E. (2017). ImageNet classification with deep convolutional neural networks. *Communications of the ACM*, 60(6).  
<https://doi.org/10.1145/3065386>
- Lagendijk, J. J. W., Raaymakers, B. W., Raaijmakers, A. J. E., Overweg, J., Brown, K. J., Kerkhof, E. M., van der Put, R. W., Hårdemark, B., van Vulpen, M., & van der Heide, U. A. (2008). MRI/linac integration. *Radiotherapy and Oncology*, 86(1).  
<https://doi.org/10.1016/j.radonc.2007.10.034>
- Lomax, A. J., Bortfeld, T., Goitein, G., Debus, J., Dykstra, C., Tercier, P. A., Coucke, P. A., & Mirimanoff, R. O. (1999). A treatment planning inter-comparison of proton and intensity modulated photon radiotherapy. *Radiotherapy and Oncology*, 51(3).  
[https://doi.org/10.1016/S0167-8140\(99\)00036-5](https://doi.org/10.1016/S0167-8140(99)00036-5)
- Lother, D., Robert, M., Elwood, E., Smith, S., Tunariu, N., Johnston, S. R. D., Parton, M., Bhaludin, B., Millard, T., Downey, K., & Sharma, B. (2023). Imaging in metastatic breast cancer, CT, PET/CT, MRI, WB-DWI, CCA: review and new perspectives. In *Cancer Imaging* (Vol. 23, Issue 1). <https://doi.org/10.1186/s40644-023-00557-8>
- Marrazzo, E., Frusone, F., Milana, F., Sagona, A., Gatzemeier, W., Barbieri, E., Bottini, A., Canavese, G., Rubino, A. O., Eboli, M. G., Rossetti, C. M., Testori, A., Errico, V., De Luca, A., & Tinterri, C. (2020). Mucinous breast cancer: A narrative review of the literature and a retrospective tertiary single-centre analysis. In *Breast* (Vol. 49).  
<https://doi.org/10.1016/j.breast.2019.11.002>
- Martins, O., & Azevedo, I. (2021). Radioterapia Paliativa para Cuidados Oncológicos em Fim de Vida. *Medicina Interna*, 27(1). <https://doi.org/10.24950/revisao/103/19/1/2020>
- Mascarenhas, S., & Agarwal, M. (2021). A comparison between VGG16, VGG19 and ResNet50 architecture frameworks for Image Classification. *Proceedings of IEEE International Conference on Disruptive Technologies for Multi-Disciplinary Research and Applications, CENTCON 2021*. <https://doi.org/10.1109/CENTCON52345.2021.9687944>
- Mathworks. (2022). *Machine Learning: Tres cosas que es necesario saber - MATLAB & Simulink*. Machine Learning Con Matlab.
- Microsoft. (2022). *Deep learning vs. machine learning - Azure Machine Learning*. Microsoft Docs.

- Mohamed, A., Krajewski, K., Cakar, B., & Ma, C. X. (2013). Targeted therapy for breast cancer. In *American Journal of Pathology* (Vol. 183, Issue 4).  
<https://doi.org/10.1016/j.ajpath.2013.07.005>
- National Cancer Institute (NIH). (2022). *Breast Cancer - Health Professional Version*. National Cancer Institute (NIH).
- NCI. (2022). Breast Cancer Treatment (Adult) (PDQ®): Patient Version. In *National Cancer Institute*.
- NIH National Cancer Institute. (2019). Radiation Therapy to Treat Cancer. *January*.
- Njeh, C. F., Saunders, M. W., & Langton, C. M. (2012). Accelerated partial breast irradiation using external beam conformal radiation therapy: A review. In *Critical Reviews in Oncology/Hematology* (Vol. 81, Issue 1).  
<https://doi.org/10.1016/j.critrevonc.2011.01.011>
- Otto, K. (2008). Volumetric modulated arc therapy: IMRT in a single gantry arc. *Medical Physics*, 35(1). <https://doi.org/10.1118/1.2818738>
- Radhakrishna, S., Agarwal, S., Parikh, P. M., Kaur, K., Panwar, S., Sharma, S., Dey, A., Saxena, K. K., Chandra, M., & Sud, S. (2018). Role of magnetic resonance imaging in breast cancer management. *South Asian Journal of Cancer*, 7(2).  
[https://doi.org/10.4103/sajc.sajc\\_104\\_18](https://doi.org/10.4103/sajc.sajc_104_18)
- Rakhlin, A., Shvets, A., Igloukov, V., & Kalinin, A. A. (2018). Deep Convolutional Neural Networks for Breast Cancer Histology Image Analysis. *Lecture Notes in Computer Science (Including Subseries Lecture Notes in Artificial Intelligence and Lecture Notes in Bioinformatics)*, 10882 LNCS. [https://doi.org/10.1007/978-3-319-93000-8\\_83](https://doi.org/10.1007/978-3-319-93000-8_83)
- Rastelli, F., & Crispino, S. (2008). Factors predictive of response to hormone therapy in breast cancer. *Tumori*, 94(3). <https://doi.org/10.1177/030089160809400314>
- Roberts, G. D., & Graham, J. P. (2001). Computed radiography. *The Veterinary Clinics of North America. Equine Practice*, 17(1). [https://doi.org/10.1016/S0749-0739\(17\)30074-3](https://doi.org/10.1016/S0749-0739(17)30074-3)
- Rogers, D. W. O. (2001). Monte Carlo Techniques for Primary Standards of Ionizing Radiation and for Dosimetry Protocols. In *Advanced Monte Carlo for Radiation Physics, Particle Transport Simulation and Applications*. [https://doi.org/10.1007/978-3-642-18211-2\\_46](https://doi.org/10.1007/978-3-642-18211-2_46)
- Ronneberger, O., Fischer, P., & Brox, T. (2015). U-net: Convolutional networks for biomedical image segmentation. *Lecture Notes in Computer Science (Including Subseries Lecture Notes in Artificial Intelligence and Lecture Notes in Bioinformatics)*, 9351.  
[https://doi.org/10.1007/978-3-319-24574-4\\_28](https://doi.org/10.1007/978-3-319-24574-4_28)
- Rosenstrom, A., Santana-Leitner, M., Rokni, S., Shumail, M., Tantawi, S., Kwofie, J., Dewji, S., & Loo, B. W. (2023). Shielding Analysis of a Preclinical Bremsstrahlung X-ray FLASH Radiotherapy System within a Clinical Radiation Therapy Vault. *Health Physics*, 125(4).  
<https://doi.org/10.1097/HP.0000000000001718>
- Samala, R. K., Chan, H. P., Hadjiiski, L. M., Helvie, M. A., Richter, C., & Cha, K. (2018). Evolutionary pruning of transfer learned deep convolutional neural network for breast

- cancer diagnosis in digital breast tomosynthesis. *Physics in Medicine and Biology*, 63(9).  
<https://doi.org/10.1088/1361-6560/aabb5b>
- Sen, R., & Das, S. (2023). Unsupervised Learning. In *Indian Statistical Institute Series*.  
[https://doi.org/10.1007/978-981-19-2008-0\\_21](https://doi.org/10.1007/978-981-19-2008-0_21)
- Serai, S. D., Ho, M. L., Artunduaga, M., Chan, S. S., & Chavhan, G. B. (2021). Components of a magnetic resonance imaging system and their relationship to safety and image quality. In *Pediatric Radiology* (Vol. 51, Issue 5). <https://doi.org/10.1007/s00247-020-04894-9>
- Sharma, A. K., Nandal, A., Dhaka, A., Koundal, D., Bogatinoska, D. C., & Alyami, H. (2022). Enhanced Watershed Segmentation Algorithm-Based Modified ResNet50 Model for Brain Tumor Detection. *BioMed Research International*, 2022.  
<https://doi.org/10.1155/2022/7348344>
- Sharma, G. N., Dave, R., Sanadya, J., Sharma, P., & Sharma, K. K. (2010). Various types and management of breast cancer: An overview. In *Journal of Advanced Pharmaceutical Technology and Research* (Vol. 1, Issue 2).
- Sood, R., Rositch, A. F., Shakoore, D., Ambinder, E., Pool, K. L., Pollack, E., Mollura, D. J., Mullen, L. A., & Harvey, S. C. (2019). Ultrasound for breast cancer detection globally: A systematic review and meta-analysis. *Journal of Global Oncology*, 2019(5).  
<https://doi.org/10.1200/JGO.19.00127>
- Sternschuss, M., Yerushalmi, R., Saleh, R. R., Amir, E., & Goldvaser, H. (2021). Efficacy and safety of neoadjuvant immune checkpoint inhibitors in early-stage triple-negative breast cancer: a systematic review and meta-analysis. *Journal of Cancer Research and Clinical Oncology*, 147(11). <https://doi.org/10.1007/s00432-021-03591-w>
- Tabouret-Viaud, C., Botsikas, D., Delattre, B. M. A., Mainta, I., Amzalag, G., Rager, O., Vinh-Hung, V., Miralbell, R., & Ratib, O. (2015). PET/MR in breast cancer. In *Seminars in Nuclear Medicine* (Vol. 45, Issue 4). <https://doi.org/10.1053/j.semnuclmed.2015.03.003>
- Taylor, A., & Powell, M. E. B. (2004). Intensity-modulated radiotherapy - What is it? *Cancer Imaging*, 4(2). <https://doi.org/10.1102/1470-7330.2004.0003>
- Teoh, M., Clark, C. H., Wood, K., Whitaker, S., & Nisbet, A. (2011). Volumetric modulated arc therapy: A review of current literature and clinical use in practice. In *British Journal of Radiology* (Vol. 84, Issue 1007). <https://doi.org/10.1259/bjr/22373346>
- Tervo, J., Vauhkonen, M., & Boman, E. (2008). Optimal control model for radiation therapy inverse planning applying the Boltzmann transport equation. *Linear Algebra and Its Applications*, 428(5–6). <https://doi.org/10.1016/j.laa.2007.03.003>
- Thawani, R., Gao, L., Mohinani, A., Tudorica, A., Li, X., Mitri, Z., & Huang, W. (2022). Quantitative DCE-MRI prediction of breast cancer recurrence following neoadjuvant chemotherapy: a preliminary study. *BMC Medical Imaging*, 22(1).  
<https://doi.org/10.1186/s12880-022-00908-0>
- Tiwari, A. (2022). Supervised learning: From theory to applications. In *Artificial Intelligence and Machine Learning for EDGE Computing*. <https://doi.org/10.1016/B978-0-12-824054-0.00026-5>

- van de Sande, D., Sharabiani, M., Bluemink, H., Kneepkens, E., Bakx, N., Hagelaar, E., van der Sangen, M., Theuws, J., & Hurkmans, C. (2021). Artificial intelligence based treatment planning of radiotherapy for locally advanced breast cancer. *Physics and Imaging in Radiation Oncology*, 20. <https://doi.org/10.1016/j.phro.2021.11.007>
- Varela, C., Valdés, R., Rojas, A., & Soffia, P. (2022). Principles of magnetic resonance imaging (MRI). In *Nuclear Medicine and Molecular Imaging: Volume 1-4* (Vol. 1). <https://doi.org/10.1016/B978-0-12-822960-6.00101-0>
- Wasif, N., Maggard, M. A., Ko, C. Y., & Giuliano, A. E. (2010). Invasive lobular vs. ductal breast cancer: A stage-matched comparison of outcomes. *Annals of Surgical Oncology*, 17(7). <https://doi.org/10.1245/s10434-010-0953-z>
- Wieser, H. P., Cisternas, E., Wahl, N., Ulrich, S., Stadler, A., Mescher, H., Muller, L. R., Klinge, T., Gabrys, H., Burigo, L., Mairani, A., Ecker, S., Ackermann, B., Ellerbrock, M., Parodi, K., Jakel, O., & Bangert, M. (2017). Development of the open-source dose calculation and optimization toolkit matRad. *Medical Physics*, 44(6). <https://doi.org/10.1002/mp.12251>
- Wieser, H.-P., Wahl, N., Gabryś, H. S., Müller, L.-R., Pezzano, G., Winter, J., Ulrich, S., Burigo, L., Jäkel, O., & Bangert, M. (2018). MATRAD-AN OPEN-SOURCE TREATMENT PLANNING TOOLKIT FOR EDUCATIONAL PURPOSES. In *MEDICAL PHYSICS INTERNATIONAL Journal* (Vol. 6, Issue 1).
- Wu, N., Phang, J., Park, J., Shen, Y., Huang, Z., Zorin, M., Jastrzebski, S., Fevry, T., Katsnelson, J., Kim, E., Wolfson, S., Parikh, U., Gaddam, S., Lin, L. L. Y., Ho, K., Weinstein, J. D., Reig, B., Gao, Y., Toth, H., ... Geras, K. J. (2020). Deep Neural Networks Improve Radiologists' Performance in Breast Cancer Screening. *IEEE Transactions on Medical Imaging*, 39(4). <https://doi.org/10.1109/TMI.2019.2945514>
- Xu, J., Zhang, Y., & Miao, D. (2020). Three-way confusion matrix for classification: A measure driven view. *Information Sciences*, 507. <https://doi.org/10.1016/j.ins.2019.06.064>
- Yamashita, R., Nishio, M., Do, R. K. G., & Togashi, K. (2018). Convolutional neural networks: an overview and application in radiology. In *Insights into Imaging* (Vol. 9, Issue 4). <https://doi.org/10.1007/s13244-018-0639-9>
- Yoon, E., Kim, J. in, Park, J. M., Choi, C. H., & Jung, S. (2023). Extension of matRad with a modified microdosimetric kinetic model for carbon ion treatment planning: Comparison with Monte Carlo calculation. *Medical Physics*, 50(9). <https://doi.org/10.1002/mp.16449>
- Zhang, X., Shi, J., Zhou, Y., Mao, F., Lin, Y., Guan, J., Liang, Z., & Sun, Q. (2017). A rare mixed breast cancer of intraductal and solid papillary with tubular carcinoma histotypes in a young woman. *Journal of Thoracic Disease*, 9(9). <https://doi.org/10.21037/jtd.2017.07.105>
- Zhu, Y., O'Connell, A. M., Ma, Y., Liu, A., Li, H., Zhang, Y., Zhang, X., & Ye, Z. (2022a). Correction to: Dedicated breast CT: state of the art—Part I. Historical evolution and technical aspects (European Radiology, (2022), 32, 3, (1579-1589), 10.1007/s00330-021-08179-z). In *European Radiology* (Vol. 32, Issue 4). <https://doi.org/10.1007/s00330-021-08491-8>

Zhu, Y., O'Connell, A. M., Ma, Y., Liu, A., Li, H., Zhang, Y., Zhang, X., & Ye, Z. (2022b). Dedicated breast CT: state of the art—Part I. Historical evolution and technical aspects. In *European Radiology* (Vol. 32, Issue 3). <https://doi.org/10.1007/s00330-021-08179-z>